Arming Adoptively Transferred T-cells with Drug-loaded Nanoparticles for Cancer Immunotherapy

Yiran Zheng
Bachelor of Science, Chemical & Biomolecular Engineering
Bachelor of Arts, Biology
Johns Hopkins University, Baltimore, MD, 2009

Submitted to the Department of Biological Engineering
In Partial Fulfillment of the Requirements for the Degree of

Doctor of Philosophy
at the

Massachusetts Institute of Technology

November 2015
[February 2016]

Signature of Author: Signature redacted
Yiran Zheng
Department of Biological Engineering
November 10, 2015

Certified by: Signature redacted
Professor Darrell J. Irvine
Department of Biological Engineering and Materials Science
Thesis Supervisor

Accepted by: Signature redacted
Forest M. White
Professor of Biological Engineering
Chairman, Graduate Program Committee for Biological Engineering

Members of Thesis Committee

Darrell J. Irvine

Professor of Biological Engineering and Materials Science & Engineering
Massachusetts Institute of Technology
Thesis Supervisor

Jianzhu Chen

Cottrell Professor of Immunology
Professor of Biology
Massachusetts Institute of Technology

K. Dane Wittrup

C.P. Dubbs Professor of Chemical Engineering and Biological Engineering
Massachusetts Institute of Technology
Thesis Committee Chair

Arming Adoptively Transferred T-cells with Drug-loaded Nanoparticles for Cancer Immunotherapy

by
Yiran Zheng

Submitted to the Department of Biological Engineering
On November 10, 2015 in partial fulfillment of the requirements for the degree of
Doctor of Philosophy in Biological Engineering

Abstract

In adoptive cell therapy (ACT), autologous tumor-specific T-cells isolated from cancer patients or genetically engineered lymphocytes are activated and expanded *ex vivo*, then infused back into the individual to eliminate metastatic tumors. A major limitation of this promising approach is the loss of ACT T-cell effector functions *in vivo* due to the highly immunosuppressive environment in solid tumors. Protection of T-cells from immunosuppressive signals can be achieved by systemic administration of supporting adjuvant drugs such as interleukins, chemotherapy, and other immunomodulators, but these adjuvant treatments are often accompanied by serious toxicities and may still fail to optimally stimulate lymphocytes in all tumor and lymphoid compartments. Here we propose a two-pronged approach to address this problem, namely 1) repeatedly reloading supporting drugs to T-cells and 2) extending the initial functional lifetime of drug carriers conjugated to cell surfaces before transfer. To achieve this, we developed a novel strategy to repeatedly stimulate or track ACT T-cells, using cytokines or ACT-cell-specific antibodies as ligands to target PEGylated liposomes to transferred T-cells *in vivo*. Using $F(ab')_2$ fragments against a unique cell surface antigen on ACT cells (Thy1.1) or an engineered interleukin-2 (IL-2) molecule on an Fc framework as targeting ligands, we demonstrate that >95% of ACT cells can be conjugated with liposomes following a single injection *in vivo*. Further, we show that IL-2-conjugated liposomes both target ACT cells and are capable of inducing repeated waves of ACT T-cell proliferation in tumor-bearing mice. These results demonstrate the feasibility of repeated functional targeting of T-cells *in vivo*, which will enable delivery of imaging contrast agents, immunomodulators, or chemotherapy agents in adoptive cell therapy regimens. On the other hand, we identified CD45 as a non-internalizing receptor on T-cells that could be used as an anchor to block internalization of cell surface-conjugated nanoparticles. Anti-CD45 decorated nanogels consisting of IL-15 superagonists remained on T-cells surfaces for over 12 days and induced 15-fold T-cell expansion in tumors *in vivo* and significant tumor regression without toxicity, while equivalent doses of free IL-15Sa were lethal. These results show that anti-CD45 can be generally employed to decorate a broad array of nanoparticles to endow them enhanced stability on cell surfaces for extracelluar drug delivery, tracking, or diagnostic purposes. We also compared the efficacy of anti-Thy1.1 liposomes and anti-CD45 liposomes in delivering SB525334, an immunosuppression-reverting drug for inhibiting TGF-β signaling pathway, to ACT T-cells. In the setting of pre-loading T-cells with liposomes *in vitro*, binding to T-cells through the non-internalizing receptor CD45

elicited greater granzyme expression in ACT T-cells systemically and particularly led to greater donor T-cell infiltration of tumors, which correlated with greater therapeutic efficacy. Nevertheless, as a proof of concept, anti-Thy1.1 liposomes allowed specific re-arming of ACT T-cells with SB525334 by *in vivo* targeting and slowed down tumor growth significantly compared to equivalent dose of free drug and anti-CD45 liposomes. These might provide us with insights into designing and selecting the right targeting nanoparticles or combination of them depending on the nature of drugs. All together, these results demonstrate the efficacy and specificity of surface-ligand decorated nanoparticles in enhancing *in vivo* persistence of transferred T-cells. These nanoparticles may be applied to significantly improve the therapeutic index of drugs in cancer immunotherapy.

Thesis Supervisor: Darrell J. Irvine
Title: Professor of Biological Engineering and Materials Science & Engineering

Table of Contents

List of Figures

Acknowledgements

Time flies. It's hard to believe that I've reached the end of my graduate studies. On the road to completing my dissertation I received help, words of encouragement and inspiration from many people, and I would like to take this opportunity to sincerely thank them.

First and foremost, I would like to thank my dear thesis advisor, Professor Darrell Irvine. Thank you for your guidance, mentorship, encouragement and patience throughout the last five years. Your enthusiasm for science is truly inspiring and motivating. Your dedication to students and attitude towards science will be my life-long role model.

To the members of my thesis committee, Professors Dane Wittrup and Jianzhu Chen, thank you for your thoughtful comments and recommendations for my project. Your expertise in engineering and biology always shed lights on the development of my project and helped me to think about the results from a different angle.

Next I would like to thank my labmates. Li, thank you for being a great friend and collaborator; I never could have achieved all of this without you. To Haipeng, Bonnie, Adrienne, Brandon, James and Matthias, thank you all for teaching me the basics behind the experiments I'd be working on and for helping me get started with animal studies. You helped me build the foundation I needed to move my project forward. Above all, your encouraging words and the experience you shared helped me get through some tough times during PhD. Llian, thank you for always working so hard with me. All those large animal experiments would not have been possible, and my life would have been miserable without you. Wuhbet, Heikyung and Alex, thank you for your kind help. You made necropsies less of a nightmare. To Talar, Sudha, Tyson, Greg, Melissa, Kavya, Sabrina, Marianne and Mark, thank you for always being there to answer questions, bounce ideas off of and to share protocols and reagents. You've all rescued my experiments on so many occasions. To my UROP Sarah, thank you for your hard work. You helped motivate me in ways I'm sure you weren't aware of, but I became a better graduate student because of you

To my collaborators and people who contributed to this project:
Kai Wucherpfennig and Michael Goldberg for thoughtful suggestions.
Technical assistance at shared facilities: Glenn Paradis and Mike Jennings (flow cytometry) and Scott Malstrom (IVIS imaging).

Lastly, I'd like to thank my family. Thank you for the patience, support and encouragement that made this PhD possible from beginning to end. I never thought I could get this far when I left home 14 years ago. Grace, thank you for your love, patience and understanding. You have been a source of unwavering support and motivation during these years of change and growth.

Thank you everyone. I have learned and grown so much because of you!

1 Background and scope of thesis

1.1 Conventional cancer therapies

For decades, surgery, radiotherapy and chemotherapy remained the frontline and only effective ways to fight against cancer. However, surgical resection is invasive and limited to localized tumors, while systemic treatment with radiotherapy and cytotoxic chemotherapy are hindered by a low maximum tolerated dose (MTD) and narrow therapeutic index due to their severe side effects [1, 2]. Increased understanding of cancer pathogenesis at a molecular basis allowed the emergence of targeted therapy which focuses on oncogenic mechanisms or biomarkers essential for tumor survival and progression [3]. The invention of the first targeted drug Imatinib (Gleevec), a tyrosine kinase inhibitor, induced complete cytogenetic responses in over 70% of chronic meylogenous leukaemia patients [4, 5]. This spurred the development and subsequent FDA approval of 21 small molecule inhibitors and monoclonal antibodies targeting various oncogenic pathways or oncoproteins (EGFR, CD33 and Her2/neu, etc.) and the list is still increasing [6]. However, most of these drugs are only effective in a small fraction of patients and even among the responding patients, tumor regressions are short-lived due to mutations in tumors and acquired resistance to the drugs (**Figure 1-1**) [3, 6-8].

1.2 The era of cancer immunotherapy

1.2.1 Boosting endogenous immunity in the suppressive tumor microenvironment

Cancer immunotherapy takes advantage of the immune system to attack tumors. Breakthroughs in our understanding of immune cell activation and immune responses in the tumor microenvironment have changed the landscape of tumor treatment dramatically. The proposed "elimination, equilibrium and escape" mechanisms in cancer immunoediting provided insight into development of new drugs focusing on restoring endogenous immune responses against tumors in the host [9]. Strategies employed by tumors to avoid T-cell responses include impairing antigen presentation, activating negative costimulatory signaling pathway and secretion of immunosuppressive factors, etc. (**Figure 1-2**) [10].

Abnormal antigen presentation involves suppressing dendritic cells function so that T-cells are tolerized instead of primed [11] or mutation to minimize recognition by cytotoxic T-cells (CTLs) [12]. The first FDA-approved cancer therapeutic vaccine, Sipuleucel-T (Provenge), utilized *ex vivo*-activated peripheral blood mononuclear cells to generate activated T-cells specific for prostate cancer in host. Despite its high cost at $104,536 per patient per therapy cycle, it only offered a 4 month of survival benefit and needs to be much more potent to be cost-effective [13-15].

Cytotoxic T-lymphocyte antigen 4 (CTLA-4) is a key negative regulator on T-cells and CTLA4 ligation efficiently inhibits T-cell activation to avoid potential autoimmune responses. However, tumors hijack CTLA-4 inhibitory signaling pathways to evade T-cell responses. Monoclonal antibody anti-CTLA4 (ipilimumab) which blocks the inhibition on T-cells from tumor, doubled the long term survival rate of metastatic melanoma patients [16, 17]. In a related manner, blockade of another immune checkpoint PD-1/PD-L1 interaction by

anti-PD-1 (nivolumab) has also recently been approved by FDA. In addition, a whole array of T-cell immunomodulators including 1) antagonistic antibodies targeting inhibitory receptors including TIM-3 and LAG-3; 2) agonistic antibodies binding activating receptors such as CD137 (41BB) and CD28 are under pre-clinical or clinical trials [16]. Due to the multiplicity and redundancy of tumor suppression mechanisms, combinations of antibodies targeting several pathways in parallel has been pursued to increase response rate.

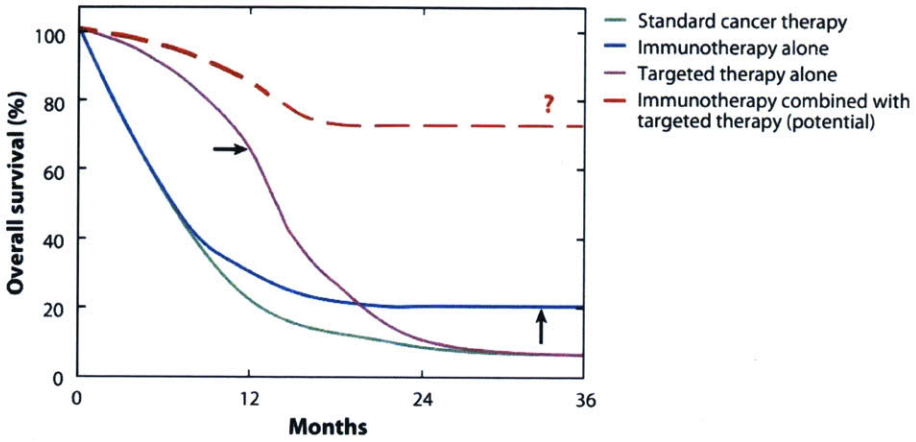

Figure 1-1: Comparison of therapeutic efficacies between different cancer therapies. Reproduced from Maus, *et al.* [18].

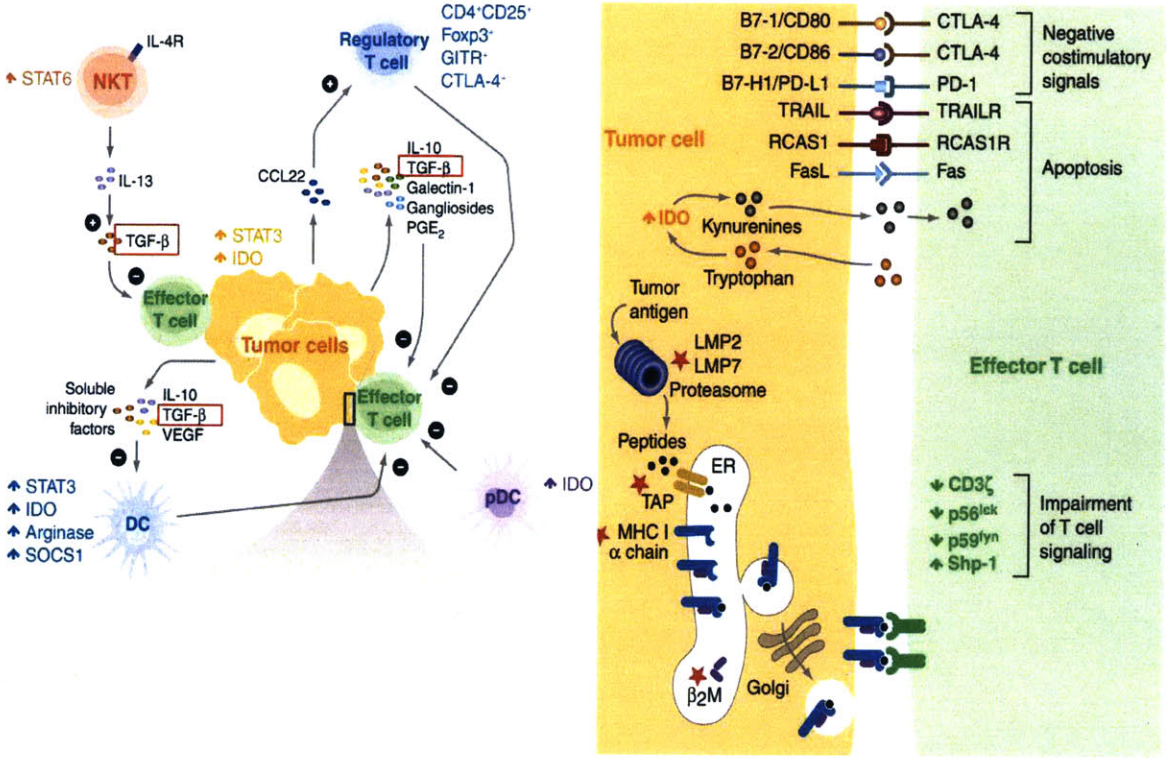

Figure 1-2: Immunosuppressive strategies and immunological checkpoints exploited by tumors to evade the immune response. Adapted from Rabinovich, *et al.* [10].

Cytokines including IFN-γ, IL-2, GM-CSF, IL-15, IL-18 and IL-21 have also been rigorously studied to boost endogenous T-cell activation and proliferation. Among them, IL-2 and IFN-γ have received FDA approval. Generally, their response rate when used alone is mediocre as their maximum tolerated dose is limited by severe systemic toxicities [16, 19]. For example, IL-2 is notorious for causing capillary leak syndrome, fever, cholestasis, diarrhea, pulmonary edema, and cardiac arrhythmias, etc. [20, 21]. Despite much less toxicity in preclinical mouse models, the first clinical trial of IL-15 in humans also reached the conclusion that IL-15 elicited serious toxicities in humans due to induction of a cytokine storm [22].

Signal transducer and activator of transcription 3 (STAT3) is actively expressed in tumor cells, myeloid cells and immune cells in the tumor microenvironment to increase secretion of immunosuppressive factors and inhibits production of Th1 cytokines that are essential for anti-tumor responses [23]. Transforming growth factor (TGF)-β and IL-10 are the two major immunosuppressive factors secreted. IL-10 attenuates DC function and downregulates TAP1 and TAP2 to protect tumor cells from cytotoxicity inflicted by CTLs [10, 24]. High levels of TGF-β in serum were found correlated to poor prognosis in prostate, gastric and bladder carcinoma [25]. TGF-β suppresses activation, differentiation and proliferation of cytotoxic T-cells (CTLs) and decreases CTLs' cytotoxicity by inhibiting production of IFN-γ, perforin, Granzyme A and B as well as FasL [26-29]. Providing soluble TGF- β receptor which neutralizes TGF-β suppressed pancreatic tumor growth in mice [30]. Furthermore, transgenic mice with expression of dominant-negative TGF-β type II receptor specifically in $CD4^+$ and $CD8^+$ T-cells rejected B16F10 and EL4 tumors [31]. Adoptive transfer of tumor specific $CD8^+$ T-cells with non-functional TGF-β receptor also eradicated prostate cancer in mice [32]. Thus, TGF-β synthesis, TGF-β interaction with its receptor and TGF-β downstream signaling transduction might provide perfect targets for restoring immune cells responses to tumors.

Overall, despite evidence that immunotherapy involving endogenous immunity can induce therapeutic benefit in cancer patients where conventional therapies have failed and significantly increase durable and complete responses, it takes time to translate immune response into survival benefits which late stage cancer patients cannot afford and the overall efficacy remains modest as only a small fraction of patients respond to the current therapies (**Figure 1-1**) [14, 18]. Thus, more rapid and robust anti-tumor T-cell responses are required to further improve the therapeutic efficacy of cancer immunotherapy.

1.2.2 Adoptive T-cell therapy

Instead of bolstering a patient's endogenous immunity, adoptive T-cell therapy (ACT) bypasses the normal process of T-cell priming to generate abundant activated tumor-specific T-cells, thus inducing an immediate and robust immune reaction against cancer [14, 33]. In the most common approach for ACT, autologous or allogeneic tumor-specific lymphocytes are selected from patient tumor biopsies, activated and expanded *ex vivo* before infusing back into patients [34]. When high avidity tumor infiltrating lymphocytes (TILs) are difficult to be found or cultured, peripheral lymphocytes can be genetically engineered to express T-cell receptors (TCRs) or chimeric antigen receptors (CARs) targeting a variety of tumor antigens

before adoptive transfer (**Figure 1-3**) [18, 35]. In phase I clinical trials, ACT has mediated up to 70% objective response rates and 22% durable complete response in patients with advanced metastatic melanoma [14, 36-38] and up to 90% sustained complete remission in chronic lymphoblastic leukemia [39, 40]. Adoptive T-cell therapy also induced promising objective responses in cervical cancer and synovial cell sarcoma patients (**Table 1-1**) [41-43].

Despite the promising results in early clinical findings, poor *in vivo* functional persistence has been one of the major limiting factors hindering the overall efficacy of adoptive T-cell therapy. The objective response rate in this therapy is not yet 100%, and the highly immunosuppressive environment generated both locally within tumors and systemically in lymphoid organs remains a major challenge to successful ACT treatment[34]. Although ACT T-cells are activated and primed *ex vivo*, they are usually quickly subjected to immunosuppression either in the lymphoid organs or tumor microenvironment just like endogenous T-cells [44]. Usually ACT T-cells become non-functional or die off before complete tumor eradication. Thus, to ensure sufficient time for T-cell killing activity, a variety of strategies are being explored to augment the function and survival of transferred T-cells (**Table 1-2**), including lymphodepletion before adoptive transfer [36, 43, 45, 46], manipulation of lymphocyte differentiation state during *ex vivo* expansion [47-49], combination treatments where patients receive adjuvant drug therapies designed to support ACT T-cells [36, 46, 47, 50] and genetic modification of T-cells to express supporting costimulatory or cytokine genes [51-55].

However, systemic exposure to adjuvant drugs or cytokine antagonists such as IL-2, IL-15 and TGF-β receptor I inhibitor might cause serious side effects as mentioned in previous section. Even when cytokines were injected subcutaneously or intratumorally, detection of administered cytokine in peripheral organs was within minutes in murine models and high circulating level of cytokines was observed within hours in humans [56, 57]. Difficulties in temporal and spatial control of expression of costimulatory or cytokine genes in genetically modified T-cells also pose safety issues [55]. Thus, complimentary solutions to specifically deliver potent adjuvants or immunomodulators to transferred T-cells to boost their function and proliferation while not inflicting systemic toxicities are in urgent need.

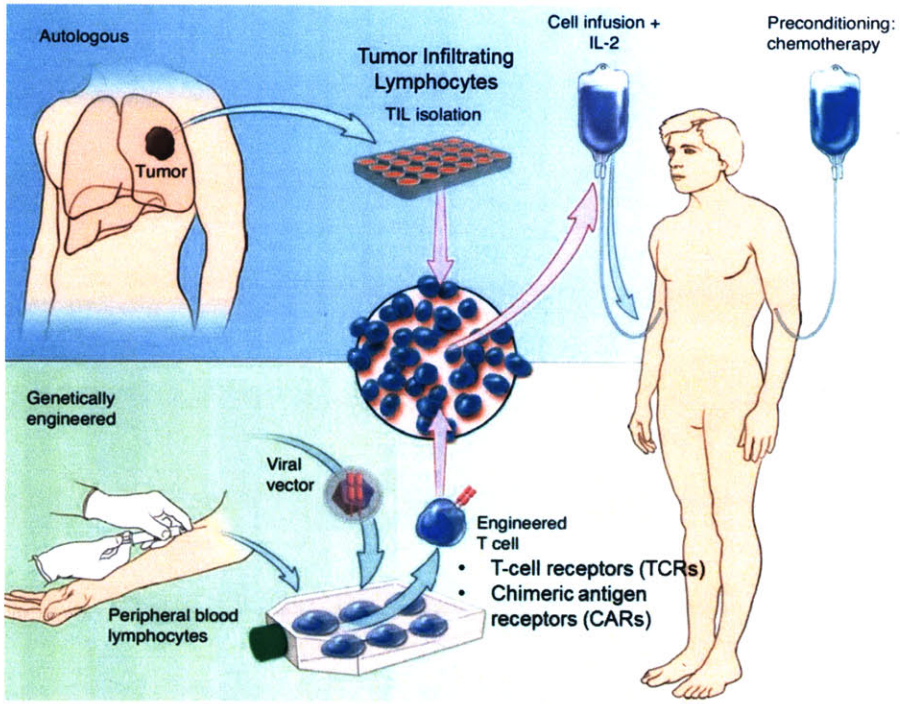

Figure 1-3: Flow chart of adoptive T-cell therapy. Reproduced from Park, *et al.* **[35].**

CELLS USED FOR ACT	YEAR	CANCER HISTOLOGY	MOLECULAR TARGET	PATIENTS	NUMBER OF ORS	COMMENTS
Tumor-infiltrating lymphocytes*	1998	Melanoma (*12*)		20	55%	Original use TIL ACT
	1994	Melanoma (*88*)		86	34%	
	2002	Melanoma (*13*)		13	46%	Lymphodepletion before cell transfer
	2011	Melanoma (*17*)		93	56%	20% CR beyond 5 years
	2012	Melanoma (*19*)		31	48%	
	2012	Melanoma (*18*)		13	38%	Intention to treat: 26% OR rate
	2013	Melanoma (*20*)		57	40%	Intention to treat: 29% OR rate
	2014	Cervical cancer (*89*)		9	33%	Probably targeting HPV antigens
	2014	Bile duct (*44*)	Mutated ERB2	1	–	Selected to target a somatic mutation
In vitro sensitization	2008	Melanoma (*90*)	NY-ESO-1	9	33%	Clones reactive against cancer-testes antigens
	2014	Leukemia (*91*)	WT-1	11	–	Many treated at high risk for relapse
Genetically engineered with CARs	2010	Lymphoma (*16*)	CD19	1	100%	First use of anti-CD19 CAR
	2011	CLL (*68*)	CD19	3	100%	Lentivirus used for transduction
	2013	ALL (*70*)	CD19	5	100%	Four of five then underwent allo-HSCT
	2014	ALL (*92*)	CD19	30	90%	CR in 90%
	2014	Lymphoma (*71*)	CD19	15	80%	Four of seven CR in DLBCL
	2014	ALL (*93*)	CD19	16	88%	Many moved to allo-HSCT
	2014	ALL (*94*)	CD19	21	67%	Dose-escalation study
	2011	Neuroblastoma (*78*)	GD2	11	27%	CR2 CARs into EBV-reactive cells
Genetically engineered with TCRs	2011	Synovial sarcoma (*81*)	NY-ESO-1	6	67%	First report targeting nonmelanoma solid tumor
	2006	Melanoma (*15, 32*)	MART-1	11	45%	

Table 1-1: Selected clinical trials of adoptive T-cell therapy for the treatment of human cancer. CLL: chronic lymphocytic leukemia; ALL, acute lymphocytic leukemia; CR: complete

response; HPC, human papillomavirus; allo-HSCT, allogeneic hematopoietic stem cell transplantation; DLBCL, diffuse large B cell lymphoma; EBV, Epstein-Barr virus. Reproduced from Rosenberg, *et al.* [43].

Adjuvants to promote maintenance of Th1 cell function, e.g., endotoxin administration to humans
Antibody infusions to prevent CTLA-4 inhibitory effects
Antibody infusions to block PD-L1–PD-1 interactions and rejuvenate exhausted T cells
Antibody infusions to enhance 4-1BB signals
Bispecific antibodies to "arm" T cells to facilitate trafficking and cytotoxicity
Cytokine administration, for example, IL-2, IL-7, IL-12, IL-15, or IL-21
Cytokine antagonists, e.g., TGF-β blockade or inhibition
$CD4^+$ Th cell infusion to sustain CTL function
Host lymphodepletion
Host Treg depletion or inhibition
Nonmyeloablative stem cell transplantation to facilitate allogeneic T cell transfers
Tumor bed manipulation via several approaches
Chemotherapy
Chemokine expression in tumor bed to promote lymphocyte trafficking
Cryoablation
Phosphodiesterase-5 inhibition
Tumor stroma and microvasculature: sensitization to induce T cell trafficking and cytotoxicity
Vaccine therapy

Table 1-2: Strategies to augment adoptive T cell therapy. Reproduced from June, *et al.* [58].

1.3 Micro-/Nano-particles for enhancing anti-tumor immunity

The efficacy of potent adjuvant drugs such as cytokines, antibody antagonists and small molecule inhibitors are limited by their maximum tolerated doses due to systemic toxicities. Micro-/nano-particles can circumvent this problem by creating artificial compartments *in vivo* and increasing local drug concentrations by targeted delivery. Application of micro-/nano-particles in cancer immunotherapy might give potent drugs with small therapeutic index a second chance in the war against cancer.

1.3.1 Endogenous immunity

Particles were designed to deploy immunomodulatory drugs and antigens in the systemic lymphoid or artificial compartments to induce anti-tumor immunity [59]. Tumor peptide antigen and adjuvant CpG-DNA cargo were linked to a lipophilic albumin binding tail to form amphiphiles which can hijack albumin for lymph node targeting. Subcutaneous injection of amphiphiles marked 30-fold increase in cytotoxic T-cell priming and significant regression of B16F10 solid tumor without systemic toxicity [60]. Mesoporous silica rods, which can self-assemble into macroporous structure to create a 3D microenvironment, recruited dendritic cells with inflammatory signal GM-CSF loaded in the pores and mounted immune response against tumor antigen [61].

Micro- and nano- particles have also been used to deliver stimulatory cytokines, agonistic antibodies, antagonist antibodies, siRNA and small molecule inhibitors to tumors to achieve therapeutically relevant drug concentrations in the tumor microenvironment while not eliciting systemic side effects. Researchers have tried to load IL-2 in biodegradable alginate polymeric microspheres and injected intratumorally to B16F10 brain metastases and CT26 liver carcinomas to gradually release IL-2 up to three weeks without eliciting overt toxicities [62]. Polyplexes of lipid-modified polyethylenimine (PEI) and STAT3 siRNA at 50nm size were injected into tumors to shut down STAT3 expression and significantly reduced tumor size [63]. Liposomes surface decorated with agonist antibody against the costimulatory receptor CD40 as well as TLR agonist CpG oligonucleotide aimed to target DCs and macrophages in the tumor microenvironment. Systemic administration of anti-CD40 elicited serious systemic inflammation and hindered its clinical application [64]. Unlike their soluble counterparts, anti-CD40 and CpG anchored to liposomes were sequestered within tumors and tumor-draining lymph nodes, minimizing the hepatic toxicity and systemic inflammatory effects [65]. The same strategy was applied to deliver IL-2 and anti-CD137, an agonistic antibody against co-stimulatory receptor CD137. This approach not only eliminated B16F10 tumor burden, but also elicited systemic immunity against distant metastases without lethal systemic toxicity which the equivalent dose of drugs had [66]. Furthermore, liposomes encapsulating biodegradable polymer hydrogel have been used to co-localize IL-2 and a small molecule TGF-β receptor I inhibitor to successfully treat B16F10 lung metastasis and subcutaneous solid tumor [67]. Intratumoral localization of micro/nanoparticles might provide a direct and potent stimulation to immune cells in the tumor microenvironment. However, it might be difficult to treat inopenable tumors or metastases.

1.3.2 Supporting adoptively transfer T-cells

Synthetic drug delivery particles have also been designed to better activate T-cells *in vitro* for adoptive transfer. For example, bundles of carbon nanotubes were employed as a platform to display MHC-I, anti-CD28 and PLGA nanoparticles encapsulating IL-2. These carbon nanotube-polymer composites served as artificial antigen presenting cells to activate and expand T-cells with 1,000-fold less soluble IL-2 required for normal activation but with enhanced anti-tumor cytotoxicity [68]. Similarly, iron dextran particles improved activation of T-cells by clustering T cell receptors (TCR) in the presence of a magnetic field. Not only were a larger number of T-cells generated, these T-cells also had significantly increased therapeutic efficacy in the B16F10 tumor model [69].

Approaches have also been taken to boost transferred T-cells' activity *in vivo*. Microparticles encapsulating IL-15 superagonist and surface decorated with anti-CD3, anti-CD28 and anti-CD137 were loaded into alginate polymer scaffolds together with adoptively transferred T cells. The scaffolds were then implanted next to the tumor site to enhance T-cell proliferation and dispersion in mouse 4T1 breast tumors [70].

In addition, strategies using T-cells themselves as delivery vehicles of supporting drugs to the tumor microenvironment have recently been reported. The efficacy of ACT can be dramatically enhanced by conjugation of cytokine- or drug-loaded nanoparticles (NPs) to the surfaces of T-cells *ex vivo* prior to transfer into tumor-bearing recipients [71, 72], creating T-cell "pharmacytes". Encapsulated cytokines or small molecule immunosuppression inhibitors

were gradually released from T-cell bound nanoparticles and provided pseudo-autocrine stimulation of transferred cells. This approach increased the effective potency of adjuvant drugs while simultaneously minimizing systemic exposure to these potent supporting signals. This strategy allowed delivery of interleukin cytokines that dramatically enhanced the efficacy of ACT T-cells in a metastatic melanoma model [71] and the delivery of immunosuppression-blocking drugs that enhanced expansion of T-cells within large established tumors in a prostate cancer model [72]. However, the method is limited by one-time nature of intervention as once the drugs are all released out, ACT T-cells will be subjected to immunosuppression again. In addition, the duration of stimulation is inherently limited by expansion of the cell population *in vivo*, since cell-bound particles are diluted with each cell division. Thus, a strategy to target supporting drugs to T-cells with nanoparticle drug carriers directly *in vivo* would enable transferred lymphocytes to be repeatedly boosted with supporting adjuvant drugs over a prolonged duration, which might be necessary for elimination of large tumor burdens.

However, targeting transferred T-cells residing in tumors via systemic administration is proven difficult. Although various reports have claimed targeted delivery of drugs to tumor microenvironment or intratumoral T_{regs} [73-76], a closer look revealed that "targeted" nanoparticles enter the tumor via the enhanced permeability and retention (EPR) effect, and increased efficacy of such treatments is generally due to improved internalization once the particles accumulate in the site due to tumor/T-cell targeting ligands [77, 78].

1.4 Scope and outline of thesis

In this thesis, we designed nanoparticles as delivery agents for cytokines and immunosuppression-reverting drugs to provide specific and long-lasting support for adoptively transferred T-cells *in vivo*. Poor *in vivo* persistence due to immunosuppression has been a major limiting factor for adoptive T-cell therapy. To tackle this problem, we tried a two-pronged approach by 1) repeatedly re-loading supporting drugs to T-cells and 2) extending the initial functional duration of drugs carriers conjugated to T-cells surface before adoptive transfer. Firstly, we developed an active-targeting liposome system which can bind to adoptive transferred T-cells specifically *in vivo* to allow reloading of drugs on T-cells. Secondly, we identified non-internalizing receptors to serve as anchors to prolong the life-span of initial cytokine carriers conjugated to T-cell surface. In the end, we target-delivered an immunosuppression-reverting drug to adoptively transferred T-cells *in vivo* to evaluate the functional impact of targeting liposome system.

Chapter 2 describes a novel strategy to repeatedly stimulate ACT T-cells, using cytokines or ACT-cell-specific antibodies as ligands to target PEGylated liposomes to transferred T-cells *in vivo*. After synthesis and characterization of the targeting liposomes, we demonstrated their targeting efficiencies to transferred T-cells *in vitro* and *in vivo*. We also used cytokine-targeted liposomes to repeatedly boost transferred T-cells in animals bearing lung metastasis as a proof-of-concept and evaluated their therapeutic efficacies in solid subcutaneous tumor model.

Chapter 3 was done in collaboration with Dr. Li Tang, who designed a novel carrier-free cytokine nanogel system in our laboratory. In this chapter, we used our targeting liposomes platform to identify CD45 as a non-internalizing receptor on T-cells that could be used as anchor to block internalization of cell-conjugated nanoparticles. Anti-CD45 decorated nanogels were then tested for internalization kinetics. We explored the effects of prolonged surface anchoring of human IL-15 superagonists (hIL-15Sa) nanogels on T-cell signaling, proliferation and therapeutic efficacy both *in vitro* and in tumor bearing mice. Furthermore, we compared the immunotoxicity of surface anchored IL-15Sa nanogels with that of systemic IL-15Sa.

In Chapter 4, we describe the use of targeting liposomes developed in previous chapters to specifically deliver an immunosuppression-reverting drug SB525334, a potent inhibitor of TGF- β receptor I (ALK5), to adoptively transferred T-cells. We explored different methods to encapsulate the drug in liposomes and optimized the formulations. We also evaluated the efficacy of liposome-encapsulated SB525334 on inhibiting the TGF-β signaling pathway and maintaining T-cell proliferation and cytotoxicity *in vitro*. As a proof of concept, we armed transferred T-cells with drug-loaded targeting liposomes in tumor bearing mice. We also compared the efficacy of different targeting liposomes in delivering SB525334 to provide insights into selecting and designing targeting nanoparticles depending on the drug choice.

Chapter 5 provides an overall summary and the broad conclusions of this thesis work as well as possible future directions. Appendix details several protocols developed for this work, as well as supplemental data. A list of bibliography of the literature cited is in the end of the thesis.

2 *In vivo* arming of adoptively transferred T-cells with targeting liposomes

The majority of this work has been published in a first author publication, *Journal of Controlled Release (2013);172(2):426-435* [79].

2.1 Introduction

Immunotherapy treatments stimulating a patient's own immune system to attack tumors are beginning to show signs of clinical efficacy, demonstrating that the immune system can be harnessed for cancer therapy even in patients with advanced disease [16, 39, 80]. Among many immunotherapy strategies in development, adoptive cell therapy (ACT) with autologous tumor-specific T-cells has shown particularly striking results in recent phase I clinical trials [36, 39]. In this approach, autologous T-cells isolated from tumor biopsies or peripheral blood are treated with cytokine/stimulatory cocktails to promote expansion of large numbers of tumor-reactive cells that can be reinfused into the patient, following which the transferred cells can home to disseminated tumor sites and destroy metastatic tumors. ACT therapy using completely autologous patient-derived tumor-infiltrating lymphocytes [36, 37] or patient T-cells transduced with genetically engineered T-cell receptors [38, 39] (TCRs, either exogenous TCR chains or chimeric antigen receptors comprised of synthetic antigen-binding Ig domains fused with TCR signaling components) have been demonstrated to elicit objective response rates in up to 70% of patients with advanced metastatic melanoma [14, 36-38] and dramatic cures in chronic lymphoblastic leukemia [39, 40].

Despite these promising early clinical findings, efforts to increase the fraction of patients showing complete responses (complete and durable elimination of all detectable tumors) in solid tumors are needed. To this end, a variety of strategies are being explored, including manipulation of lymphocyte differentiation state during *ex vivo* expansion [47-49], combination treatments where patients receive adjuvant drug therapies designed to support ACT T-cells [36, 47, 50], and genetic modification of T-cells to express supporting costimulatory or cytokine genes [51-53]. We recently demonstrated that the efficacy of ACT can be dramatically enhanced by conjugation of cytokine- or drug-loaded nanoparticles (NPs) to the surfaces of T-cells *ex vivo* prior to transfer into tumor-bearing recipients [71, 72], creating T-cell "pharmacytes". T-cell-bound particles provided pseudo-autocrine drug delivery to the transferred cells that greatly increased the effective potency of adjuvant drugs while simultaneously minimizing systemic exposure to these potent supporting signals. This approach allowed autocrine delivery of interleukin cytokines that dramatically enhanced the efficacy of ACT T-cells in a metastatic melanoma model [71] and the delivery of immunosuppression-blocking drugs that enhanced expansion of T-cells within large established tumors in a prostate cancer model [72].

A limitation of the pharmacyte approach is the one-time nature of the intervention: ACT T-cells can only be loaded once with a cargo of adjuvant drug prior to transfer, and the

duration of stimulation is inherently limited by expansion of the cell population *in vivo*, since cell-bound particles are diluted with each cell division. We hypothesized that a strategy to target supporting drugs to T-cells with nanoparticle drug carriers directly *in vivo* would enable transferred lymphocytes to be repeatedly stimulated with supporting adjuvant drugs, and thereby provide continuous supporting signals over the prolonged durations that might be necessary for elimination of large tumor burdens. Such "Re-arming" of T-cells with supporting drugs could be achieved by repeated administration of targeted particles, allowing adoptively-transferred T-cells to be restimulated multiple times directly *in vivo*, while the use of internalizing targeting ligands would minimize the likelihood of immune responses against the nanoparticle carrier. To our knowledge, only two prior studies have attempted to target nanoparticles to T-cells *in vivo* [81, 82]. In both of these studies, particles were targeted to T-cells via peptide-MHC ligands that bind to specific T-cell receptors. However, peptide-MHC-functionalized nanoparticles have recently been shown to deliver an anergizing/tolerizing signal to T-cells [82, 83]– which is ideal for treating graft rejection or autoimmunity, but runs counter to the goals of cancer immunotherapy.

Here we report on initial results illustrating the feasibility of specifically targeting ACT T-cells *in vivo* using stimulatory or non-stimulatory immunoliposomes. We synthesized and characterized PEGylated liposomes conjugated with 2 types of targeting molecules: (1) antibodies against unique cell surface antigens expressed only by the ACT T-cells (here, we employ the congenic marker Thy1.1), mimicking unique surface markers introduced clinically in genetically-engineered ACT T-cells [84, 85]; and (2) recombinant interleukin-2 (IL-2), a cytokine that binds the trimeric IL-2 receptor (IL-2R) expressed by activated T lymphocytes [86]. These two ligands provide contrasting targeting strategies; anti-Thy1.1 provides highly specific targeting without overt stimulation of target cells, while IL-2 provides potentially less specific targeting (IL-2R can be expressed by some endogenous T-cells) but also delivers a direct stimulatory signal to T-cells. We characterized the efficacy of targeting particles to anti-tumor T-cells *in vitro* and internalization of liposomes triggered by these ligands, and then analyzed targeting of ACT T-cells *in vivo* in healthy animals and in a model of metastatic melanoma. Targeted liposomes labeled T-cells in multiple systemic compartments *in vivo*, with anti-Thy1.1 liposomes binding to >90% of transferred cells following a single injection. We also showed that dual-targeting liposomes, empowered by both IL-2 and anti-Thy1.1 could overcome some of the limitations IL-2-liposomes have. Further, we demonstrate the proof of concept that targeted stimulatory IL-2-liposomes can drive repeated expansion of ACT T-cells *in vivo*, following multiple periodic injections of targeted vesicles. In a therapy in murine tumor model, IL-2-liposomes suppressed tumor growth and prolonged survival of tumor bearing mice. We believe this strategy could provide a safe means to amplify the efficacy of ACT while avoiding systemic toxicity associated with many adjuvant drug treatments, and would be translatable to other immunotherapy settings, such as enhancement of cancer vaccines and therapeutic interventions in infectious diseases such as HIV.

2.2 Materials and methods

2.2.1 Materials

All lipids and polycarbonate membranes (0.2 μm) for size extrusion were from Avanti Polar Lipids (Alabaster, AL) and used as received. DiD, ACK lysis buffer, Calcium Phosphate Transfection Kit, HEK293 Free Style Cells, Max Efficiency ® DH5α™ Competent cells and Phoenix eco viral packaging cells were obtained from Invitrogen Life Technologies (Grand Island, NY). Anti-Thy1.1 (clone 19E12) and mouse IgG_{2a} isotype control antibodies were purchased from BioXCell (West Lebanon, NH). Dithiothreitol (DTT), Fluorescein isothiocyanate (FITC) isomer I, Concanavalin A Type VI (ConA), and Triton X-100 were from Sigma-Aldrich (St. Louis, MO) and used as received. Recombinant IL-2 and IL-7 were purchased from PeproTech (Rocky Hill, NJ). Anti-mouse CD16/32, anti-CD25, anti-CD25-Alexa 488, anti-CD8-PE, anti-Thy1.1-Percp-Cy5.5 and anti-Thy1.1-FITC were from eBiosceince (San Diego, CA). Protein A agarose column and Amicon Ultra-15 30kDa MWCO Centrifugal Filter Units were from Millipore (Billerica, MA). Polyethylenimine (PEI) was from Polysciences (Warrington, PA). $F(ab')_2$ Preparation Kits, BCA Protein Assay Kits, and 7k MWCO Zeba spin desalting columns were from Pierce Thermo Scientific (Rockford, IL). IL-2 ELISA Kits were obtained from R&D Systems (Minneapolis, MN). Ficoll-Pague Plus was from GE Health Care (Waukesha, WI). EasySep™ Mouse $CD8^+$ T Cell Enrichment Kit was from Stemcell (Vancouver, BC, Canada). Collagenase II and Hank's Balanced Salt Solution were purchased from (Gibco-Invitrogen, Carlsbad, CA). EndoFree Plasmid Maxi Kit was from Qiagen (Valencia, CA). Retronectin Recombinant Human Fibronectin Fragment was from Clontech (Mountain View, CA). D-Luciferin was from Caliper Life Sciences (Hopkinton, MA). B16F10 melanoma cells were from American Type Culture Collection (Manassas, VA). IL-2-Fc was a generous gift from Dane Wittrup's lab at MIT.

2.2.2 Preparation of targeting ligands IL2-Fc and antibody F(ab)2

IL-2-Fc is a bivalent fusion protein of the C-terminus of murine wild type IL-2 linked to a mouse IgG_{2a} backbone [66]. A D265A mutation was introduced in the IgG_{2a} Fc region to minimize interaction of IL-2-Fc with Fc receptors [87]. IL-2-Fc gene was transformed into DH5α cells via heat shock and extracted after clone expansion using an EndoFree Plasmid Maxi Kit following the manufacturer's instructions. HEK293 Freestyle cells were transfected with IL-2-Fc gene/Polyethylenimine (PEI) complexes and grown in roller bottles at 37 °C for a week before harvest. Cells were spun down and secreted IL-2-Fc in the supernatant was purified by gravity flow/elution through Protein A agarose columns and concentrated by using centrifugal filter units (Amicon Ultra-15 30kDa MWCO). Monoclonal antibodies (Abs) against Thy1.1 were digested with pepsin to generate the $F(ab')_2$ using a $F(ab')_2$ Preparation Kit following the manufacturer's instructions. IL-2-Fc and anti-Thy1.1 $F(ab')_2$ concentrations were determined by the BCA Protein Assay Kit. IL-2-Fc bioactivity concentration relative to wild type murine IL-2 was quantified by an IL-2 ELISA Kit.

2.2.3 Synthesis of liposomes

Vacuum dried lipid films composed of 1,2-distearoyl-*sn*-glycero-3-phosphoethanolamine-N-[maleimide(polyethylene glycol)-2000 (maleimide-PEG_{2000}-DSPE)/

cholesterol /hydrogenated Soy L-α-phosphatidylcholine (HSPC) in a molar ratio of 2.5/27.5/69 together with 1% of a fluorescent lipophilic tracer dye 1,1'-Dioctadecyl-3,3,3',3'-Tetramethylindodicarbocyanine, 4-Chlorobenzenesulfonate Salt (DiD) were rehydrated in 250 µl of 50 mM HEPES/150 mM NaCl-buffer (pH6.5). Lipids were vortexed every 10 min for 1 hr at 62°C to form vesicles and size extruded through a polycarbonate membrane (0.2 µm). After washing in excess phosphate buffered saline (PBS) pH7.4 and spinning down by ultracentrifugation at 110,000xg for 4 hr, liposomes were re-suspended in 100 µl PBS per 1.4 mg of lipids.

2.2.4 Coupling of ligands to liposome surface

IL-2-Fc and anti-Thy1.1 $F(ab')_2$ were coupled to liposomes as previously described [66]. Briefly, Ab, cytokine and mixtures of antibodies/cytokine at different molar ratio (2-5 mg/ml) were treated with 1.8 mM DTT in the presence of 10 mM EDTA at 25°C for 20 min to expose hinge region free thiols. DTT was subsequently removed by using Zeba desalting columns before mixing with maleimide-bearing liposomes (1 mg protein/1 mg lipid) in PBS pH 7.4. After incubation for 18 hr at 25°C on a rotator, excess protein was removed by ultracentrifugation in excess PBS. Liposome sizes were characterized before/after coupling by dynamic light scattering (90Plus Particle Size Analyzer, Brookhaven, Holtsville, NY).

2.2.5 Quantification of ligands coupled to liposomes

Anti-Thy1.1-FITC or anti-CD45-FITC was concentrated to 3-5 mg/ml using Ultra-15 Centrifugal Filters before coupling to liposomes as previously described. After liposomes were solubilized in 2% Triton X-100 at 37°C for 5 min with gentle vortexing, FITC fluorescence was measured at ex/em wavelengths of 490/520nm using a fluorescence plate reader (Tecan Systems, San Jose, CA) and converted to protein concentrations using standard curves prepared from serial dilutions of neat anti-Thy1.1-FITC or anti-CD45-FITC stock solutions. IL-2-Fc-Lips were solubilized in the same manner and the amount of IL-2 coupled was determined using an IL-2 ELISA Kit (R&D Systems, Minneapolis, MN) following the manufacturer's instructions.

2.2.6 Activation of Pmel-1 Thy1.1$^+$ CD8$^+$ T cells

Animals were cared for in the USDA-inspected MIT Animal Facility under federal, state, local and NIH guidelines for animal care. Spleens from pmel-1 Thy1.1$^+$ mice were ground through a 70 µm cell strainer and red blood cells were removed by incubating with ACK lysis buffer (2 ml per spleen) for 5 min at 25°C. After 1 wash in PBS, the remaining cells were cultured at 37°C in RPMI 1640 medium containing 10% fetal calf serum (FCS). ConA at a final concentration of 2 µg/ml and IL-7 at 1 ng/ml were added to activate and expand splenocytes. After two days, dead cells were removed by Ficoll-Pague Plus gradient separation and CD8$^+$ T-cells were isolated via magnetic negative selection using an EasySep™ Mouse CD8$^+$ T Cell Enrichment Kit. Purified CD8$^+$ T-cells were re-suspended at 1.5×10^6 per ml RPMI containing 10 ng/ml recombinant murine IL-2. After 24 hr, cells were washed 3 times in PBS and re-suspended in 100×10^6 per ml for adoptive transfer.

For bioluminescence imaging experiments, Click Beetle Red luciferase (CBR-luc) [72] was introduced into pmel-1 T-cells (post ficoll purification and magnetic selection) by retroviral transduction. Phoenix eco viral packaging cells were seeded at $4x10^6$ cells per 10 cm tissue culture dish in 10ml DMEM medium containing 10% FCS. After incubation

overnight at 37°C, phoenix cells were exchanged with 10ml fresh DMEM with 10% FCS, transfected with CBR-luc plasmid and phoenix eco plasmid using a Calcium Phosphate Transfection Kit and cultured at 32°C for 24 hr. DMEM was then replaced with 6 ml RPMI containing 10% FCS and transfected phoenix eco cells were incubated for another 24 hr. Supernatant containing the retrovirus-packaged CBR-luc gene was collected and replaced with fresh RPMI for another 24 hr incubation. Supernatant was collected again and combined with that collected 24 hr earlier, and sterile filtered (0.45 μm). Six-well non-tissue culture plates (BD Falcon) were coated with 1 ml RetroNectin (15 μg/ml) 18 hr at 4°C, then excess RetroNectin was aspirated. Pmel-1 T-cells post ficoll purification and magnetic selection were suspended in filtered viral sups (RPMI collected previously) with 10 ng/ml IL-2 at $1.8x10^6$/ml, 3 ml was added to each RetroNection-coated well, and spinoculation was conducted by centrifuging at 2000x g for 1 hr at 25°C. Transduced T-cells were then incubated at 37°C. Six hours later, 1 ml of fresh RPMI was added with 10 ng/ml IL-2. Transduced, activated pmel-1 T-cells were used 1 day later for adoptive transfer studies.

2.2.7 In vitro liposome binding to T cells

DiD-labeled protein-conjugated liposomes (0.7 mg lipids in 100 μl) were incubated with 15×10^6 activated pmel-1 Thy1.1$^+$ T-cells in 1ml complete RPMI supplemented with 10% FCS for 30 min at 37°C with gentle agitation every 10 min. In competitive conjugation assays, 100-fold molar excess soluble IL-2-Fc or anti-Thy1.1 free antibody (compare to the amount coupled to liposomes) was added 30 min before targeting liposomes to saturate IL-2 or Thy1.1 receptors on the cells, respectively. For IL-2-Fc-Liposome (IL-2-Fc-Lip) competition assays, $2.5x10^6$ activated pmel-1 CD8$^+$ T-cells were mixed with $2.5x10^6$ naïve C57Bl/6 splenocytes in 100 μl complete RPMI with 10% FCS. The cell mixture was incubated with or without 0.24 mg/ml soluble IL-2-Fc, followed by incubation with 0.07 mg/ml IL-2-Fc-Lip for 30 minutes at 37°C with total volume topped up to 300 μl. For competition assays with anti-thy1.1.-Liposome (anti-Thy1.1-Lip), 0.15 mg/ml liposomes (Lip) were incubated with a mixture of $2.5\ x10^6$ activated pmel-1 T-cells and $2.5\ x10^6$ naïve C57Bl/6 splenocytes (with or without pre-blocking by 1.34 mg/ml anti-Thy1.1). Cells without any liposomes added served as a control for cellular autofluorescence and cells conjugated with 0.15 mg/ml IgG_{2a}-Liposomes (IgG_{2a}-Lip) were used to test non-specific binding of non-targeting liposomes.

For dual targeting liposome binding, 0.05 mg/ml Lip with different mole fraction of IL-2-Fc/anti-Thy1.1 or anti-CD45/anti-Thy1.1 on the surface were incubated with a mixture of $2.5\ x10^6$ activated C57Bl/6 CD8$^+$ T-cells and CFSE labeled $2.5\ x10^6$ activated pmel-1 T-cells in total 200 μl complete RPMI with 10% FCS for 30 minutes at 37°C. Mixture were gently agitated every 15 minutes to ensure homogenous distribution of cells and liposomes.

For all *in vitro* conjugation experiments, cells were stained with anti-CD8 and anti-Thy1.1 after two washes in ice cold PBS to remove unbound liposomes, and analyzed by flow cytometry on a BD FACS Canto except competition assays which were done on a BD LSR II.

2.2.8 Titration of liposome concentration for in vitro conjugation

Varying amounts of DiD-labeled anti-Thy1.1-Lip were added to 5×10^6 activated pmel-1 Thy1.1$^+$ T-cells in 100 μl complete RPMI with 10% FCS. The total volume for all groups was topped up with RPMI with 10% FCS to 300 μl and incubated at 37°C for 30 min. After

two washes in ice cold PBS to remove unbound liposomes, cells were resuspended in FACS buffer, surface stained with fluorescently labeled anti-CD8 and anti-Thy1.1, and analyzed by flow cytometry on a BD LSR II.

2.2.9 *In vitro* kinetics study of internalization of by using CF-DOPE

Anti-Thy1.1-Liposomes were labeled with 1% (mol) carboxyfluorescein- 1,2-dioleoyl-*sn*-glycero-3-phosphoethanolamine lipid (CF-DOPE) instead of DiD during the synthesis stage and incubated with 6×10^6 activated pmel-1 Thy1.1$^+$ T-cells per 0.7 mg of lipids for 60 min at 4°C with gentle agitation every 15 min. After two washes in ice cold PBS pH7.4 to remove unbound liposomes, T-cells were re-suspended in RPMI and aliquotted into four equal portions for 0, 2, 4 and 6 hr time points, respectively. After each incubation interval at 37°C, T-cells were washed 2x in ice cold PBS and re-suspended in 2% FCS in PBS. Cells were placed on ice to minimize further internalization and analyzed by flow cytometry on a BD LSR II. Cells were also imaged directly without fixation on a Zeiss LSM 510 laser scanning confocal microscope.

2.2.10 Adoptive transfer and in vivo liposome targeting

Albino C57BL/6 female mice 6-8 weeks of age were from the Jackson Laboratory (Bar Harbor, ME). One day before adoptive transfer, mice were sublethally lymphodepleted with 5Gy total body irradiation. 15×10^6 activated pmel-1 CD8$^+$ T-cells in 150 µl PBS were injected intravenously (i.v.) into each recipient animal. DiD-labeled immunoliposomes (1.4 mg lipids) were re-suspended in 100 µl PBS and injected i.v. immediately or three days after adoptive transfer. For *in vivo* targeting dose titration, various amount of anti-Thy1.1-Lip (1.4 mg, 0.35 mg and 0.18 mg) were injected i.v. immediately after adoptive transfer. Twenty-four hr after administration of liposomes, mice were euthanized and blood, lymph node, and spleen cells were analyzed by flow cytometry on a BD FACS Canto to assess liposome binding to T-cells.

2.2.11 Adoptive transfer of CBR-Luc T-cells and bioluminescence imaging

B16F10 melanoma cells (authenticated from American Type Culture Collection and cultured <6 months before use) were suspended at 1×10^6 cells per 200 µl in Hank's Balanced Salt Solution and injected i.v. to induce lung metastases in albino C57Bl/6 mice (Day -8). Animals were then sublethally lymphodepleted by total body irradiation (5 Gy) 7 days post tumor inoculation (Day -1). Pmel-1 CD8$^+$ T-cells transduced with CBR-Luc (12×10^6) were resuspended in 150 µl PBS and administered i.v. one day after lymphodepletion (Day 0). IL-2-Fc-Lip (1 mg of liposomes) or PBS were injected i.v. immediately after ACT and on day 6. D-Luciferin, a substrate for CBR-luc, was suspended in PBS (15 mg/ml) and 150 mg luciferin/kg body weight was injected Intraperitoneally (i.p.) in anesthetized animals 10 min before bioluminescence imaging acquisitions (5 min, 3 min, 2min and 1min) on a Xenogen IVIS Spectrum Imaging System (Caliper Life Sciences). Images were collected every two days starting from day 0 (2hrs after ACT) to day 14. Living Image software version 3.0 (Caliper Life Sciences) was used to acquire and quantitate the bioluminescence imaging data sets. To compare the stimulatory effects of soluble IL-2 and IL-2-Fc-Lip, a similar experiment was repeated with 1st/2nd dose as 0.5 mg/1 mg IL-2-Fc-Lip or 10 µg/20 µg soluble recombinant wild type mouse IL-2 (PeproTech, Rocky Hill, NJ), equivalent to the amount of IL-2 coupled on IL-2-Fc-Lip). On day 12, mice were sacrificed and T-cells from

inguinal lymph nodes were collected and surface stained for CD8 and vβ13 before analyzing by flow cytometry on a BD FACS Canto to assess the percentage of tumor-specific T-cells in each group.

2.2.12 *In vivo* therapy experiment

B16F10 melanoma cells were suspended at 0.25×10^6 cells per 100 µl in Hank's Balanced Salt Solution and inoculated subcutaneously (*s.c.*) to induce tumor in C57Bl/6 mice (Jackson Laboratory, Bar Harbor, ME) (Day 0). Animals were then sublethally lymphodepleted by total body irradiation (5 Gy) 7 days post tumor inoculation (Day 7). Activated Pmel-1 $CD8^+$ T-cells (15×10^6) were resuspended in 150 µl PBS and administered i.v. one day after lymphodepletion (Day 8). IL-2-Fc-Lip (0.35 mg of liposomes) or PBS were injected i.v. immediately after ACT, on day 12 and day 16. Tumor size was measured every two days since adoptive transfer and tumor area was calculated as the product of 2 measured orthogonal diameters (D_1xD_2). Mice with tumor area larger than 100 mm^2 were considered dead.

2.2.13 Necropsy and sample preparation for flow cytometry analysis

Inguinal lymph nodes and spleens were ground through a 70 µm cell strainer and washed once with ice cold PBS. Splenocytes were then lysed with ACK lysis buffer (2 ml per spleen) for 4 min at 25°C to remove red blood cells before washing in ice cold PBS. Blood samples were lysed with 2X 1ml ACK lysis buffer for 5 min at 25°C and then washed 1x with ice cold PBS. All cells were washed in flow cytometry buffer (PBS with 2% Fetal Calf Serum) once before surface-staining with Ab. After staining, cells were washed 2x in FACS buffer and analyzed on a BD FACS Canto Flow Cytometer. All data was processed using FlowJo software.

2.2.14 Statistical analysis

Statistical analysis was done using GraphPad Prism software and two-tailed unpaired t-tests were conducted between groups of experimental data. Graphs show the mean ± SEM of sample groups. Tumor growth curves were compared using two-way ANOVA, and Kaplan-Meier survival curves were compared by log rank test.

2.3 Results and discussion

2.3.1 Synthesis and Characterization of IL-2-Fc-Lip, anti-Thy1.1-Lip and dual-ligands liposomes

To generate cytokine- or antibody (Ab)-conjugated liposomes (IL-2-Fc-Lip or anti-Thy1.1-Lip) for T-cell targeting, PEGylated liposomes incorporating maleimide-headgroup PEG-lipids (Mal-PEG-DSPE) were prepared from high-T_m lipids and sized by membrane filtration to a mean diameter of 173±13 nm (**Schematic 2-1**, **Figure 2-1A**). Murine IL-2 fused to the C-terminus of mouse IgG_{2a} Fc or anti-Thy1.1 $F(ab')_2$ were coupled to the maleimide termini of PEG chains to serve as targeting ligands of the immunoliposomes. To minimize interaction of liposomes with phagocyte Fc receptors, a D265A mutation was introduced in the Fc portion of IL-2-Fc [87] and $F(ab')_2$ fragments of anti-Thy1.1

monoclonal antibodies were generated by pepsin digestion. Prior to $F(ab')_2$/cytokine coupling, IL-2-Fc and anti-Thy1.1 $F(ab')_2$ were mildly reduced by DTT to expose hinge region free thiols for reaction with the liposome maleimide functional head groups. We tested liposomes containing two different mole fractions of maleimide-PEG lipid (1 or 2.5 mol% of total lipids), and found greater targeting ligand conjugation with higher fractions of maleimide-lipid, as expected (**Figure 2-1B**). Negligible IL-2 or $F(ab')_2$ binding to liposomes was observed in the absence of the maleimide reactive groups. Liposomes with 2.5 mol% mal-PEG-DSPE gave 23 ± 2 μg of IL-2 (cytokine equivalent, or 1.4 nmol IL-2) or 76 ± 7 μg of anti-Thy1.1 (0.5 nmol $F(ab')_2$) per mg lipid after overnight coupling at 25°C. As shown in **Figure 2-1A**, targeting ligand conjugation caused a slight increase in the mean size of the vesicles from 173 ± 13 nm to 186 ± 16 nm.

Dual-targeting liposomes were formed by adding mixture of IL-2-Fc and anti-Thy1.1 $F(ab')_2$ to maleimide functionalized liposomes (**Schematic 2-2**). The amount of each type of ligands on the surface could be controlled by varying the mole ratios of antibodies or cytokines in the feeding ligand cocktail. The amount of IL-2 equivalent coupled dropped around 50% from 21 μg to 11 μg when 50 mole % of IL-2-Fc was in the ligand cocktail and further down to 2 μg when only 10 mole % of IL-2-Fc was fed (**Figure 2-2A**). When FITC-labeled anti-CD45 and IL-2-Fc were used to couple liposomes, amount of anti-CD45 conjugated was also positively correlated to the mole ratio of anti-CD45 in the feeding ligand cocktail (**Figure 2-2B**), indicating this strategy could be generalized to decorate liposomes with an array of targeting candidates or even combination of them.

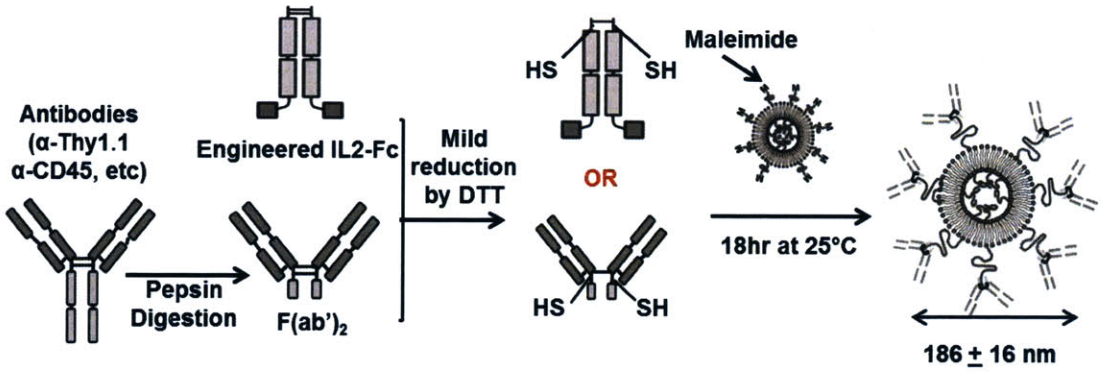

Schematic 2-1: Synthesis of cytokine-or antibody-conjugated liposomes.

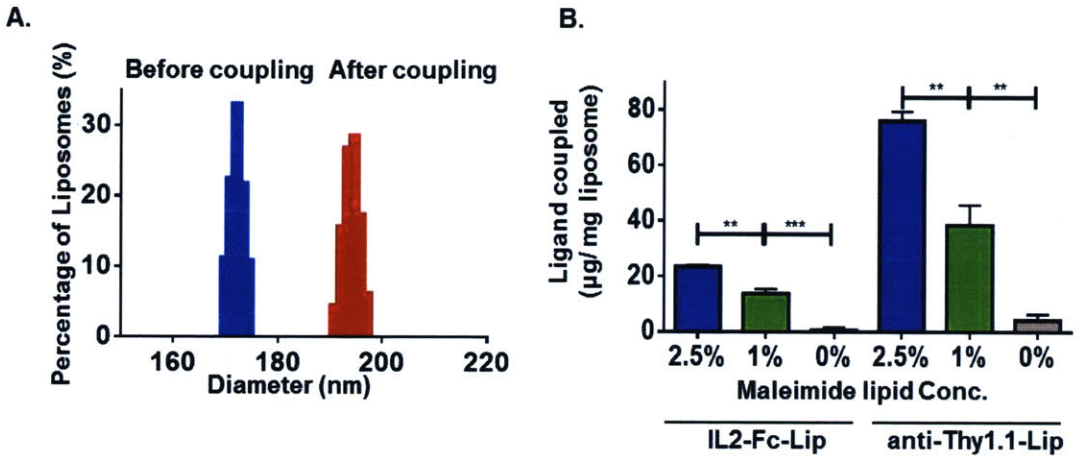

Figure 2-1: T-cell-targeted liposome characterization. (**A**) Typical particle size distributions for liposomes before antibody conjugation (open bars) and after conjugation (black filled bars) determined by dynamic light scattering. (**B**) Quantification of ligand (IL-2 cytokine equivalent or anti-Thy1.1) coupled to liposomes incorporating different mole fractions of maleimide-PEG lipid: 2.5% (black filled bar), 1% (open bar) or 0% (striped bar), assessed by IL-2 ELISA and measuring FITC-labeled anti-Thy1.1 incorporation respectively. *, $p<0.05$; **, $p<0.01$; ***, $p<0.001$.

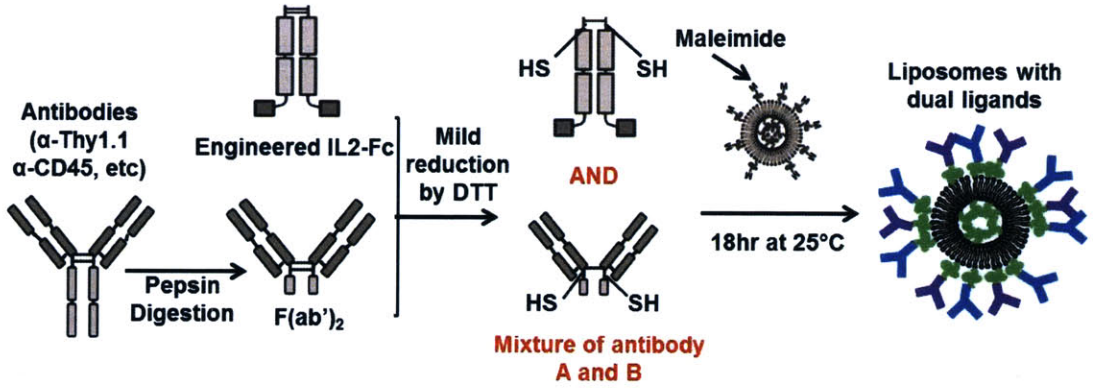

Schematic 2-2: Synthesis of dual antibodies/cytokines conjugated liposomes.

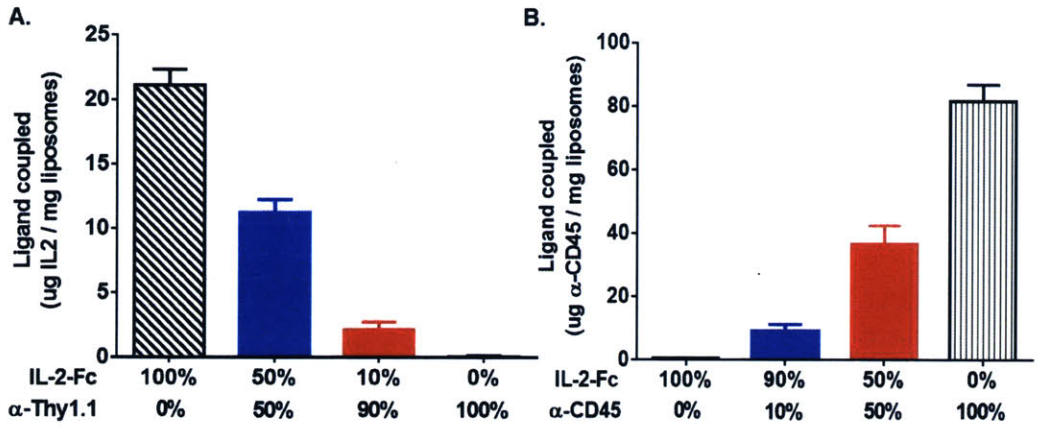

Figure 2-2: Quantification of surface ligands on dual-targeting liposomes. Quantification of ligand (IL-2 cytokine equivalent or anti-CD45) coupled to liposomes when different mole fractions of IL2-Fc and anti-Thy1.1 (**A**) or IL2-Fc and anti-CD45 (**B**) were added to maleimide functionalized liposomes, assessed by IL-2 ELISA and measuring FITC-labeled anti-CD45 incorporation respectively. Total amount of ligands added for each case were the same.

2.3.2 IL-2-Fc-Lip and anti-Thy1.1-Lip binding to T-cells in vitro

To generate a target population of T-cells to be used in adoptive transfer studies, $CD8^+$ T-cells from pmel-1 $Thy1.1^+$ mice (which express a transgenic T-cell receptor specific for the gp100 antigen of melanoma [88]) were isolated by magnetic negative selection from activated splenocytes, and expanded by culturing with IL-2 for 1 day to obtain an elevated expression of CD25 (the α-chain of the trimeric IL-2 receptor) compared to naive pmel-1 or naive polyclonal C57Bl/6 $CD8^+$ T-cells (**Figure 2-3A** and data not shown). Fluorescently labeled PEGylated vesicles showed very low background binding to activated pmel-1 T-cells following a 30 min incubation at 37° *in vitro*, but IL-2-Fc-Lip or anti-Thy1.1-Lip containing 1% or 2.5% maleimide functional groups efficiently bound to activated pmel-1 T-cells (**Figure 2-3B**). The Mean Fluorescence Intensities (MFI) of cells after conjugation with different types of liposomes was quantified; the high expression levels of Thy1.1 on pmel-1 T-cells led to much greater per-cell binding of anti-Thy1.1-Lip vs. IL-2-Fc-Lip (**Figure 2-3C**). For both targeting ligands, liposomes containing 2.5 mol% mal-PEG-DSPE (and therefore with higher ligand densities) achieved much greater binding to T-cells than vesicles with 1 mol% of the maleimide lipid, with MFIs of bound liposomes increased by 6-fold and 4-fold for anti-Thy1.1-Lip and IL-2-Fc-Lip, respectively (**Figure 2-3B, C**).

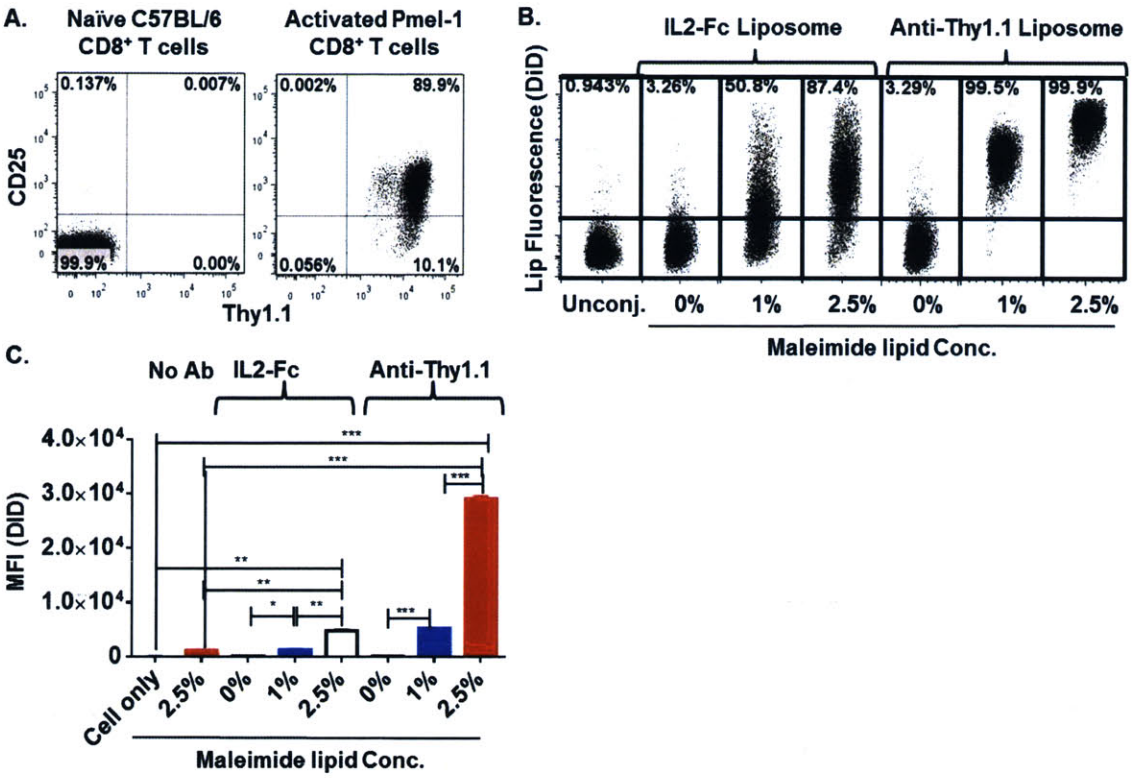

Figure 2-3: *In vitro* binding of IL-2-Fc-Lip and anti-thy1.1 F(ab')$_2$ -Lip to primary T-cells. **(A)** Flow cytometry analysis of cell surface expression of CD25 and Thy1.1 on naïve C57BL6/J (Thy1.1$^-$) splenocytes vs. activated pmel-1 Thy1.1$^+$CD8$^+$ T-cells. **(B, C)** Pmel-1 CD8$^+$ Thy1.1$^+$ T-cells were incubated with 0.7 mg/ml (per 15×10^6 cells) DiD-labeled liposomes (IL-2-Fc or anti-Thy1.1 F(ab')$_2$ conjugated) for 30 min at 37 °C in complete RPMI, then analyzed by flow cytometry for liposome binding. Shown are representative flow cytometry scatter plots (B) and quantification of Mean Fluorescence Intensity (MFI) of pmel-1 T-cells as a function of mol% of mal-PEG-DSPE included in the vesicles (C). *, $p<0.05$; **, $p<0.01$; ***, $p<0.001$.

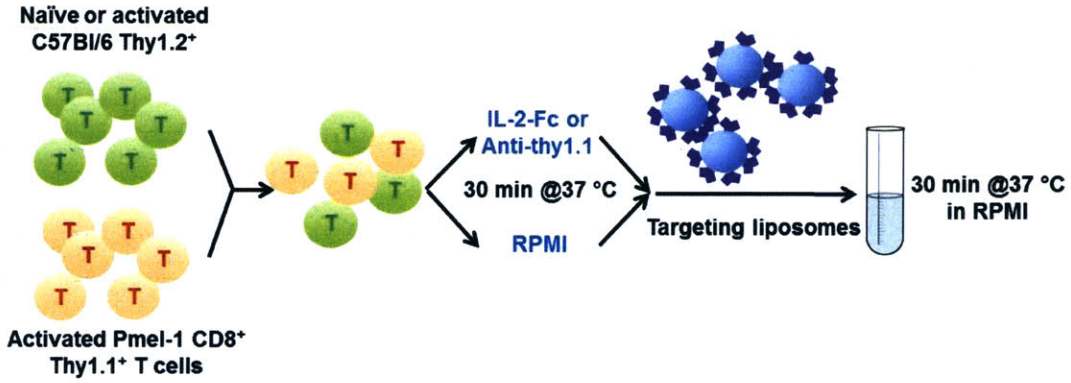

Schematic 2-3: Flowchart of testing targeting specificity of liposomes *in vitro*.

To evaluate the specificity of anti-Thy1.1-Lip and IL-2-Fc-Lip binding, we assessed T-cell labeling in the presence of competing free IL-2-Fc or anti-Thy1.1 Abs added to a 1:1 mixture of naïve C57Bl/6 lymphocytes and pmel-1 T-cells 30 min before the targeted vesicles (**Schematic 2-3**). IL-2-Fc-Lip bound to activated pmel-1 T-cells, but not naïve C57Bl/6 $CD8^+$ T cells that lack IL-2 receptors (**Figure 2-4A middle left**). Pre-blocking pmel-1 T-cells with soluble IL-2-Fc blocked 90% of binding to pmel-1 T-cells (**Figure 2-4A middle right, Figure 2-4B**). Similarly, anti-Thy1.1-Lip selectively targeted pmel-1 $CD8^+$ T cells but not naive C57Bl/6 ($Thy1.2^+$) $CD8^+$ T cells (**Figure 2-4A bottom left**). Pre-incubation of pmel-1 T-cells with anti-Thy1.1 lowered anti-Thy1.1-Lip binding by 99% (**Figure 2-4A bottom right, Figure 2-4B**). Autofluorescence and non-specific binding of non-targeted control IgG_{2a}-Lip were neglibible (**Figure 2-4A top left and right, Figure 2-4B**). As expected from the pM affinity of IL-2 for its receptor [89, 90] and the typical nM affinity of commercial antibodies, liposomes at concentration of 0.4 mg/ml (equivalent to 2 nM of liposomes) labeled 100% of activated pmel-1 T-cells *in vitro*, and liposome binding reached a plateau at concentrations higher than 0.4 mg/ml (equivalent to 2 nM liposomes) (**Figure 2-4C**). Thus, both IL-2- and anti-Thy1.1-targeted stealth liposomes achieve specific and avid binding to primed pmel-1 $CD8^+$ T-cells. Even when the concentration was titrated down to 0.1mg/ml, nearly 100% of cells were still labeled with liposomes, albeit with fewer liposomes bound per cell.

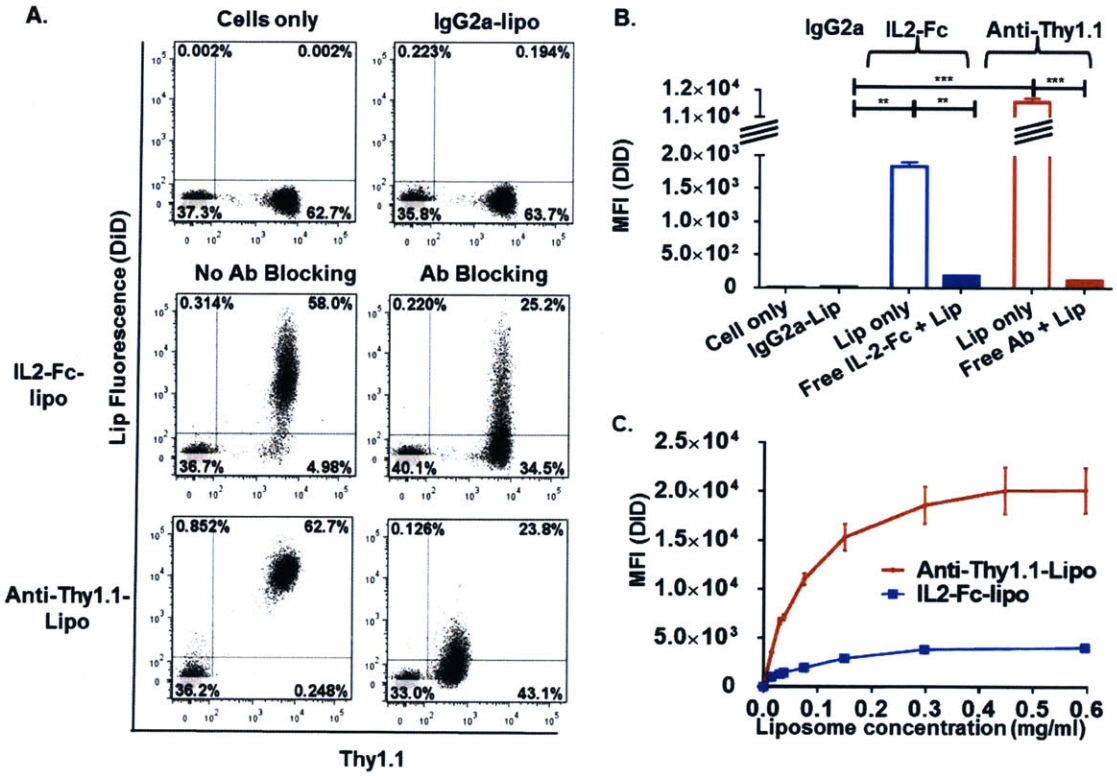

Figure 2-4: IL-2-Fc-Lip and anti-thy1.1 F(ab')$_2$–Lip achieve specific and avid binding to T-cells. (**A, B**) Activated pmel-1 CD8$^+$ T-cells were mixed with naive C57BL/6 splenocytes in a 1:1 ratio and incubated with 0.07 mg/ml IL2-Fc-Lip or 0.15 mg/ml anti-Thy1.1-Lip for 30 min at 37°C, then analyzed by flow cytometry. (A) Shown are scatter plots representing liposome fluorescence on naive C57BL/6 CD8$^+$ T cells (Thy1.1$^-$) and activated pmel-1 CD8$^+$ T-cells (Thy1.1$^+$) with/without 0.24 mg/ml soluble IL2-Fc or 1.34 mg/ml anti-Thy1.1 antibody added for 30 min prior to addition of liposomes. Cells incubated with 0.15 mg/ml IgG2a-lipo are also shown. (B) Quantification of the MFI of Pmel-1 CD8$^+$ T cells when bound with respective liposomes or pre-blocked by free Ab/IL-2. (**C**) Titrated concentrations of fluorescent liposomes were added to 5 $\times 10^6$ activated pmel-1 T-cells and incubated at 37°C for 30 min, then analyzed by flow cytometry for MFI of T-cell-associated liposomes. *, $p<0.05$; **, $p<0.01$; ***, $p<0.001$.

2.3.3 Anti-Thy1.1-Lip triggered liposome endocytosis quickly

After binding targeting-liposomes to T-cells, we tried to find out the internalization kinetics of them. We added anti-Thy1.1-Lip incorporating a carboxyfluorescein (CF)-headgroup lipid to pmel-1 T-cells at 4°C to allow binding without internalization, then warmed the cells to 37°C and assessed cell-associated fluorescence over time. Fluorescein has highly pH-sensitive fluorescence that is strongly quenched at acidic pHs [91]. The high avidity of liposome binding to cells led to no measurable release of free liposomes into the supernatant over 6 hr at 37°C (not shown); we thus attributed loss of the CF tracer signal to endocytic uptake by labeled cells. Over a time course of 6 hr, the MFI of liposome-labeled T-cells steadily dropped, corresponding to roughly 90% internalization over this time course (**Figure 2-5A**). Confocal imaging also showed that anti-Thy1.1-Lip fluorescence initially localized to the plasma membrane of labeled cells was largely lost by 6 hr (**Figure 2-5B**).

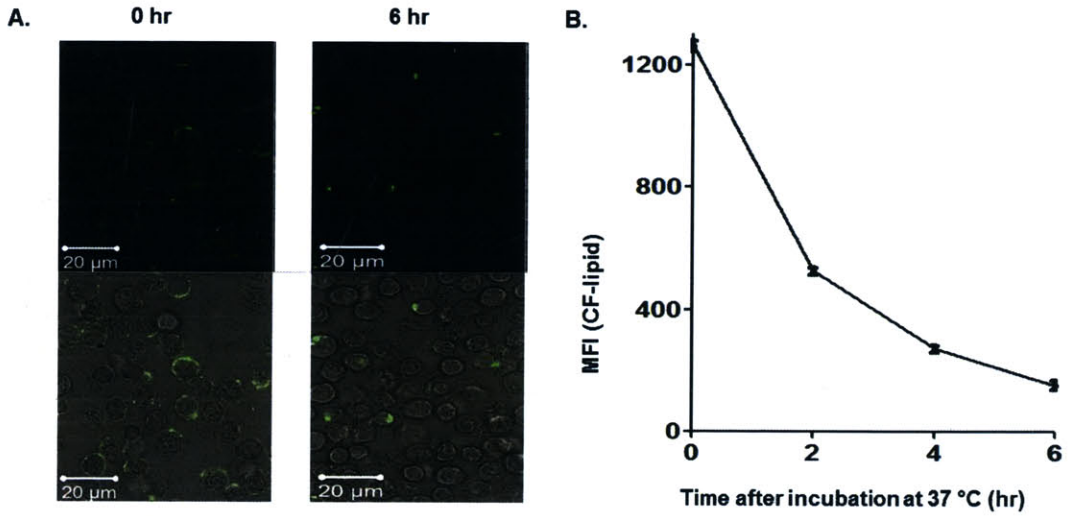

Figure 2-5: Internalization of Thy1.1-targeted liposomes. Carboxy-fluorescein (CF)-labeled anti-Thy1.1-Lip (1.4 mg/ml) were incubated with 12x10^6 activated pmel-1 CD8$^+$ T-cells in 500 µl RPMI containing 10% FCS for 1 hr at 4°C, washed, then incubated in RPMI at 37°C until analysis by flow cytometry 2 hr, 4 hr or 6 hrs later. (**A**) MFI of T-cell-associated CF fluorescence. (**B**) Confocal images of cells at time zero or after 6 hr at 37°C. Scale bar= 20 µm.

2.3.4 IL2-Fc-Lip and anti-Thy1.1-Lip targeted adoptively transferred T cells in healthy mice

Next, we tested the capacity of anti-Thy1.1-Lip and IL-2-Fc-Lip to target pmel-1 T-cells *in vivo* in healthy mice. PEGylated liposomes conjugated with isotype control murine IgG_{2a} were prepared to serve as a control non-T-cell-targeting liposome. To model clinical adoptive T-cell therapy, recipient Thy1.2$^+$ C57Bl/6 mice were lymphodepleted by sublethal irradiation, followed by i.v. injection of $15x10^6$ activated pmel-1 Thy1.1$^+$CD8$^+$ T-cells one day later. Lymphodepletion removes cytokine sinks and regulatory T-cells to allow more efficient expansion and effector function of transferred T-cells [92, 93]. To assess T-cell targeting, IgG_{2a}-Lip, IL-2-Fc-Lip, or anti-Thy1.1-Lip fluorescently labeled with the non-pH-sensitive tracer DiD were injected i.v. either immediately after adoptive transfer or 3 days after T-cell injection. Twenty-four hours after liposome injection, cells from the blood, lymph nodes (LNs), and spleens were analyzed by flow cytometry to assess binding of fluorescent liposomes (**Figure 2-6A**). Thy1.1 expression allowed liposome binding to transferred pmel-1 T-cells to be distinguished from endogenous T-cells (**Figure 2-6B**). Sample flow cytometry histograms are shown in **Figure 2-6C**, illustrating conjugation efficiencies of IgG_{2a}-Lip, IL-2-Fc-Lip, and anti-Thy1.1-Lip obtained when liposomes were injected immediately after ACT T-cells. The percentage endogenous or ACT CD8$^+$ T-cells labeled by each type of liposome in the blood (**Figure 2-6D**), lymph nodes (**Figure 2-6E**) and spleens (**Figure 2-6F**) were assessed; this analysis revealed that IgG_{2a}-Lip exhibited low binding to both T-cell populations. In contrast, anti-Thy1.1-Lip labeled nearly 100% of the transferred T-cells in the blood and spleen whether injected on day 0 or day 3. The targeting specificity of anti-Thy1.1-Lip on day 0 was still maintained even when the dose was lowered to 0.18 mg (approximately ~0.1 mg/mL liposomes in the blood) (**Figure 2-7A-C**). The drop in mean liposome fluorescence intensity on transferred T-cells indicated fewer particles bound per transferred T-cell with lower doses of targeting liposomes (**Figure 2-7D**) and can be potentially exploited to control amount of drug to be delivered. The slightly greater background binding of isotype control IgG2a-Lip to ACT vs. endogenous T-cells in spleens was found to be an artifact of the liposome dose; injection of lower liposome doses of 0.18 mg led to a similar efficiency of specific T-cell binding but eliminated the low differential background binding to ACT vs. endogenous T-cells (data not shown). A lower fraction of T-cells in lymph nodes were labeled by anti-Thy1.1-Lip following a day 3 injection, which may reflect a combination of poor entry of targeted liposomes into LN and/or incomplete recirculation of T-cells from LN back into the blood in the 24 hr time window between liposome injection and our analysis. Anti-Thy1.1-Lip also showed low levels of background binding to endogenous (Thy1.1$^-$) T-cells. IL-2-Fc-Lip labeled the majority of pmel-1 T-cells in the LNs, spleen and blood when injected just after T-cells, and also showed relatively low binding to endogenous T-cells. Injection of IL-2-Fc-Lip on day 3 led to relatively poor T-cell labeling in the blood and LNs, while still labeling a majority of ACT T-cells in the spleen (**Figure 2-6D-F**). Poor labeling by IL-2-Fc-Lip on day 3 might reflect the rapid downregulation of the IL-2R *in vivo* following T-cell transfer in the absence of antigen (data not shown). Overall, both IL-2-Fc and anti-Thy1.1 $F(ab')_2$ can be effective for specifically targeting adoptively transferred T-cells *in vivo*, though modulation of IL-2R levels by T-cells over time is an important consideration for achieving effective targeting.

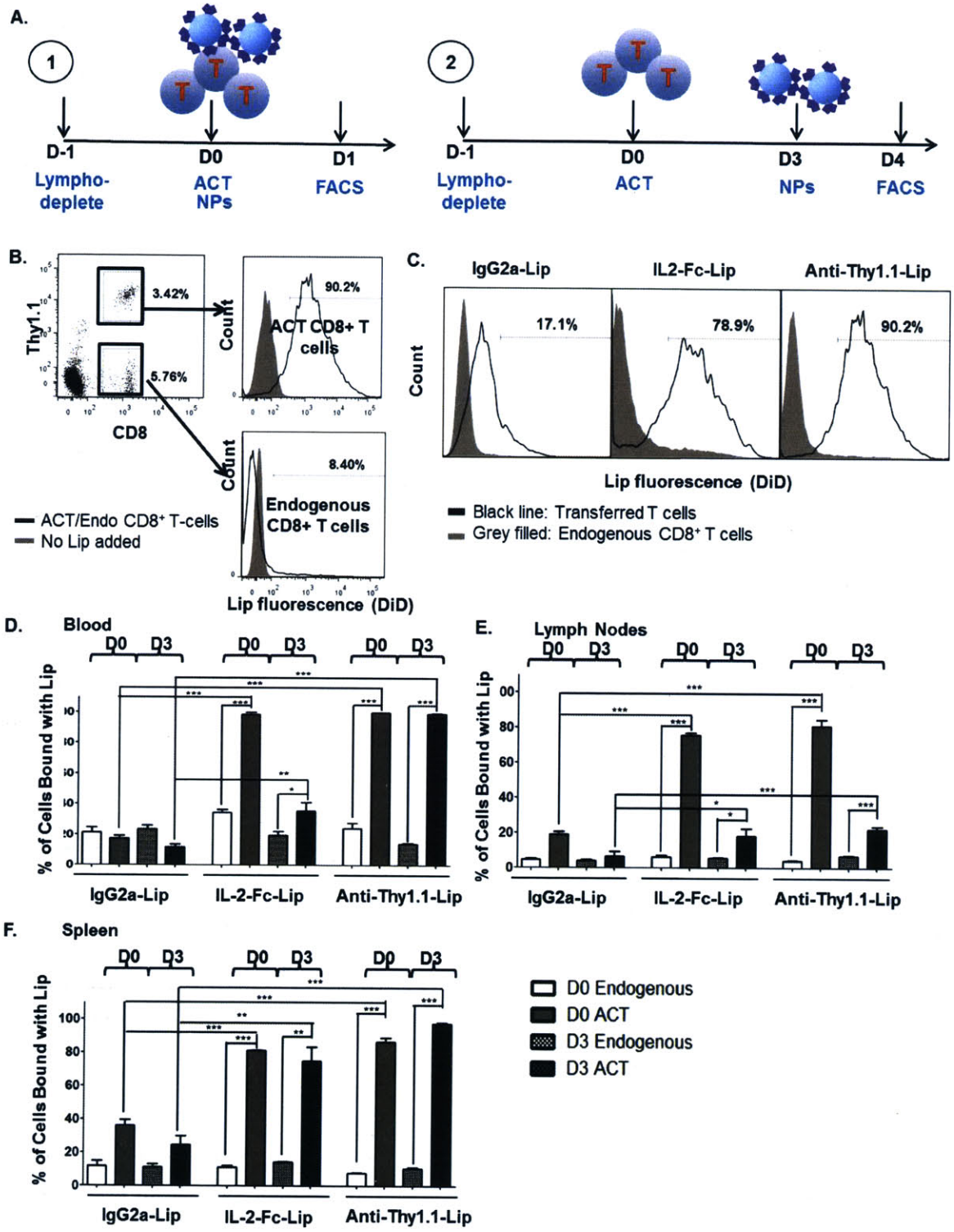

Figure 2-6: IL-2-Fc- and anti-Thy1.1-Liposomes target transferred T-cells *in vivo*. C57Bl/6 mice received i.v. adoptive transfer of $15x10^6$ pmel-1 $CD8^+Thy1.1^+$ T-cells, followed by i.v. injection of 1.4 mg IL-2-Fc-Lip, anti-Thy1.1-Lip, or isotype control IgG_{2a}-Lip either

immediately after the T-cells or 3 days after the T-cells. Liposome binding to cells recovered from lymphoid organs and blood was analyzed 24 hr after liposome injections by flow cytometry. (**A**) Timeline of injections and analysis. (**B**) Representative flow cytometry plots illustrating gating strategy for analysis of liposome binding to transferred pmel-1 T-cells or endogenous $CD8^+$ T-cells. (**C**) Representative histograms of pmel-1 T-cell or endogenous $CD8^+$ T-cell labeling following day 0 liposome injections. (**D-F**) Quantification of percentages of endogenous or transferred T-cells labeled by day 0 or day 3 liposome injections in the blood (D), lymph nodes (E), and spleen (F). n=5 animals/group for IgG_{2a}-Lip and anti-Thy1.1-Lip and n=3 for IL-2-Fc-Lip. *, $p<0.05$; **, $p<0.01$; ***, $p<0.001$.

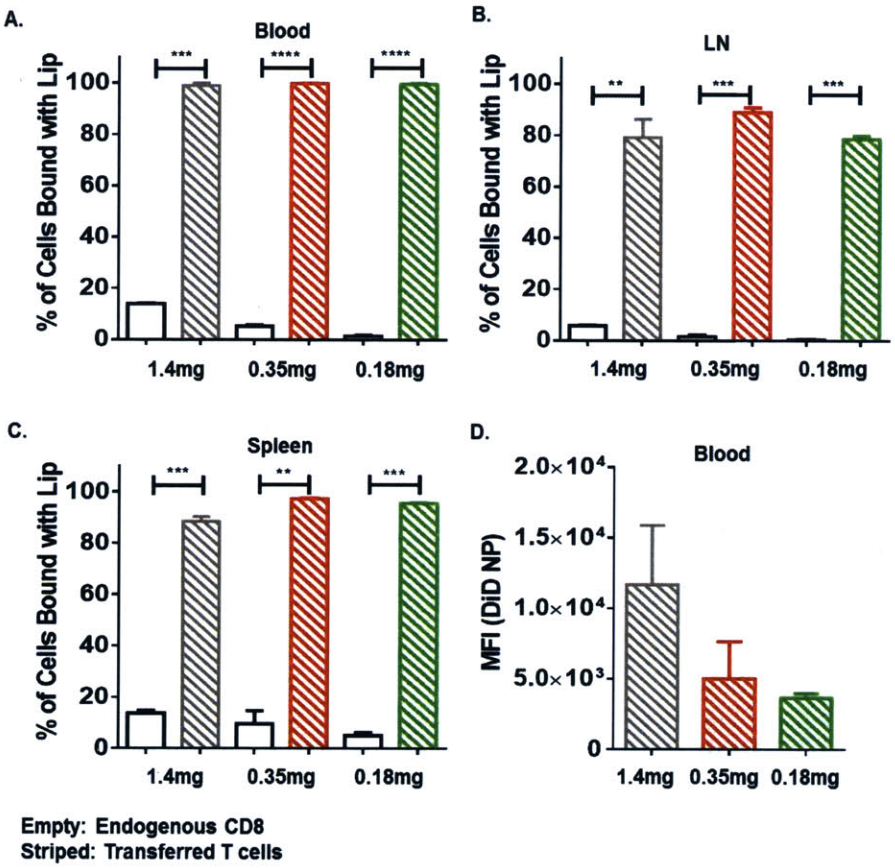

Figure 2-7: Anti-Thy1.1-Liposomes can target transferred T-cells *in vivo* at lower doses. C57Bl/6 mice received i.v. adoptive transfer of $15x10^6$ pmel-1 $CD8^+Thy1.1^+$ T-cells, followed by i.v. injection of 1.4 mg, 0.35 mg or 0.18 mg anti-Thy1.1-Lip immediately after the T-cells. Liposome binding to cells recovered from lymphoid organs and blood was analyzed 24 hr after liposome injections by flow cytometry. **(A-C)** Quantification of percentages of endogenous or transferred T-cells labeled by liposome injections in the blood (A), lymph nodes (B), and spleen (C). **(D)** Mean DiD fluorescence intensity of transferred T cells in blood after injection of different doses of anti-Thy1.1 liposomes. *, $p<0.05$; **, $p<0.01$; ***, $p<0.001$; ****, $p<0.0001$.

2.3.5 IL2-Fc-Lip permitted repeated boosting of ACT T-cells in a murine lung metastasis model

To test the potential functional impact of stimulatory T-cell targeted liposomes, we assessed the response of pmel-1 melanoma-specific T-cells *in vivo* during ACT treatment of B16F10 tumors in a metastatic lung tumor model. B16F10 melanoma cells were injected via the tail vein to allow lung metastases to establish for 7 days, then animals were lymphodepleted and received adoptive transfer of luciferase-expressing pmel-1 melanoma-specific $CD8^+$ T-cells (**Figure 2-8A**). In one group of animals, T-cell expansion was followed over time by bioluminescence imaging without further treatment, while in other two groups of mice, the adoptively-transferred cells were boosted on days 0 and 6 by injection of IL-2-Fc-Lip. Adoptively transferred cells without further adjuvant support showed a low level persistence in the tumor-bearing recipients that gradually declined over 14 days, as expected in the absence of additional stimulation or protection from tumor immunosuppression [88] (**Figure 2-8B, C**). In contrast, following injection of the first dose of IL-2-Fc-Lip, pmel-1 T-cells expanded 3-fold more than the control T-cell therapy group. These boosted T-cells began to contract again between day 4 and day 6, but following a second dose of IL-2-Fc-Lip, re-expanded to an even greater level, reaching a peak by day 10 with 6-fold greater T-cell numbers relative to the T-cell-only treatment group (**Figure 2-8B, C**). To assess the relative potency of stimulation achieved by IL-2-Fc-Lip compared to traditional systemic IL-2 therapy, we repeated this ACT experiment and compared the expansion of T-cells following injection of IL-2-Fc-Lip or soluble IL-2 (at an equivalent total amount of cytokine to that bound to the liposomes) on day 0 and day 6. Flow cytometry analysis of T-cells pooled from the inguinal lymph nodes 12 days after adoptive transfer confirmed that the frequency of tumor-specific $CD8^+$ T-cells (pmel-1 T-cells express the Vβ13 TCR β chain) was nearly 3 times greater in animals that received IL-2-Fc-Lip injections compared to T-cells alone (**Figure 2-8D-E**). Further, soluble IL-2 at these doses showed no enhancement in T-cell expansion. The difference between the potency of IL-2-Fc-Lip and soluble IL-2 may reflect the very short half-life of IL-2 *in vivo* [94], which the PEGylated liposomes may partly overcome. Notably, this enhanced potency was not accompanied by overt toxicity as assessed by changes in animal weights during the therapy (data not shown). Thus, IL-2-targeted liposomes allow multiple boosts of ACT T-cells *in vivo*, leading to repeated waves of T-cells expansion in tumor-bearing animals, which exceed the response elicited by systemic free IL-2.

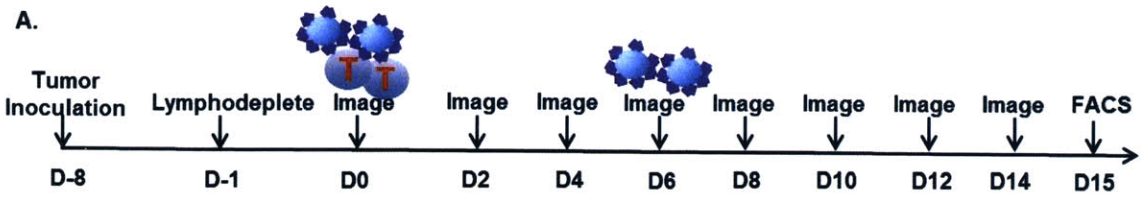
A.
Tumor Inoculation
Lymphodeplete
Image
Image
Image
Image
Image
Image
Image
Image
FACS
D-8
D-1
D0
D2
D4
D6
D8
D10
D12
D14
D15

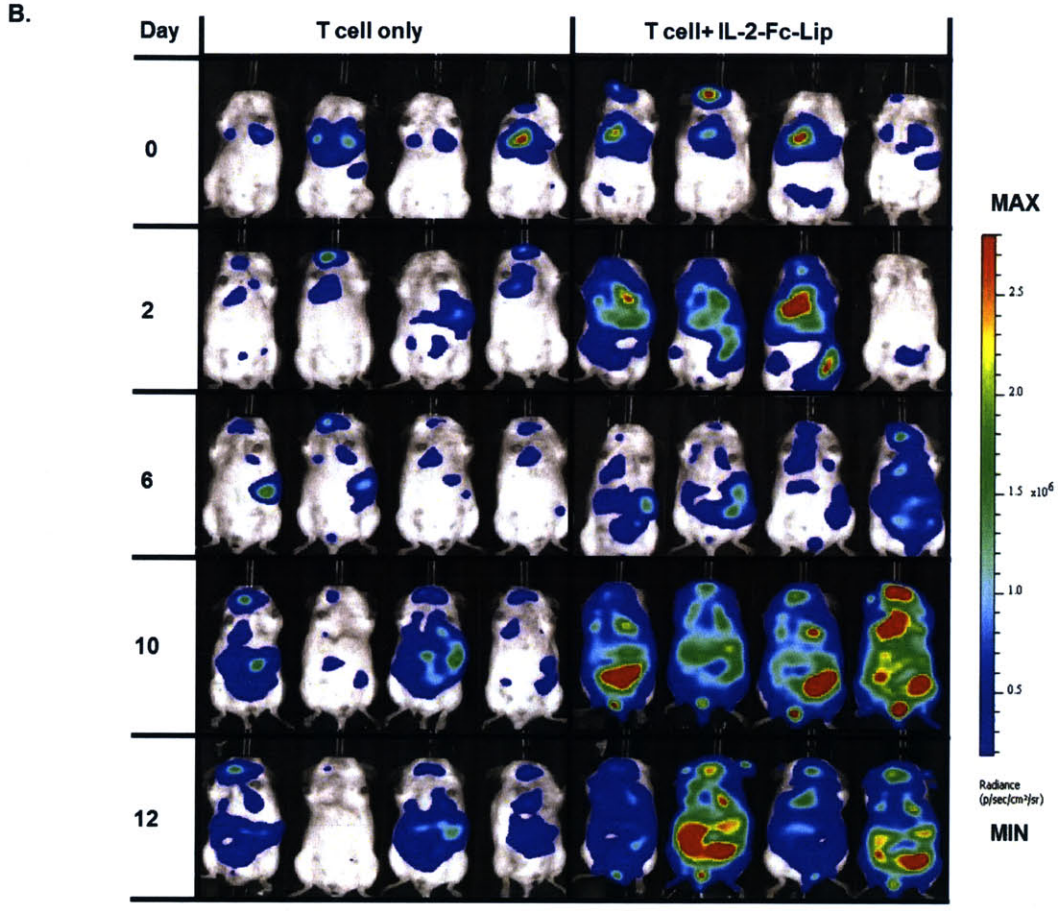
B.
Day
T cell only
T cell+ IL-2-Fc-Lip
0
2
6
10
12
MAX
2.5
2.0
1.5 x10^6
1.0
0.5
Radiance (p/sec/cm²/sr)
MIN

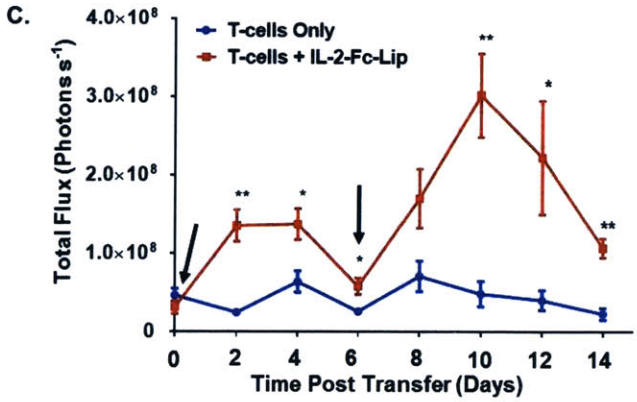
C.
T-cells Only
T-cells + IL-2-Fc-Lip
Total Flux (Photons s⁻¹)
4.0×10⁸
3.0×10⁸
2.0×10⁸
1.0×10⁸
0
0
2
4
6
8
10
12
14
Time Post Transfer (Days)

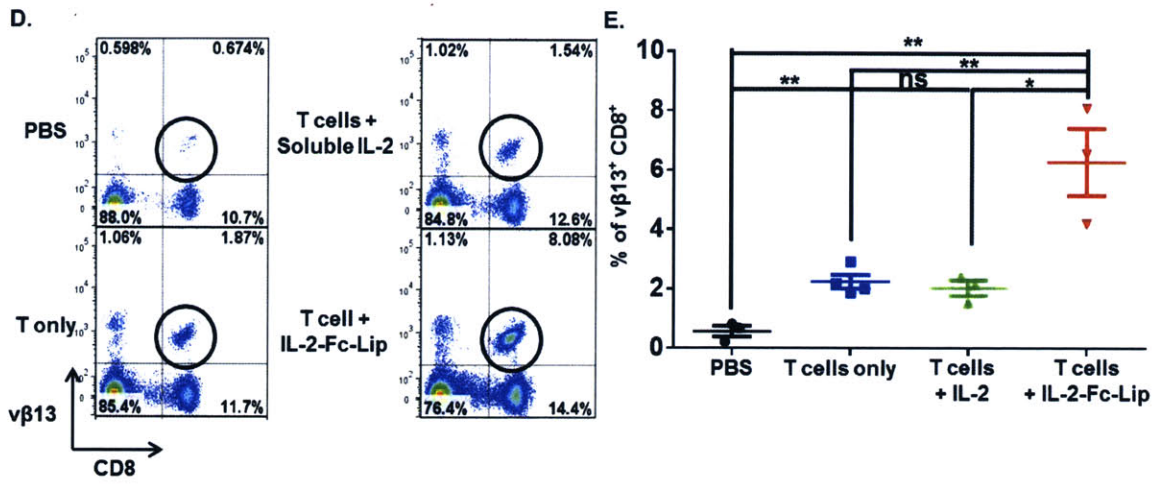

Figure 2-8: IL-2-Fc-liposomes allow repeated expansion of target ACT T-cells *in vivo* in tumor-bearing animals. (A-C) B16F10 tumor cells ($1x10^6$) were injected i.v. into albino C57Bl/6 mice and allowed to establish lung metastases for 7 days. Animals were then sublethally lymphodepleted by irradiation and received i.v. adoptive transfer of $12x10^6$ luciferase-expressing pmel-1 $CD8^+$ T-cells the next day. One group of mice additionally received injections of IL-2-Fc-Lip (1 mg, carrying 60 µg IL-2-Fc or 20 µg IL-2 cytokine equivalent) i.v. immediately after T-cell transfer and again on day 6. **(A)** Timelines of cell/liposome injections and bioluminescence imaging of T-cells. **(B)** Representative bioluminescent images of ACT T-cells over time. **(C)** Quantification of average whole-body T-cell bioluminescence over time. **(D-E)** Groups of C57B/6 mice with established lung metastases were left untreated or were treated with T-cells as in A, then received either IL-2-Fc-Lip or equivalent total doses of systemic free IL-2 injected i.v. on day 0 (10 µg and day 6 (20 µg). **(D)** Sample flow cytometry analyses showing percentages of tumor-specific (vβ13 TCR^+) $CD8^+$ T-cells among T-cells in inguinal lymph nodes 12 days after adoptive transfer. **(E)** Quantification of average frequency of tumor-specific (vβ13 TCR^+) $CD8^+$ T-cells in inguinal lymph nodes 12 days after adoptive transfer. n=3-4 animals/group. *, $p<0.05$; **, $p<0.01$.

2.3.6 IL2-Fc-Lip prevent tumor outgrowth of subcutaneous B16F10 melanoma.

To evaluate the therapeutic efficacy of stimulatory T-cell targeted liposomes, we also investigated the tumor eradication potential of pmel-1 melanoma-specific T-cells in a B16F10 subcutaneous solid tumor model. B16F10 melanoma cells were injected subcutaneously to allow tumor to establish for 7 days, then animals were lymphodepleted and received adoptive transfer of pmel-1 melanoma-specific $CD8^+$ T-cells (**Figure 2-9A**). In one group of animals, the adoptively-transferred cells were boosted immediately after, 4 days after and 8 days after adoptive transfer by injection of IL-2-Fc-Lip. In the other group, PBS was injected at the same time points (**Figure 2-9A**). Tumors outgrew rapidly in the group without further adjuvant support for transferred T cells whereas the infusion of stimulatory T-cell targeted liposomes delayed tumor growth for 14 days after adoptive transfer (**Figure 2-9B**). IL-2-Fc-Lip support for transferred T cells also endowed mice better survival advantage than T-cells alone group. All mice in the T-cell alone group had tumor size larger than 100 mm^2 on day 20 while on day 32, only two mice in the IL-2-Fc-Lip supporting group

reached 100 mm^2 tumor size and one mouse has tumor almost eradiated with only a small bump left over (**Figure 2-9C**).

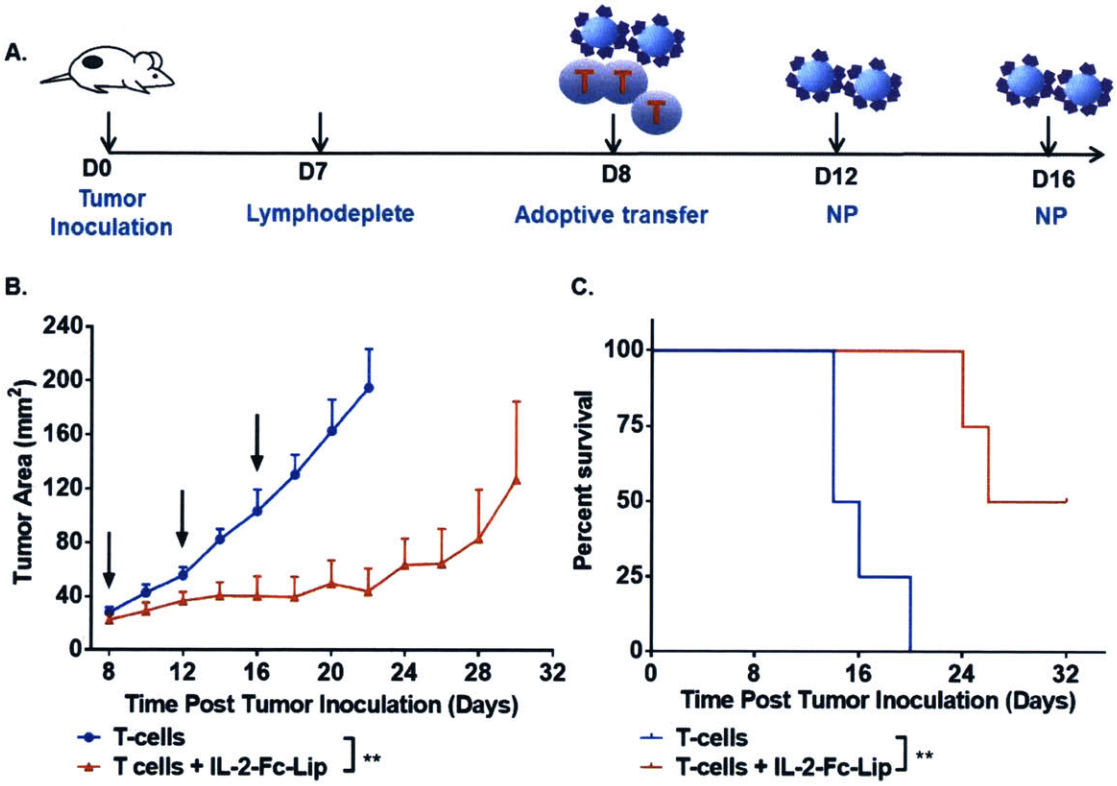

Figure 2-9: IL-2-Fc-liposomes slow down tumor growth significantly.
B16F10 tumor cells ($0.25x10^6$) were injected subcutaneously into C57Bl/6 mice and allowed to establish tumor for 8 days. Animals were then sublethally lymphodepleted by irradiation and received i.v. adoptive transfer of $15x10^6$ pmel-1 $CD8^+$ T-cells the next day. One group of mice additionally received injections of IL-2-Fc-Lip (0.35 mg, carrying 21 μg IL-2-Fc or 7 μg IL-2 cytokine equivalent) i.v. immediately after T-cell transfer and four days after for 3 doses in total. **(A)** Timelines of cell/liposome injections. **(B)** Average tumor growth curves of mice with adoptive transfer only (blue circle) and adoptive transfer with IL-2-Fc-Lip (red triangle). **$p<0.01$ by two way anova. (**C**) Kaplan-Meier survival curve of mice treated with adoptive transfer (blue) and adoptive transfer with IL-2-Fc-Lip (red). Mice with tumor area larger than 100 mm^2 were considered dead. n=4 animals/group, **$p<0.01$ by log-rank test.

2.3.7 Anti-Thy1.1/IL-2-Fc dual-targeting liposomes improved targeting consistency and specificity of IL-2-Fc-Lip

Despite the demonstrated therapeutic efficacy of stimulatory T-cell targeting liposomes, we strived to improve the targeting consistency and specificity of IL-2-Fc-Lip when injected at later time points. When activated T cells ready to transfer were incubated without further cytokine support *in vitro*, IL-2R expression was rapidly downregulated (**Figure 2-10A**),

suggesting external environment impacts the modulation of IL-2R greatly. To combine the targeting consistency of anti-Thy1.1 and stimulatory effect of IL-2-Fc, we generated dual-targeting liposomes to synergize targeting with stimulation, but with less interference from modulation of IL-2R expression. Fluorescently labeled liposomes with different mole ratios of IL-2-Fc and anti-Thy1.1 on their surfaces were incubated with mixtures of activated Pmel-1 Thy1.1$^+$ CD8$^+$ T-cells and naive C57BL/6 Thy1.2$^+$ CD8$^+$ T-cells. Liposomes with 10% or 50% IL-2-Fc bound to Thy1.1$^+$ cells similar to 100% anti-Thy1.1-Lip (**Figure 2-10B**). This result indicates the possibility to specifically target low IL-2R-expressing ACT T-cells by anti-Thy1.1 without consideration for modulation of IL-2R level and still stimulate bound T-cells by IL-2 on the same liposome.

Furthermore, when activated Thy1.1$^+$ and activated Thy1.2$^+$ cells were mixed for anti-Thy1.1/IL-2-Fc liposome binding, IL-2-Fc-Lip (100% IL-2-Fc) showed binding to both Thy1.1$^+$ and Thy1.2$^+$ cells due to expression of IL-2R on both type of cells (**Figure 2-10C**). However, liposomes with 10% and 50% IL-2-Fc (90% anti-Thy1.1 and 50% anti-Thy1.1 respectively) still preferably bound to Thy1.1$^+$ T-cells despite the high expression of IL-2R on Thy1.2$^+$ T-cells (**Figure 2-10C**). Thus, dual targeting liposomes could possibly minimize off-targeting to IL-2R expressing endogenous cells while still stimulating targeted cells. The high expression of Thy1 relative to IL-2R may allow the dual-ligand liposomes to still preferentially bind to the target Thy1.1+ cells even in the presence of other CD25+ lymphocytes. If this were true, then dual-ligand liposomes functionalized with anti-Thy1.1 and a second antibody/ligand targeting a more highly expressed protein would be expected to show loss of target cell specificity. To test this, we explored antibodies against CD45, a universal marker expressed on all lymphocytes, which was abundantly expressed by both Thy1.1$^+$ and Thy1.2$^+$ T-cells. Dual-targeting liposomes with anti-Thy1.1 and anti-CD45 were also produced. Although liposomes with 0.5% and 1% anti-CD45 showed preferable binding to Thy1.1$^+$ T-cells, they also increasingly bound to Thy1.2$^+$ T-cells, and liposomes with 20% anti-CD45 bound equivalently to both cell types (**Figure 2-10D**), demonstrating a much smaller range of mole ratios between anti-Thy1.1 and anti-CD45 could be exploited for specific Thy1.1$^+$ T-cell targeting. Thus, when other antibody candidates were used for dual targeting, further characterization of each combination might be necessary.

Next we tried to test the specificity of dual targeting liposomes in healthy mice. Two days after adoptive transfer, a low dose (0.25 mg) of 10% IL-2-Fc/ 90% anti-Thy1.1 liposomes were injected into C57BL/6 mice, which were sacrificed one day after injection for analysis (**Figure 2-11A**). At this low dose and time point, IL-2-Fc-Lip showed little binding to transferred T-cells in blood and LN while dual-targeting liposomes still bound to almost 100% of transferred T-cells in blood and spleen and enhanced targeting in lymph nodes (**Figure 2-11B, C**). Both dual-targeting liposomes and IL-2-Fc-Lip exhibited little binding to endogenous CD8$^+$ T-cells (**Figure 2-11B, C** and data not shown). Overall, addition of anti-Thy1.1 on the surface of IL-2-Fc-Lip improved targeting efficiency of IL-2-Fc-Lip both *in vitro* and *in vivo* and decreased the binding dependency on expression level of IL-2R.

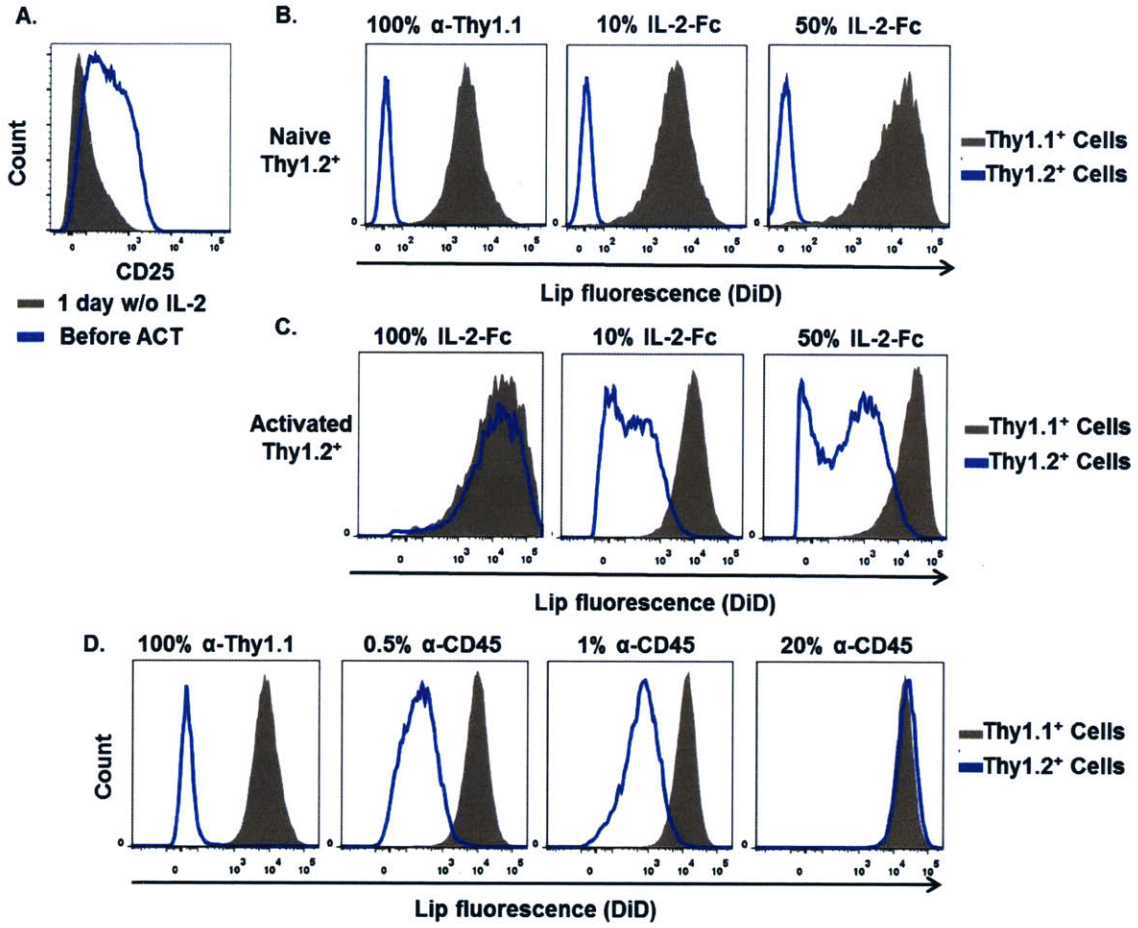

Figure 2-10: *In vitro* targeting of liposomes with dual ligands. (A) CD25 expression was assessed by flow cytometry for activated T cells before adoptive transfer (blue line) and after they were cultured in complete RPMI without IL-2 for one day (grey filled). (B-D) Naïve or C57BL/6 $CD8^+$ T-cells primed with conA/IL-7 + IL-2 for 3 days were mixed with CFSE-labeled activated pmel-1 $CD8^+$ T-cells in a 1:1 ratio. The cell mixture was incubated with 0.05 mg/ml fluorescently-labeled liposomes surface decorated with different mole fractions of IL-2-Fc and anti-Thy1.1 or liposomes conjugated with varying ratios of anti-CD45 and anti-Thy1.1, respectively. After incubation for 30 min at 37°C, unbound particles were washed off and cells were analyzed by flow cytometry. (B) Representative overlaying histograms of activated pmel-1 $Thy1.1^+$ T-cells (grey filled) or naive C57BL/6 $Thy1.2^+$ T-cells (blue line) labeling following incubation with liposomes with 0% (100% anti-Thy1.1, left), 10% (middle) and 50% (right) mole fraction of IL-2-Fc on surface. (C) Representative overlaying histograms of activated pmel-1 $Thy1.1^+$ T-cell (grey filled) or activated C57BL/6 $Thy1.2^+$ T-cell (blue line) labeling following incubation with liposomes with 100% (left), 10% (middle) and 50% (right) mole fraction of IL-2-Fc on surface. (D) Representative overlaying histograms of pmel-1 $Thy1.1^+$ T-cell (grey filled) or C57BL/6 $Thy1.2^+$ T-cell (blue line) labeling following incubation with liposomes having 0% (left), 0.5% (middle left), 1% (middle right) and 20% (right) mole fraction of anti-CD45 on surface.

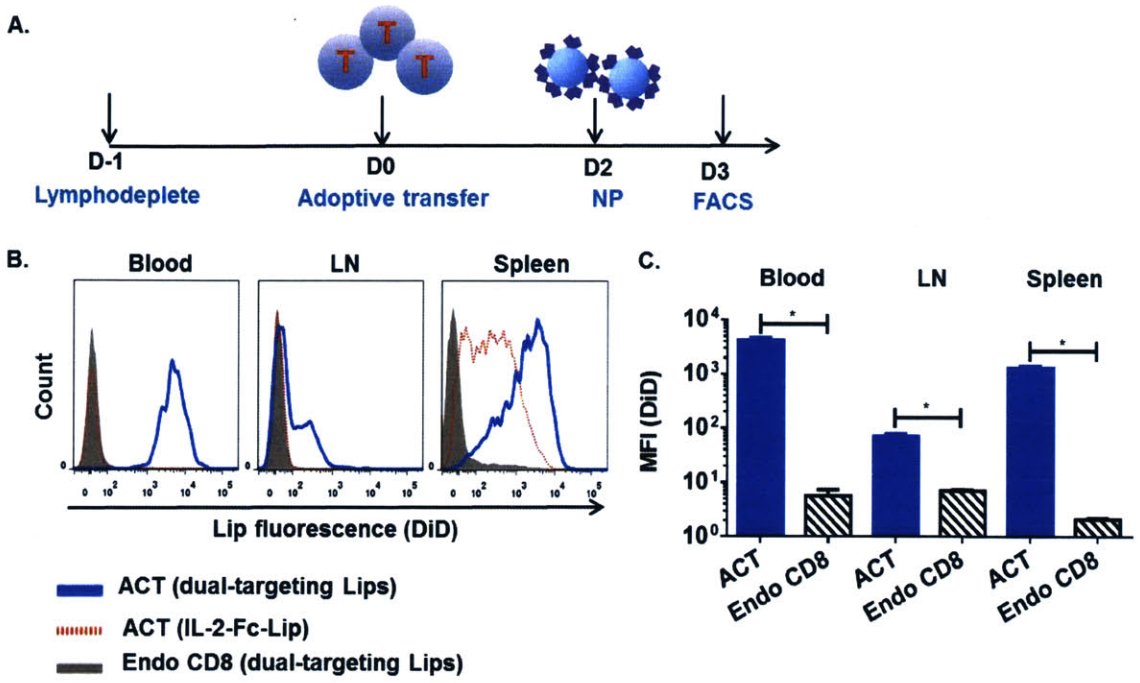

Figure 2-11: Dual-targeting liposomes achieve better targeting efficiency than IL-2-Fc-Lip *in vivo*. C57Bl/6 mice received i.v. adoptive transfer of $15x10^6$ pmel-1 $CD8^+Thy1.1^+$ T-cells, followed by i.v. injection of 0.25 mg IL2-Fc-Lip or 10% IL-2-Fc/90% anti-Thy1.1-Lip 2 days after the T-cells. Liposome binding to cells recovered from lymphoid organs and blood was analyzed 24 hr after liposome injections by flow cytometry. (**A**) Timeline of injections and analysis. (**B**) Representative histograms of endogenous $CD8^+$ T-cell labeling (grey filled) or pmel-1 T-cell labeling by dual targeting liposome (blue line) and IL-2-Fc-Lip (red line). (**C**) Quantification of mean liposome fluorescence intensity of endogenous or transferred T-cells after binding by 10% IL-2-Fc/90% anti-Thy1.1-Lip in the blood, lymph nodes, and spleen. *, $p<0.05$.

2.4 Conclusion

Here we synthesized and characterized antibody-, cytokine- or combinations of antibody/cytokine- decorated immunoliposomes targeting unique cell surface antigens or activation markers on T-cells, respectively. Targeting liposomes bound to ACT T-cells specifically *in vitro,* and further, anti-Thy1.1-Lip also labeled nearly 100% of transferred T-cells in systemic compartments and most of transferred T-cells in LN *in vivo* following a single injection of targeted vesicles. Despite its lower targeting specificity compared to anti-Thy1.1-Lip, IL-2-Fc-Lip was able to repeatedly boost transferred T-cells *in vivo* in tumor-bearing animals and provide direct stimulation to ACT T-cells. IL-2-Fc-Lip also suppressed tumor growth in murine B16F10 tumor model. We focused here on an initial characterization

of *in vitro* and *in vivo* T-cell targeting, and future work will examine the therapeutic efficacy of ACT cell targeting with drug-loaded liposomes. However, these results demonstrate the concept of repeated targeting of ACT T-cells for adjuvant stimulation *in vivo*. This data sets the stage for functional targeting of supporting adjuvant drugs or imaging contrast agents to T-cells, in order to enhance the efficacy of ACT and/or permit longitudinal tracking of ACT T-cells *in vivo*.

3 Enhancing adoptively transferred T-cells function with surface retaining nanoparticles

The work described in this chapter was carried out collaboratively with a postdoctoral associate, Li Tang in the Irvine laboratory. Experiments with IL-15Sa/anti-CD45 nanogels part were done collaboratively unless otherwise indicated in figure caption.

3.1 Introduction

3.1.1 Different internalization rates of nanoparticles

Extensive research has been done to take advantage of internalization of ligand-targeted drugs/nanoparticles for cancer treatment [95-99]. However, much less is known about cell surface receptors that show little/no internalization. We previously reported that IL-2-Fc-conjugated liposomes are rapidly internalized by activated T-cells *in vitro* [65]. Similarly, anti-Thy1.1-Lip also quickly triggered liposome endocytosis [79]. On the contrary, prior work in our laboratory showed that lipid vesicles conjugated to T-cell surface proteins through maleimide-thiol coupling could stay on cell surface for over four days [71, 100]. A mass spectrometry analysis of the surface proteins these multilamellar vesicles bound to most abundantly revealed a candidate pool of receptors which might contribute to the non-internalizing property of the particles [72]. Among them, leukocyte common antigen (CD45), CD11a, CD29, CD97 and CD2 were top hits.

In this chapter, we describe our studies seeking to identify non-internalizing receptors on T-cells that could be used as anchors to block internalization of cell-conjugated nanoparticles. Starting from the list of receptors described above as promising candidate molecules, we identified binding to CD45 as a key contributor to the slow internalization of lipid vesicles, and further discovered that co-binding to CD45 could dominantly suppress internalization triggered by other ligands on a nanoparticle surface. We believe that anti-CD45 can also be generally employed to decorate a broad array of nanoparticles to endow them enhanced stability on cell surfaces for extracelluar drug delivery, tracking, or diagnostic purposes.

3.1.2 IL-15 as a cancer immunotherapy

Both interleukin-2 (IL-2) and interleukin-15 (IL-15) have key roles in maintenance, activation and proliferation of $CD8^+$ T cells and natural killer (NK) cells [101, 102]. Despite their similarities in functions and sharing of IL-2/15R$\beta\gamma_c$ receptors, IL-15 has several advantages over IL-2 as it does not promote activation-induced cell death (AICD), is not associated with capillary leak syndrome, and induce less regulatory T-cell (T_{reg}) expansion [103-107]. IL-15 focuses more on promoting survival of naïve and memory $CD8^+$ T cells [108, 109] and has been proven a more effective adjuvant than IL-2 in adoptive cell therapy in mice [110-112]. In addition, research has shown that IL-15 superagonists (IL-15Sa) formed by complexing IL-15 with a soluble form of its receptor α chain are even more potent

than IL-15 alone as binding of IL-15Rα to IL-15 may create a conformational change that potentiates IL-15 recognition by the $\beta\gamma_c$ receptor on T-cells [113, 114].

Despite the promising pre-clinical results of IL-15, the first clinical trial of IL-15 in humans reached a conclusion that IL-15 elicited serious toxicities due to induction of a cytokine storm [22]. Although researchers have shown that systemic toxicity could be mitigated by continuous i.v injection of small dose of IL-15 in rhesus macaques [115], the practice is inconvenient and maybe impractical in the real clinical setting. Thus, novel ways to deliver safe but also effective doses of IL-15 are in urgent need for IL-15 to move forward as an agent for cancer immunotherapy.

Previously, our lab circumvented the systemic toxicity of adjuvant cytokines by generating T-pharmacytes. Lipid vesicles encapsulating IL-15Sa were conjugated to T-cell surface as "backpacks" of supporting drugs. Loaded cytokines were gradually released out to provide pseudo-autocrine stimulation of the T-cells carrying them [71]. However, the poor encapsulation efficiency, low drug/cargo weight ratio and loss of cytokines during synthesis of lipid vesicles limited the efficacy of the T-pharmacytes approach.

In this chapter, we describe a novel carrier free strategy to allow uniform encapsulation of high levels of protein drugs compared to lipid vesicles. Cytokines were cross-linked by a reversible crosslinker to form nanogels which release cytokines in their native form in reducing environment such as maintained on cell surface [116]. In nanogels, up to 70% of the molecular weight can be the actual protein drugs and there was minimal loss during synthesis. Encouraged by the potency of IL-15Sa, we formed nanogels by cross-linking human IL-15Sa (**Figure 3-1**). IL-15Sa nanogels were conjugated to the surface of adoptively transferred T-cells as backpacks and released IL-15Sa gradually to provide specific stimulation of T-cells carrying them without causing systemic toxicity. However, binding of nanogels formed by IL-2 or IL-15Sa to IL-2Rα and IL-2/15R$\beta\gamma_c$ chain triggered rapid internalization of the complex consistent with the biology of these ligand-receptor interactions [117, 118], causing premature removal of nanogels from cell surfaces and rendering un-released cytokines ineffective (**Figure 3-2**). In order for cross-linked IL-15Sa to be fully released before internalization, it is crucial to find ways to anchor nanogels on cell surface for a prolonged period of time. Thus, cytokine nanogels are the perfect systems to test application of the identified non-internalizing receptor CD45. IL-15Sa nanogels surface decorated with anti-CD45 were retained on T-cell surfaces for over 12 days and elicited prolonged stimulation via the IL-15 signaling pathway, leading to 3-6-fold increases in T-cell proliferation compared to equivalent dose of free IL-15Sa. In a murine tumor model, IL-15Sa/anti-CD45 nanogels specifically expanded adoptively transferred T-cells 16 times more than systemic IL-15Sa, suppressed tumor growth and prolonged the survival of mice. More importantly, IL-15Sa/anti-CD45 nanogels allowed a large dose of IL-15 (~700 μg IL-15 equivalent/kg body weight) to be infused in one injection without systemic toxicity while free IL-15Sa caused severe immunotoxicity.

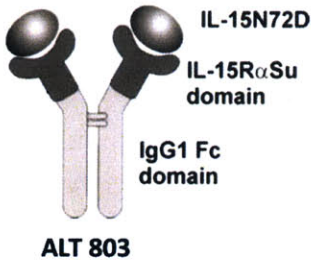

Figure 3-1: Structure of human IL-15Sa. Reproduced from Han, *et al.* [114].

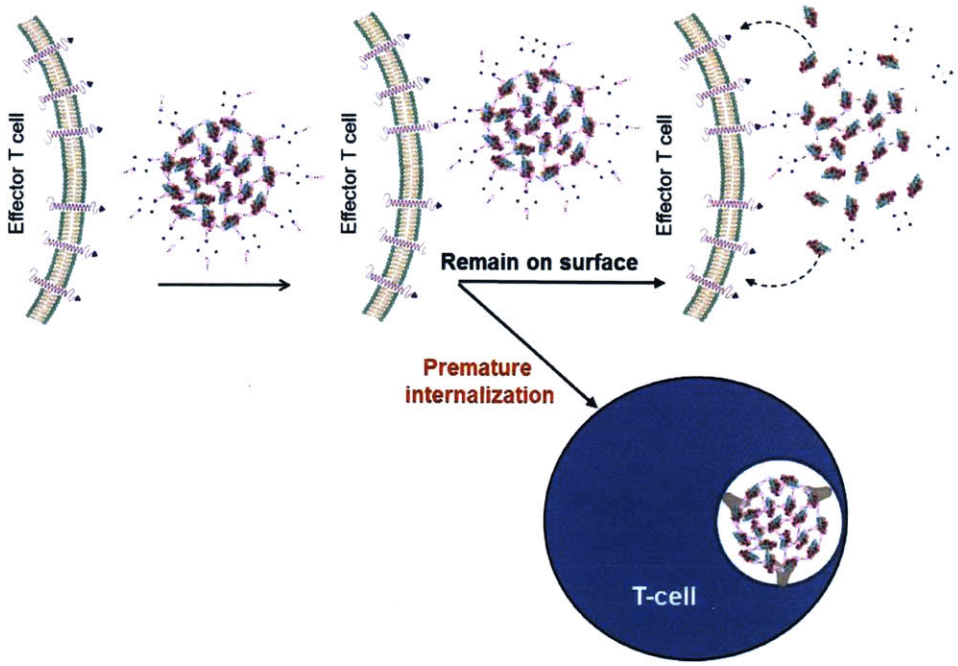

Figure 3-2: Illustration of removal of nanogels from cell surface due to premature internalization.

3.2 Materials and methods

3.2.1 Materials

Anti-CD2, anti-CD45, anti-Thy1.1-PE, anti-Foxp3-Percp-Cy5.5, anti-NK1.1-FITC, anti-ki67-PE-Cy7, Streptivadin-PE-Cy7 and Foxp3/transcription factor staining buffer set were purchased from eBiosceince (San Diego, CA). Anti-CD45RB (clone HB220) and anti-CD11a (clone M17/4) was obtained from BioXCell (West Lebanon, NH). All lipids were from Avanti Polar Lipids (Alabaster, AL) and used as received. Live/Dead fixable Aqua dead cell stain kit and mouse anti-CD3/CD28 dynabeads were obtained from Life Technologies

(Grand Island, NY). AccuCount rainbow fluorescent count beads (10.1 μm) was bought from Spherotech (Lake forest, IL). EZ-Link NHS-LC-LC-Biotin was from Thermo scientific (Tewkbury, MA). Human IL-15Sa was gift from Altor Bioscience (Miramar, FL).

3.2.2 Pmel-1 T-cell activation

Pme-1 splenocytes were activated, Ficoll-Pague Plus gradient separated and isolated as previously described (**Section 2.2.6**). Purified $CD8^+$ T-cells were re-suspended at 0.75×10^6 per ml RPMI containing 10 ng/ml recombinant murine IL-2. After 48 hr, cells were washed 2 times in PBS and re-suspended in HBSS for nanogel conjugation or adoptive transfer.

3.2.3 *In vitro* kinetics study of internalization by using biotin lipids

Vacuum dried lipid films composed of maleimide-PEG_{2000}-DSPE/ cholesterol / HSPC/ 1,2-distearoyl-*sn*-glycero-3-phosphoethanolamine-N-[biotinyl(polyethylene glycol)-2000 (biotin-PEG_{2000}-DSPE) in a molar ratio of 2.5/27/68/1.5 together with 1% of a fluorescent lipophilic tracer dye DiD were rehydrated in 250 μl of 50 mM HEPES/150 mM NaCl-buffer (pH6.5). Lipids were vortexed and liposomes were formed as previously described (**Section 2.2.1**). Concentrations of antibodies used for liposome coupling were measured by Direct Detect (Milipore, Antibody against CD2, CD11, CD45, anti-CD2/anti-CD45 in a molar ratio 1/1 and anti-CD11/anti-CD45 in a molar ratio 1/1 were coupled to maleimide functionalized liposomes as before (**Section 2.2.4**). Antibody-conjugated liposomes (0.7 mg lipids in 100 μl) were incubated with 20×10^6 activated pmel-1 $Thy1.1^+$ T-cells in 0.5 ml complete RPMI supplemented with 10% FCS for 30 min at 37°C with gentle agitation every 15 min. Conjugated T-cells were washed 2x to remove unbound particles and incubated at 0.5 $\times10^6$/ml RPMI media with 1.5 ng/ml recombinant IL-7 and 10% FCS at 37°C. At 0 hr, 19 hr, 49 hr and 69 hr, replicates of cells were spun down, washed once with ice cold FACS buffer before surface-staining with streptavidin-fluorophore. For internalization kinetics study of anti-Thy1.1/anti-CD45 liposomes and IL-2-Fc/anti-CD45 liposomes, anti-Thy1.1/anti-CD45 or IL-2-Fc/anti-CD45 at different molar ratio were coupled to prepared liposomes as previously described. Antibody-conjugated liposomes (0.7 mg lipids in 100 μl) were incubated with 20×10^6 activated pmel-1 $Thy1.1^+$ T-cells in 0.5 ml complete RPMI supplemented with 10% FCS for 30 min at 37°C with gentle agitation every 15 min. After incubation with liposomes, cells were washed 2x to remove unbound particles and incubate in RPMI supplemented by 10% FCS and 1.5 ng/ml IL-7. At 0 hr, 19 hr, 45 hr and 69 hr, replicates of cells were spun and stained by streptavidin-fluorocphore. All samples were analyzed on a BD FACS Canto Flow Cytometer and processed using FlowJo software.

3.2.4 CFSE labeling of cells

Naïve $CD8^+$ T cells were isolated from Pmel-1 splenocytes via magnetic negative selection using an EasySep™ Mouse $CD8^+$ T Cell Enrichment Kit. Isolated $CD8^+$ T cells were re-suspended in 10×10^6 /ml pre-warmed serum free RPMI. CFSE at 5mM in DMSO were added to cells with final concentration at 2 μM before incubation at 37°C for 15 minutes. Staining were quenched by adding at 1:1 volume ratio of cold RPMI with 10% FCS and cells were spun down followed by two more washes in cold RPMI with FCS.

3.2.5 Safety check for anti-CD45-Lips

Naïve $CD8^+$ T-cells were activated by anti-CD3/CD28 beads with 1:1 beads to T-cells ratio for 3 days. After removal of anti-CD3/CD28 beads, activated $CD8^+$ T-cells were CFSE stained and incubated with IL2-Fc-Lip (0.2 μg lipo/ml; 5 ng/mL IL-2 equivalent) in the presence or absence of 0.2 μg/ml α-CD45-Lips. After 2 days, cells were added with counting beads and analyzed by flow cytometry.

3.2.6 Synthesis of anti-CD45 decorated nanogels

Amine reactive cross-linker NHS-SS-NHS (93.5 μg, 0.214 μmol) dissolved in 9.35 μL DMSO was added to human IL-15-Sa (1320 μg, 0.0143 μmol) solution in 132 μL PBS buffer. The mixture was rotated at rt for 30 min followed by the addition of 1188 μL PBS buffer. Mouse anti-CD45 (215 μg, 0.0014 μmol) in 31.7 μL PBS buffer was then added to the diluted solution. The reaction mixture was rotated at rt for another 30 min. The resultant hIL-15-Sa nanogels with surface-coated anti-CD45 was collected with Millipore Amicon ultra-centrifugal filter (molecular weight cutoff = 100, 000 Da) and washed with PBS (1.5 mL × 3). The purified h IL-15-Sa nanogels solution was diluted to 1 μg/μL followed by the addition of $mPEG_{5K}$-*b*-PLKC (43.6 μg, 0.0011 μmol) in 43.6 μL PBS. The mixture was rotated at rt for 30 min and used without further purification. The final concentration of h IL-15-Sa nanogels was determined with Nanodrop (A280). The purified hIL-15-Sa nanogel was stored in PBS at 4 °C before use. IL-2-Fc nanogels was prepared in the same way.

To prepare hIL-15Sa nanogels with biotin labeling, EZ-Link NHS-LC-LC-Biotin (40.6 μg, 0.072 μmol) in 7.5 μL DMSO was added to the mixture after amine reactive cross-linker reacted with hIL-15Sa. The mixture was then diluted with 1188 μL PBS buffer and added with mouse anti-CD45 (215 μg, 0.0014 μmol) in 31.7 μL PBS buffer. The following reaction and washing steps were the same as nanogels without biotin.

3.2.7 Conjugation of nanogels to T-cell surface

In a typical experiment, h IL-15-Sa nanogels (950 μg) in 950 μL PBS was added to activated or naïve $CD8^+$ T cells (95 million, 475 μL HBSS) followed by incubation at 37 °C for 1 hr with gentle agitation every 15 min. The T cells with surface conjugated h IL-15-Sa nanogels were collected by centrifugation at 800 rcf, washed with PBS (1.0 mL × 2), and resuspended in HBS (50×10^6/ml) for injection to mice or for *in vitro* experiments. Supernatants from all washes were collected to determine the amount of unbound hIL-15-Sa nanogels in the supernatant, thus the amount of conjugated hIL-15-Sa nanogels on T-cells.

3.2.8 *In vitro* kinetics study of internalization of Nanogels

Biotin labeled IL-2-Fc and IL-15Sa nanogels were synthesized with or without anti-CD45 on the surface. Nanogels were incubated with activated $CD8^+$ T-cells (IL-2-Fc nanogels) or CFSE stained naïve $CD8^+$ T-cells (IL-15Sa nanogels) for 1 hr at 37°C in HBSS. T-cells were washed 2x to remove unbound nanogels and were incubated in RPMI with 10% serum. For the experiment with IL-15Sa nanogels, naïve $CD8^+$ T-cells were also supplemented with anti-CD3/CD28 beads at 1:2 T-cells to beads ratio. At staggered time points, replicates of cells were added with counting beads, collected, washed once with ice cold FACS buffer and then stained with streptavidin-fluorophore to detect surface-localized

nanogels followed by flow cytometry analysis. For experiment with IL-15Sa nanogels, the fluorescence intensity of streptavidin-fluorophore was also normalized by the CFSE (FTIC) fluorescence to account for the decrease in streptavidin-fluorophore fluorescence due to cell proliferation. All samples were analyzed on a BD FACS Canto Flow Cytometer and processed using FlowJo software.

3.2.9 *In vitro* proliferation of T cells with IL-15Sa/anti-CD45 Nanogels

CFSE labeled naïve Pmel-1 $CD8^+$ T cells were conjugated with IL-15Sa, IL-15Sa nanogels and IL-15Sa/anti-CD45 nanogels respectively as previously described. After removing unbound IL-15Sa or nanogels, T-cells (0.1×10^6 per well) were resuspended in RPMI with 10% FCS and added with anti-CD3/CD28 beads at a 1:3 beads to T-cells ratio in 96-well plates. Free IL-15Sa were added to control group at 700 ng/ml to match the amount of IL-15Sa conjugated to T-cells in IL-15Sa/anti-CD45 group. Activated Pmel-1 $CD8^+$T cells were conjugated with IL-15Sa/anti-CD45 nanogels and incubated in complete RPMI with 10% FCS. Control group was added 3.6 μg /10^6 T-cells to match the actual IL-15Sa amount conjugated to T-cells in IL-15Sa/anti-CD45 group. Replicates of T-cells were added with counting beads and spun every day. All samples were re-suspended in FACS buffer before flow cytometry analysis on BD FACS Canto Flow Cytometer.

3.2.10 *In vivo* therapy with IL-15Sa/anti-CD45 nanogels

B16F10 melanoma cells were suspended at 0.5×10^6 cells per 200 μl in HBSS and inoculated subcutaneously (*s.c.*) to induce tumor in C57Bl/6 mice (Jackson Laboratory, Bar Harbor, ME) (Day 0). Animals were then sublethally lymphodepleted by total body irradiation (5 Gy) 5 days post tumor inoculation (Day 5). Activated Pmel-1 $CD8^+$ T-cells were washed 2 times in PBS and re-suspended in HBSS for incubation with IL-15Sa/anti-CD45 nanogel or equivalent volume of HBSS.

For FACS analysis, activated Pmel-1 $CD8^+$ T-cells or T-cells with nanogel backpacks were re-suspended at 13.5×10^6 per 100 μl HBSS and administered i.v. one day after lymphodepletion (Day 6). HBSS or 57 μg of free IL-15Sa was injected i.v. immediately after adoptive transfer. Mice were sacrificed on day 13 for necropsy and flow cytometry study. For high dose IL-15Sa tumor growth study, one day after lymphodepletion (Day 6), activated T-cells or T-cells with nanogel backpacks at 11×10^6 per 100 μl HBSS were i.v. infused. HBSS, 10 μg and 40 μg of free IL-15Sa were injected i.v. immediately after adoptive transfer. The group received 10 μg IL15-Sa was boosted with three more doses of 10 μg IL15-Sa on day 8/10/12. For lower dose IL-15Sa long term tumor growth, 5 μg and 20 μg of free IL-15Sa were injected i.v. immediately after adoptive transfer of 14×10^6 T-cells. The group received 5 μg IL15-Sa was boosted with three more doses of 5 μg IL15-Sa on day 9/12/15.

Tumor size was measured every two days since adoptive transfer and tumor area was calculated as the product of 2 measured orthogonal diameters (D_1xD_2). Body mass of treated mice was measured daily as an indicator of overall body condition and systemic toxicity.

3.2.11 Necropsy and sample preparation for flow cytometry analysis

Inguinal lymph nodes and spleens were ground through a 70 μm cell strainer and washed once with ice cold PBS. Splenocytes were then lysed with ACK lysis buffer (1 ml per spleen) for 4 min at 25°C to remove red blood cells before washing in ice cold FACS buffer (PBS

with 1% Bovine Serum Albumin). Blood samples were lysed with 2X 1ml ACK lysis buffer for 5 min at 25°C and then washed 1x with ice cold PBS. Tumors were weighed and ground through a 70 μm cell strainer and washed once with ice cold FACS buffer. All cells were added with counting beads and washed in ice cold PBS once before Aqua live/dead staining. After Aqua staining, cells were washed 1x in FACS buffer followed by surface-staining with Ab. Cells were then washed 1x in FACS buffer, fixed, permeabilized and intracellularly stained for Foxp3 and ki67. After one wash in FACS buffer, cells were re-suspended in FACS buffer before analyzing on a BD FACS Canto Flow Cytometer. All data was processed using FlowJo software.

3.2.12 Statistical analysis

Statistical analysis was done using GraphPad Prism software and two-tailed unpaired t-tests were conducted between groups of experimental data. Graphs show the mean ± SEM of sample groups. Tumor growth curves were compared using two-way ANOVA, and Kaplan-Meier survival curves were compared by log rank test.

3.3 Results and discussion

3.3.1 Discovery of CD45 as a dominant non-internalizing receptor

3.3.1.1 Identification of slowly internalizing receptors

We previously showed that conjugation of multilamellar lipid vesicles to T-cell surfaces through maleimide-thiol coupling provided stable retention of ~200 nm particles on the surfaces of T-cells over extended time periods of many days in vitro [71]. However, why these particles were not endocytosed remained unclear. To test whether the lipid vesicles were non-internalized due to their size, we coupled anti-CD8 to liposomes with similar diameter and tested the internalization rate of anti-CD8 liposomes when bound to cell surface. Liposomes were firstly produced by hydrating dried high-T_M phospholipid films containing 2.5% PEG-maleimide and 1.5% biotin head groups before decoration with anti-CD8. Anti-CD8 liposomes were then incubated with $CD8^+$ T cells to allow liposome binding for 30 minutes at 37°C. Unbound liposomes were washed off before T-cells were incubated in RPMI media at 37°C. At different time points, replicates of cells were stained by streptavidin-fluorophore and analyzed by flow cytometry (**Schematic 3-1**). Only T-cells with surface-bound liposomes would be fluorescently labeled as streptavidin-dye did not have access to internalized liposomes. Instead of remaining on cell surface, these liposomes were internalized readily over 3 days (**Figure 3-3A, B**). Thus particle size should not be a contributing factor to the long surface retention and the interaction between particle maleimide and cell surface thiol might play a role. We previously used mass spectrometry to determine what proteins the particles anchored to on the cell surface [72], and identified CD2, the α and β chains of the T-cell integrin LFA-1 (CD11a and CD29, respectively), and CD45 as key anchoring proteins. We thus focused on these candidate cell surface receptors and prepared antibody targeting or dual-targeting liposomes against each of these molecules. Individual antibodies (Ab) against respective surface receptors (CD2, CD45, or CD11a), or combinations of anti-CD2/anti-CD45 at 1:1 molar ratio or anti-CD11/anti-CD45 at 1:1 molar ratio were coupled to biotin functionalized liposomes via maleimide-thiol reactions. Among

the three receptors, CD45 internalized the slowest. After 3 days, almost 100% of cells still had α-CD45-Lip anchoring on their surface while surface anti-CD2-Lip were only found on about 30% of cells after 19 hr and anti-CD11a-Lip was only on about 65 % of T-cells surface after 3 days. (**Figure 3-4A, B**). More importantly, the non-internalizing property of CD45 dominated over the faster internalization receptors CD2 and CD11. When anti-CD45 was used in combination with anti-CD2 or anti-CD11 to surface decorate liposomes, anti-CD2/anti-CD45-Lip and anti-CD11/-anti-CD45-Lip remained on the surface of nearly 100% of cells after three days regardless of binding to the faster internalization receptor CD2 or CD11 (**Figure 3-4A, B**).

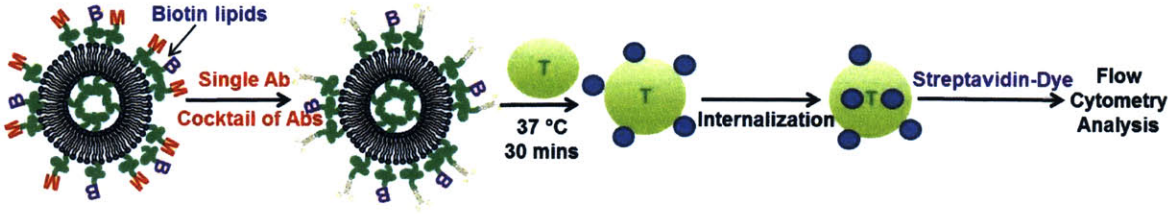

Schematic 3-1: Illustration of using biotin lipids and streptavidin conjugate dye to detect liposomes on cell surface.

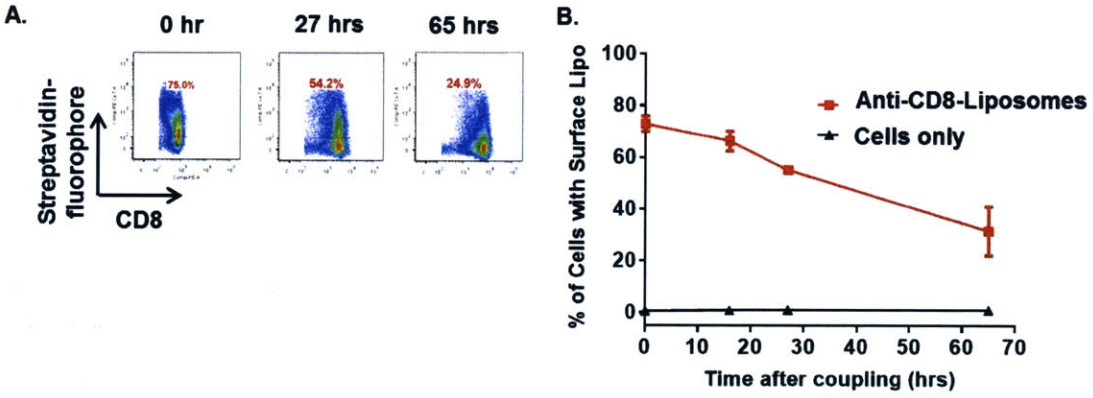

Figure 3-3: Anti-CD8 liposomes with 200 nm diameter get internalized over time. Activated $CD8^+$ T cells were incubated with anti-CD8 liposomes for 30 minutes at 37°C in complete RPMI. Unbound particles were washed off and cells were further incubated at 37°C in complete RPMI supplemented with 1ng/ml IL-7. At staggered time points, cells were stained by streptavidin-fluorophore and analyzed by flow cytometry. (**A**) Representative flow cytometry plots illustrating percentage of cells with surface liposomes. (**B**) Percentage of fluorescently labeled cells with anti-CD8 liposomes were plotted over time.

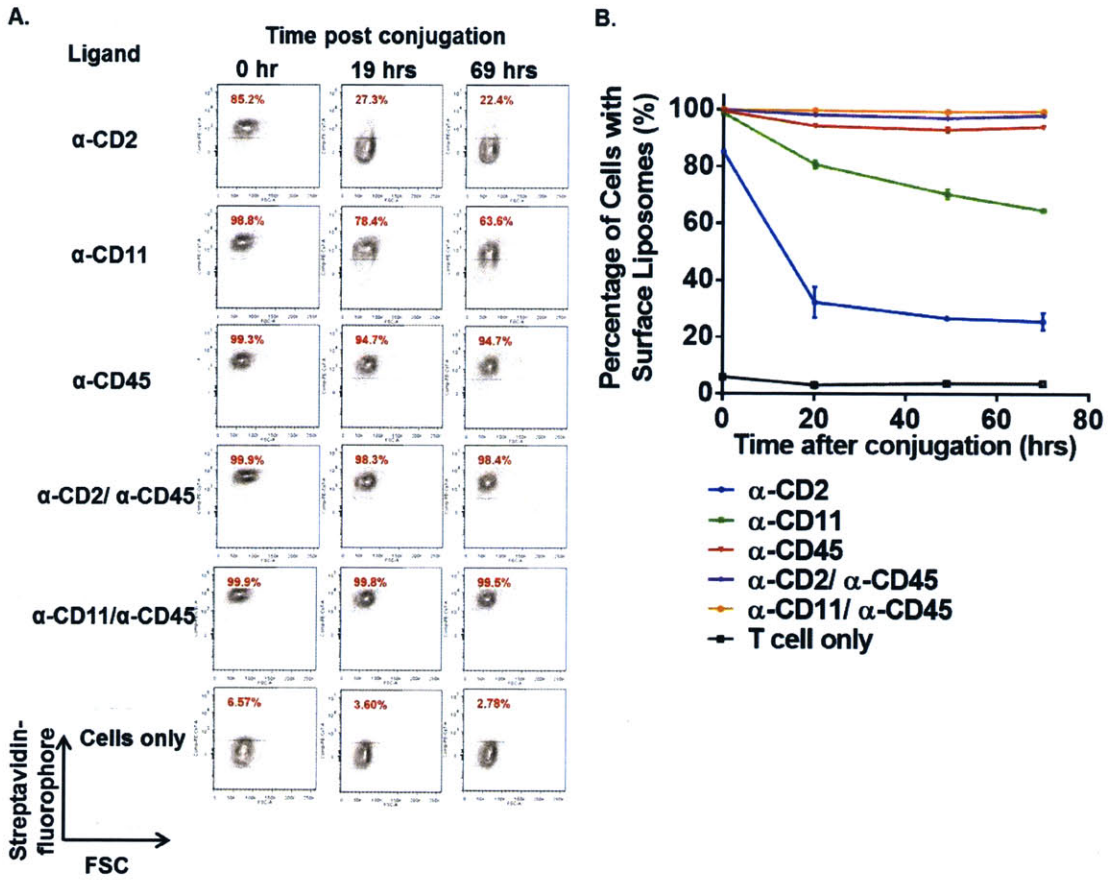

Figure 3-4. Anti-CD45 liposomes remain non-internalized for days. Internalization kinetics of anti-CD2-Lip, anti-CD11-Lip, anti-CD45-Lip, anti-CD2/α-CD45-Lip (1:1 molar ratio) and anti-CD11/anti-CD45-Lip (1:1 molar ratio). Activated $CD8^+$ T cells were incubated with respective liposomes for 30 minutes at 37°C in complete RPMI. Unbound particles were washed off and cells were further incubated at 37°C in complete RPMI. 0 hr, 19 hr, 49 hr and 69 hr after conjugation, cells were stained by streptavidin-fluorophore and analyzed by flow cytometry. (**A**) Representative flow cytometry plots illustrating percentage of cells with various surface liposomes. (**B**) Percentage of fluorescently labeled cells with anti-CD2-Lip (blue), anti-CD11-Lip (green), anti-CD45-Lip (red) , anti-CD2/α-CD45-Lip (purple) and anti-CD11/anti-CD45-Lip (orange) and T cells alone (black) were plotted over time.

3.3.1.2 Small quantities of anti-CD45 slow internalization of liposomes that co-display ligands for rapidly internalizing receptors

To further confirm the non-internalizing behavior of CD45, we tested it together with two rapidly internalizing receptors we had previously characterized- IL-2R and Thy1. Anti-CD45-Lip, IL-2-Fc-Lip, anti-Thy1.1/anti-CD45-Lip and IL-2-Fc/anti-CD45-Lip were synthesized as previously described. After conjugation to activated T-cells, more than 90% of IL2-Fc-Lip and 70% of anti-Thy1.1-Lip were internalized within 19 hours (**Figure 3-5A, B**). However, co-coupling of just 1 mol% of anti-CD45 together with anti-Thy1.1 led to 50% of

cells having anti-Thy1.1/anti-CD45 liposomes on their surface by 19 hrs and 33% of cells with surface liposomes even by 69hr, when all anti-Thy1.1-Lip have been internalized. Strikingly, inclusion of 5 mol% of anti-CD45 reversed the fast internalization of both IL-2R and Thy1, assuring almost 100% of cells retained surface-bound liposomes after 3 days *in vitro* (**Figure 3-5A, B**).

When activated T-cells were co-incubated with IL-2-Fc-Lip (0.2 μg/ml) and anti-CD45-Lip (0.2 μg/ml), the presence of anti-CD45-Lip did not affect T-cells proliferation as cell counts were about the same (**Figure 3-6**). It indicates that firstly binding of CD45 did not negatively interfere with IL-2 signaling despite the fact that CD45 is a protein tyrosine phosphatase [119] while IL-2/IL2-R triggers complex signaling cascade by tyrosine phosphorylation [120]. Secondly, this extent of crosslinking of CD45 with targeting liposomes, in the presence of IL-2 signaling, also did not elicit overt toxicity as observed in co-crosslinking anti-CD45 mAb on thymocytes [121] or naïve T lymphocytes when co-crosslinking with T-cell receptor (TCR) [122]. This might be due to the change in signaling pathways for activated T-cells or difference in ligand spacing between 200 nm liposomes and smaller secondary antibodies or larger 6 μm beads [123].

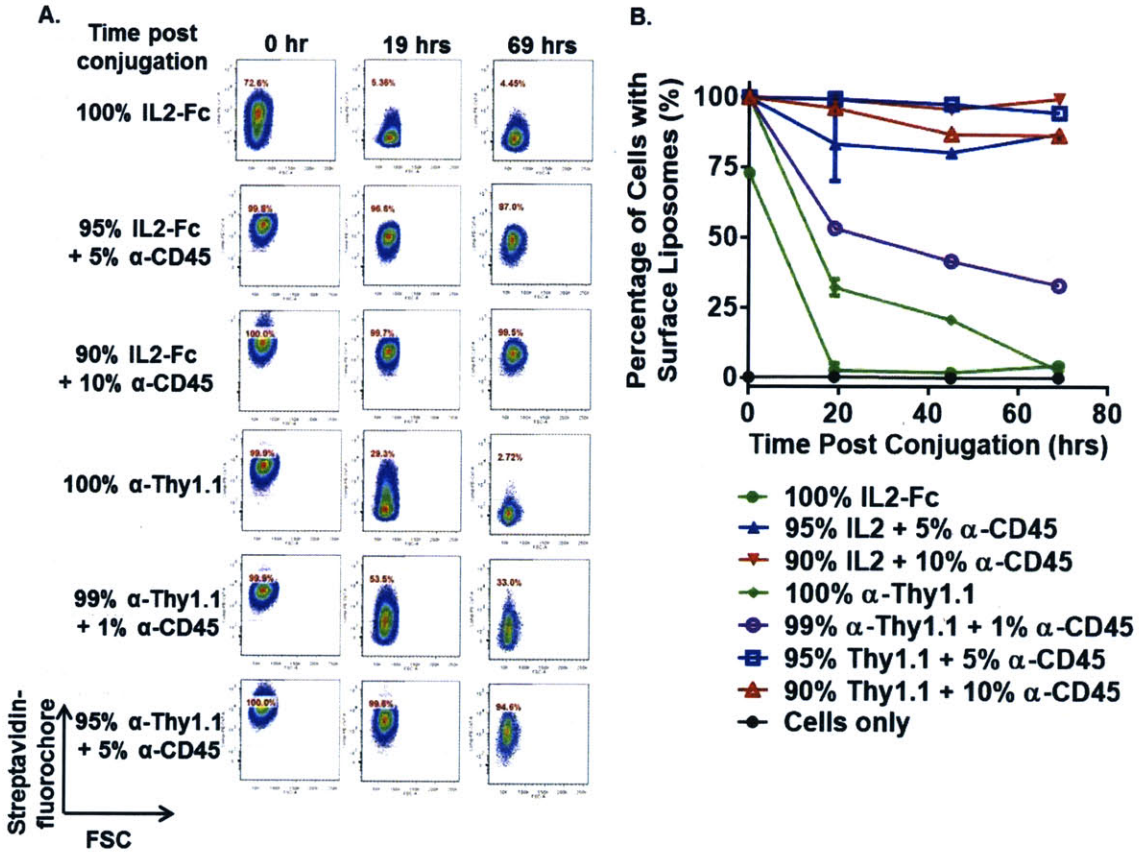

Figure 3-5: Co-functionalization of liposomes with anti-CD45 limits internalization triggered by IL-2-Fc or anti-Thy1.1. Internalization kinetics of liposomes with surface-

decorated IL2-Fc, α-Thy1.1, mixture of IL2-Fc/α-CD45 or mixture of α-Thy1.1/α-CD45. Activated $CD8^+$ T cells were incubated with respective liposomes for 30 minutes at 37°C in complete RPMI. Unbound particles were washed off and cells were incubated at 37°C in complete RPMI. 0hr, 19hr, 45hr and 69hrs after conjugation, cells were stained by streptavidin-fluorophore and analyzed by flow cytometer. FACS sample plots of fluorescently labeled cells at different time points (**A**). A quantification of percentage of cells with surface labeled lipos over time (**B**).

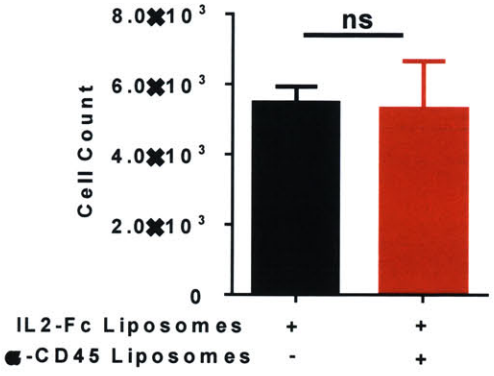

Figure 3-6: Binding of CD45 liposomes does not affect T cell proliferation. CFSE stained activated $CD8^+$ T-cells were incubated with IL2-Fc-Lip (0.2 μg/ml) in the presence or absence of 0.2 μg/ml anti-CD45-Lip. After 2 days, cells were added with counting beads and analyzed by flow cytometry. Cell numbers were counted by flow cytometer.

3.3.2 Synthesis of cytokine nanogels

To test the value of anti-CD45-mediated cell surface "trapping" of nanoparticles, we sought to apply this approach to a novel nanoparticle formulation developed in the laboratory. We previously used lipid vesicles encapsulating therapeutic proteins as drug carriers to be linked to T-cell surfaces [71]. However, a limitation of liposome-based drug carriers is the inconsistency and generally poor encapsulation efficiency for proteins in general. To overcome this issue, Dr. Li Tang in the laboratory developed a novel "carrier free" strategy for formation of drug-based nanoparticles. In this approach, an amine-reactive crosslinker NHS-S-S-NHS reversibly cross-linked cytokines (IL-2-Fc or IL-15Sa) in solution, forming nanogels with mean diameters of 85.6 ± 1.9 nm (**Schematic 3-2A**, **Figure 3-7A, B**). In a reducing environment such as maintained at the surface of T-cells [116], the disulfide bond in the linker will be reduced to release the native form of IL-2-Fc or IL-15Sa (**Schematic 3-2B**). However, in order for these cytokine nanogels to continuously signal to their carrier cell, nanogels need to retained on cell surfaces to gradually release cytokines for prolonged stimulation of IL-2Rα or the shared IL-2/15Rβγ complex, which are also present on cell surface [86, 103, 104].

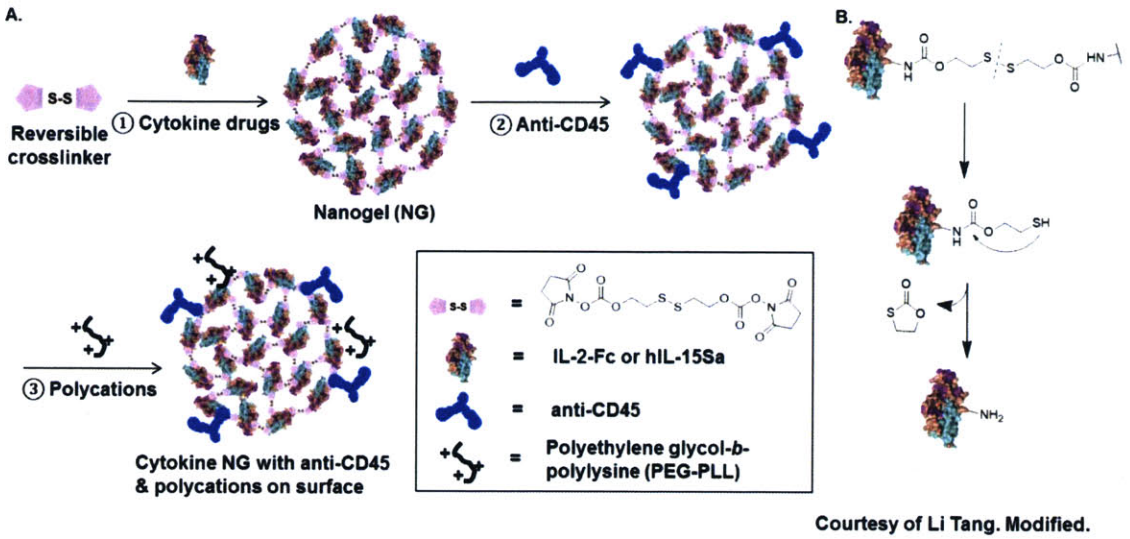

Schematic 3-2: Preparation and surface modification of cytokine nanogels for cell surface coupling.

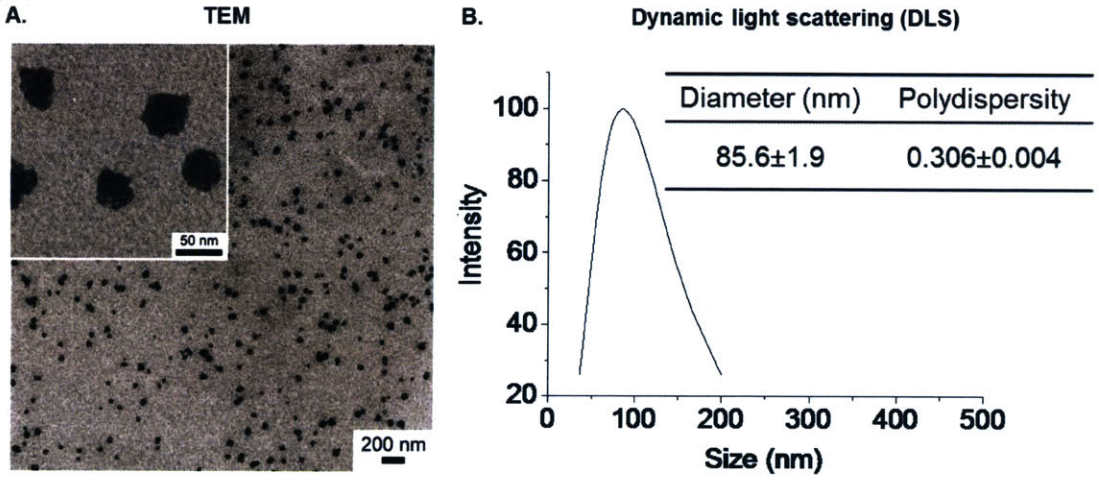

Figure 3-7: Size of nanogels. (**A**) Particle size measured by transmission electron microscopy (TEM). (**B**) Particle size measured by dynamic light scattering. Courtesy of Li Tang.

3.3.3 Anti-CD45 enabled stable anchoring of IL-2-Fc and IL-15Sa nanogels on T-cell surfaces

To couple IL-2-Fc or IL-15Sa nanogels to T-cells, we coated the particles with a low density of low molecular weight poly-L-lysine, to promote initial electrostatic adsorption of the nanogels to T-cells prior to antibody/cytokine conjugation to respective receptors. However, coupling of nanogels containing only the cytokines led to rapid clearance of

nanogels from the cell surfaces due to rapid internalization of IL-2R or IL-2/15R$\beta\gamma_c$. More than 75% of cells lost surface IL-2-Fc nanogels due to rapid IL-2R internalization over 1 day. After three days, almost all nanogels had been internalized (**Figure 3-8A**). Similarly, 90% of IL-15Sa nanogels were internalized within three days (**Figure 3-8B**). To block internalization, we prepared nanogels that co-incorporated a small quantity (10 mol% relative to IL-2-Fc) of anti-CD45 into the nanogel network (**Schematic 3-2A**). In contrast to the cytokine-only nanogels, almost 100% of T-cells still had IL-2-Fc/anti-CD45 nanogels remaining on surface after three days (**Figure 3-8A**). For IL-15Sa nanogels, anti-CD45 retained them on cell surface even for more than 12 days, greatly expanding the lifetime of nanogels without premature internalization (**Figure 3-8B**). The gradual drop of percentage of cells with surface IL-15Sa/anti-CD45 nanogels was probably due to the loss of biotin when nanogels gradually broke down to release cytokines.

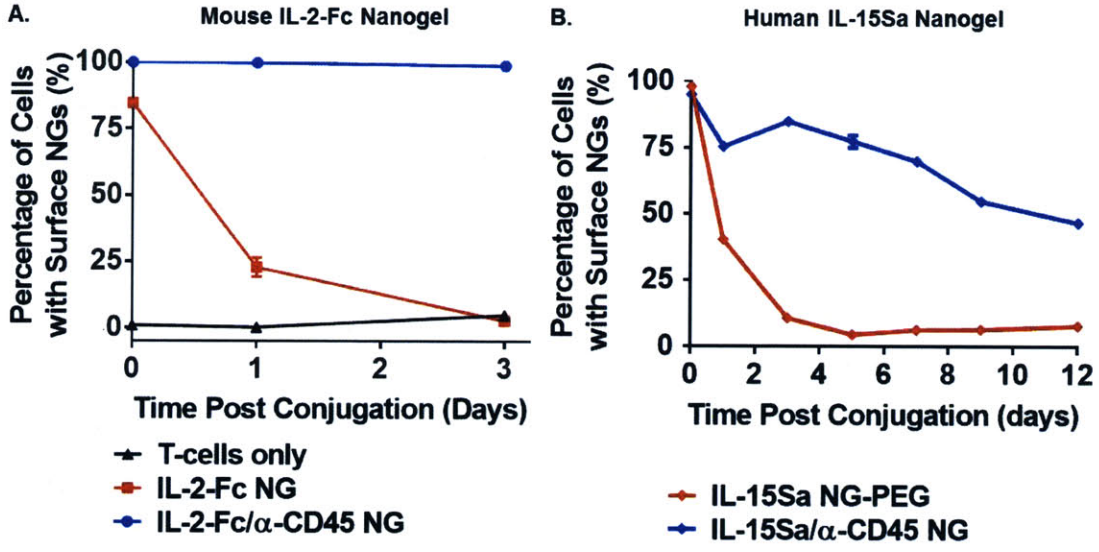

Figure 3-8: Anti-CD45 enables stable anchoring of nanogels on T-cells surface. Biotin-labeled IL-2-Fc and IL-15Sa nanogels were synthesized with or without surface anti-CD45. Nanogels were incubated with activated $CD8^+$ T cells (IL-2-Fc nanogels) or CFSE stained naïve $CD8^+$ T-cells (IL-15Sa nanogels) for 1 hr at 37°C in HBSS. T-cells were washed 2X to remove unbound nanogels and then incubated in RPMI with 10% serum. For the experiment with IL-15Sa nanogels, naïve $CD8^+$ T-cells were also supplemented with anti-CD3/CD28 beads at 1:2 T-cells to beads ratio. At staggered time points, replicates of cells were collected and stained with streptavidin-fluorophore to detect surface-localized nanogels followed by flow cytometry analysis. For experiment with IL-15Sa nanogels, the fluorescence intensity of streptavidin-fluorophore was also normalized by the CFSE (FTIC) fluorescence to account for decrease in streptavidin-fluorophore fluorescence due to cell proliferation. (**A**) Percentage of T-cells with IL-2-Fc nanogels on surface over three days. (**B**) Percentage of T-cells with IL-15Sa nanogels on surface over 12 days.

3.3.4 Surface retained nanogels allowed greater proliferation of both naive and activated T cells *in vitro*

Stable anchoring of IL-15Sa/anti-CD45 nanogels to cell surfaces should permit prolonged stimulation of the T-cells carrying them. This might be due to the combined effects of 1) longer surface retention of IL-15Sa/anti-CD45 nanogels thus more IL-15Sa released before internalization and/or 2) more IL-15Sa conjugated to the cell surfaces. After conjugation, the mean fluorescence intensity on T-cells increased 16 times with the addition of anti-CD45 on surface (**Figure 3-9A**) corresponding to an increase in loading of IL-15Sa from 0.9 μg to 3 μg/$\times 10^6$ T-cells. When naïve $CD8^+$ T cells were suboptimally activated, the presence of anti-CD45 in the nanogels induced a 3-fold increase in T-cell expansion compared to IL-15Sa nanogels without anti-CD45 (**Figure 3-9B**). CFSE proliferation patterns of T-cells further confirmed that IL-15Sa/anti-CD45 nanogels were more potent in inducing cell proliferation compared to conjugated IL-15Sa nanogels (**Figure 3-9C**). Interestingly, IL-15Sa/anti-CD45 nanogels also induced more CFSE dilution and a 3-fold increase in cell number for naïve T-cells and 6-fold increase for activated T cells compared to equivalent doses of free IL-15Sa *in vitro* (**Figure 3-9B, C, D**).

Next, we assessed whether the additional T-cell proliferation stimulated by nanogels was due to prolonged IL-15 signaling from surface-anchored IL-15Sa/anti-CD45 nanogels. STAT5 is a downstream phosphorylation target of IL-15 signaling and is an essential signal transducer for effector $CD8^+$ T cell survival and proliferation [124-126]. We also tried to look into Ki67 which is a proliferation marker [127, 128] and has been used as a predictive and prognostic marker in cancer [129, 130]. We evaluated the amount of phosphorylated STAT5 and Ki67 in naïve $CD8^+$ T-cells during suboptimal activation by anti-CD3/CD28 beads with a 1:2 beads to T-cells ratio over 13 days. T-cells were either conjugated with IL-15Sa/anti-CD45 nanogels or pulsed with an equivalent dose of free IL-15Sa for 1 hr. Both T-cells alone and T-cells with free IL-15Sa had upregulated pSTAT5 on day 1. This transient upregulation went down on day 3 and the amount of pSTAT5 of the two groups remained similar afterwards (**Figure 3-10A, B**). However, IL-15Sa/anti-CD45 nanogels allowed T-cells to have prolonged upregulation of STAT5 with pSTAT5 peaked on day 3 and gradually declined afterwards. Even on day 13, pSTAT5 was still more than 3 time upregulated compared to the free IL-15Sa group (**Figure 3-10A, B**). Similarly, IL-15Sa/anti-CD45 nanogels increased Ki67 in T-cells for over 13 days with maximum on day 3, corresponding to the pSTAT5 upregulation pattern (**Figure 3-10A, C**). This indicated that conjugated IL-15Sa/anti-CD45 nanogels continued to stimulate T-cells even after 13 days.

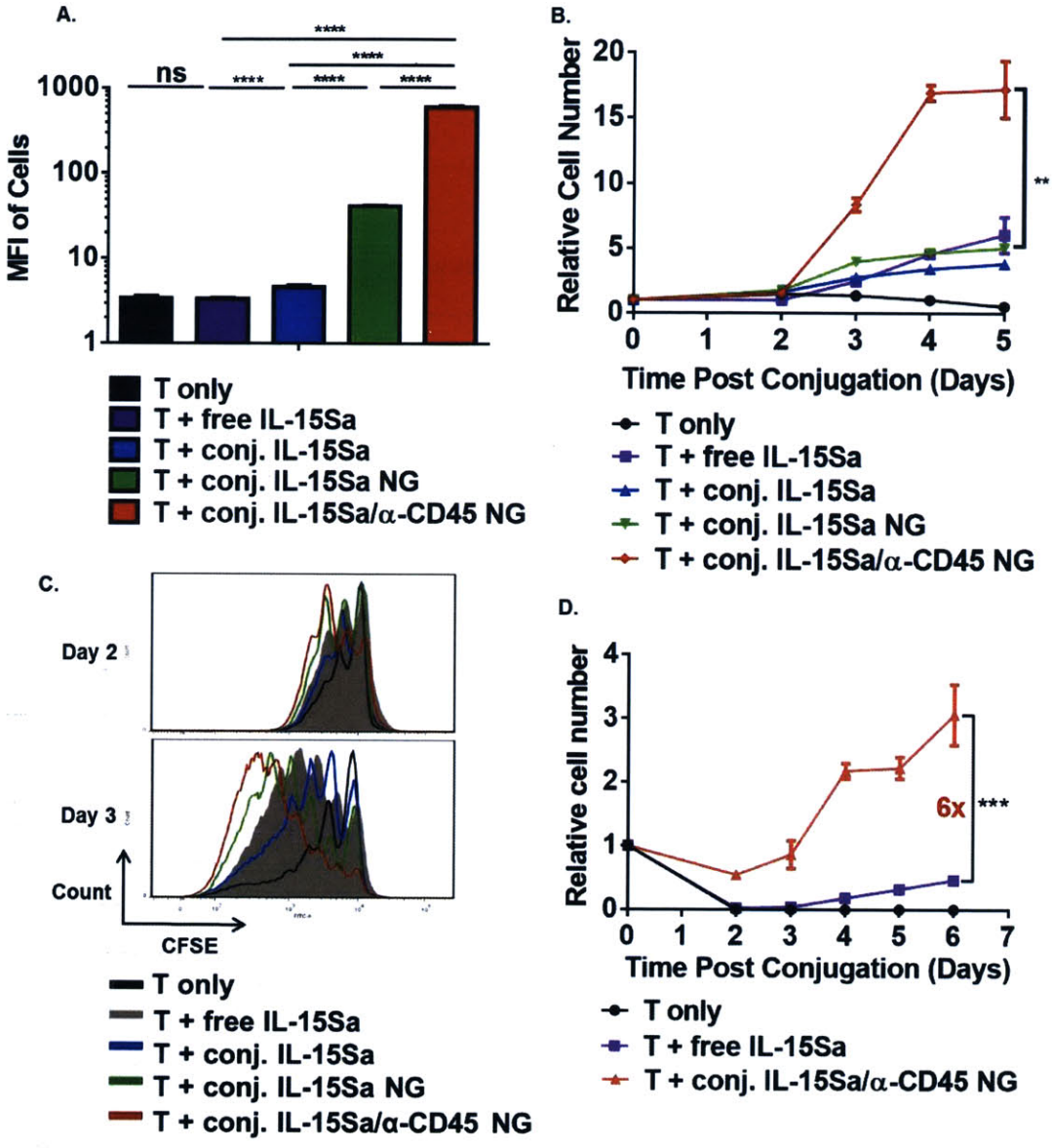

Figure 3-9: Stable surface IL-15Sa/α-CD45 nanogel allow greater T cell expansion *in vitro*. (**A-C**) CFSE stained naïve pmel-1 $CD8^+$ T cells were activated by anti-CD3/CD28 beads with a 3:1 T cells to beads ratio. T cells were either supplemented with free IL-15Sa (0.7 μg/ml) or conjugated with IL-15Sa (0.4 μg/10^6), IL-15Sa nanogel (0.9 μg/10^6) or IL-15Sa/α-CD45 nanogel (3 μg/10^6) before addition of beads. (**A**) Mean fluorescence intensity of T-cells after conjugation was measured by flow cytometry. (**B**) Cell numbers were monitored every day and relative cell numbers normalized to that on day 0 were plotted over time. (**C**) CFSE proliferation pattern of respective group were overlaid for day 2 and day 3. (**D**) Activated pmel-1 $CD8^+$ T-cells were conjugated with 3.6 μg/10^6 IL-15Sa/anti-CD45 nanogel, washed and resuspended in complete RPMI with 10% FCS. Another group of T-cells were supplemented with 1.2 μg/ml of soluble IL-15Sa. Cell numbers were monitored every day and relative cell number were plotted over time.

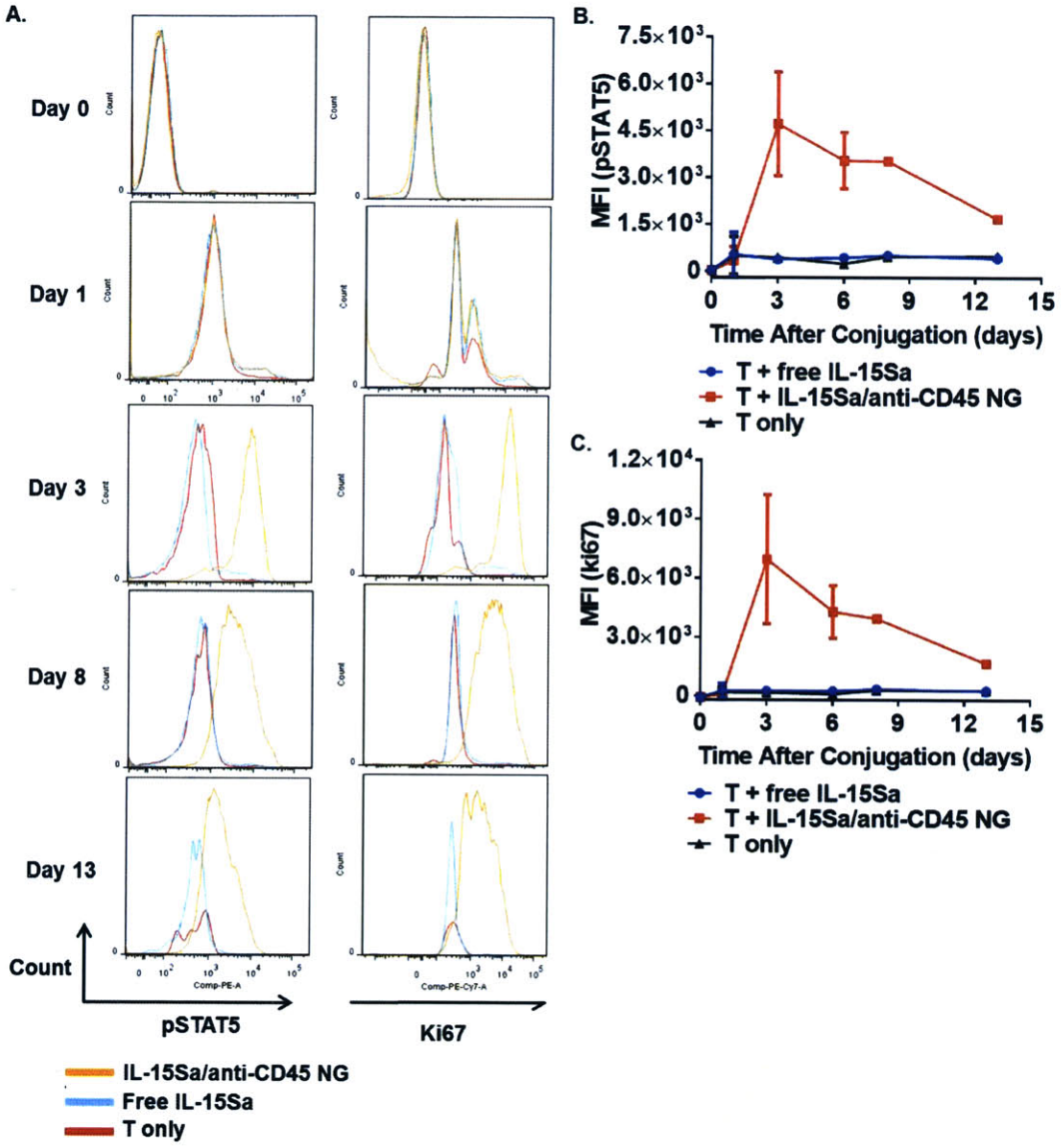

Figure 3-10: IL-15Sa/anti-CD45 nanogels prolong activation of IL-15 signaling pathway and maintain T-cell proliferation. Naïve $CD8^+$ T-cells were conjugated with IL-15Sa/anti-CD45 nanogels or pulsed with equivalent dose of free IL-15Sa before resuspension in complete RPMI with 10% serum. Anti-CD3/CD28 beads were added to all groups with 1:2 beads to T-cells ratio. Replicates of cells were stained for pSTAT5 and ki67 on day 0, 1, 3, 6, 8 and 13 and analyzed by flow cytometry. (**A**) Sample histograms of pSTAT5 (left) and ki67 (right) expression of T-cells on day 0, day 1, day 3, day 8, and day 13. (**B**) Quantification of mean fluorescence intensity of pSTAT5 of T-cells (black), T-cells pulsed with free IL-15Sa (blue) and T-cells conjugated IL-15Sa/anti-Cd45 nanogels (red) over time. (**C**) Quantification of mean

fluorescence intensity of Ki67 of T-cells (black), T-cells pulsed with free IL-15Sa (blue) and T-cells conjugated IL-15Sa/anti-Cd45 nanogels (red) over time.

3.3.5 IL-15Sa/anti-CD45 nanogels specifically expanded ACT T cells in murine tumor and suppressed tumor growth without overt toxicity

To test the potential functional impact of IL-15Sa/anti-CD45 nanogels, we assessed the response of transferred pmel-1 melanoma-specific T-cells *in vivo* during an ACT treatment in B16F10 solid tumor model. B16F10 tumor cells (0.5×10^6) were subcutaneously inoculated into Thy1.2$^+$ C57Bl/6 mice and allowed to establish tumors for 5 days. Animals were then sublethally lymphodepleted by irradiation and received i.v. adoptive transfer of 13.5×10^6 activated pmel-1 Thy1.1$^+$ CD8$^+$ T-cells the next day (Day 6). In one group of animals, T-cells were conjugated with IL-15Sa/anti-CD45 nanogels prior to transfer while in other groups, an equivalent dose of soluble IL-15Sa (56.9 μg) or equivalent volume of PBS were injected. On day 13, mice were sacrificed and tumor were processed and analyzed by flow cytometry (**Figure 3-11A**).

As IL-15Sa/anti-CD45 nanogels were conjugated to the T-cell surfaces, IL-15Sa could be gradually released to provide specific pseudo-autocrine stimulation of ACT T-cells carrying them. In this therapy, long surface-anchoring IL-15Sa/anti-CD45 nanogels allowed specific expansion of transferred T-cells to around 1×10^6 per gram of tumor weight, corresponding to a 16-fold increase compared to systemic free IL-15Sa (**Figure 3-11B left**). Similarly, IL-15Sa nanogels also raised the number of proliferating ACT T-cells (Ki67$^+$) 15 times more than systemic free IL-15Sa to 0.6×10^6 per gram of tumor (**Figure 3-11B middle**). The percentage of transferred T-cells in tumor infiltrating lymphocytes were also increased 7-fold in the nanogel group, indicating specific expansion of ACT T-cells in the tumor (**Figure 3-11B right**). The nanogel group also had higher ACT T-cell numbers in the spleen and a similar number of ACT T-cells in the inguinal lymph nodes compared to free IL-15Sa group (**Figure 3-11C**).

Surprisingly, free IL-15Sa elicited stronger ACT T-cell proliferation in blood (**Figure 3-11D**). However, the expansion of transferred T-cells due to systemic IL-15Sa was non-specific. For example, in blood, not only ACT T-cells, but also endogenous CD8$^+$ T cells and Tregs were expanded 17-fold and 9-fold respectively (**Figure 3-11D**). A similar pattern was observed in lymph nodes and spleen (data not shown). This non-specific expansion caused spleen enlargement (**Figure 3-11E**) and systemic toxicity reflected by a drop of 20% body weight in free IL-15Sa group (**Figure 3-11F**). Mice still suffered from more than 20% decrease in body weight when the dose of IL-15Sa decreased to 40 μg or even 20 μg (**Figure 3-12D, E**). Lower dose at 10 μg every two days (total 40 μg) also elicited similar accompanying inflammatory toxicities as one dose at 40 μg (**Figure 3-12D**) Even with 5 μg every three days (total 20 μg), mice still lost average 10% of body weight during the course while IL-15Sa nanogels backpacks did not elicit overt toxicity for doses up to 60 μg (**Figure 3-11E, F; Figure 3-12D, E**). Interestingly, all doses of systemic IL-15Sa caused a delayed toxicity response as mouse body weight started to drop about 4-5 days after infusion. This might be due to the impact of systemic IL-15sa on the reconstituted host endogenous T-cells,

natural killer cells and myeloid suppressor cells which were removed by lymphodepletion in the beginning [131].

Prolonged surface anchoring allowed IL-15Sa/anti-CD45 nanogels to induce tumor regression and increase the life span of mice significantly (**Figure 3-12B, C**). Therapeutic efficacy of surface anchoring nanogels might be stronger if mouse IL-15 is used in murine model. Human IL-15 is active on murine T-cells, but binds to the murine IL-2/15R$\beta\gamma_c$ with lower affinity, resulting 3-10 fold less activity on mouse T-cells [132].

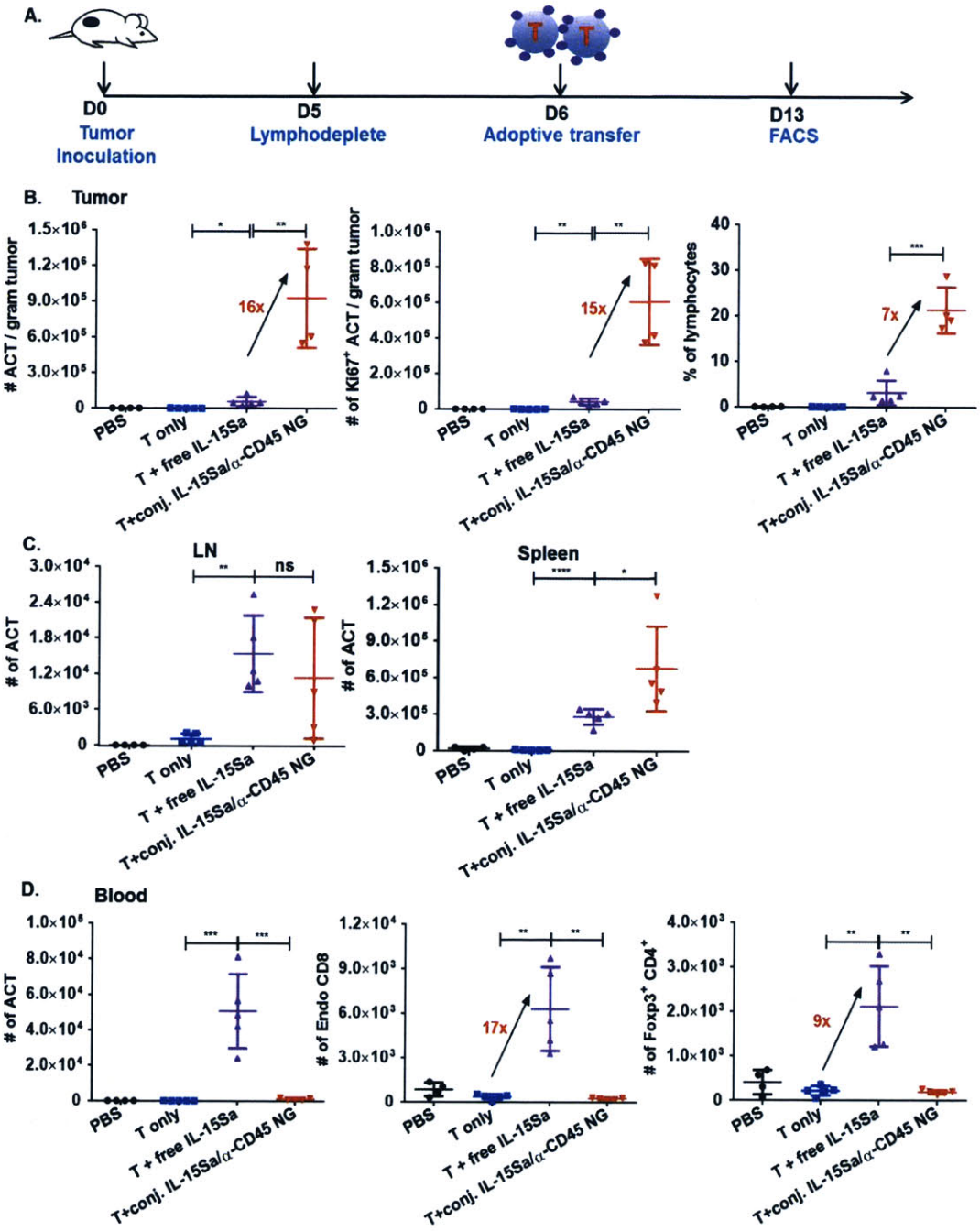
A.
D0
Tumor Inoculation
D5
Lymphodeplete
D6
Adoptive transfer
D13
FACS
B. Tumor
ACT / gram tumor
16x
# of Ki67+ ACT / gram tumor
15x
% of lymphocytes
7x
C.
LN
ns
# of ACT
Spleen
# of ACT
D.
Blood
# of ACT
# of Endo CD8
17x
# of Foxp3+ CD4+
9x
PBS
T only
T + free IL-15Sa
T+conj. IL-15Sa/α-CD45 NG

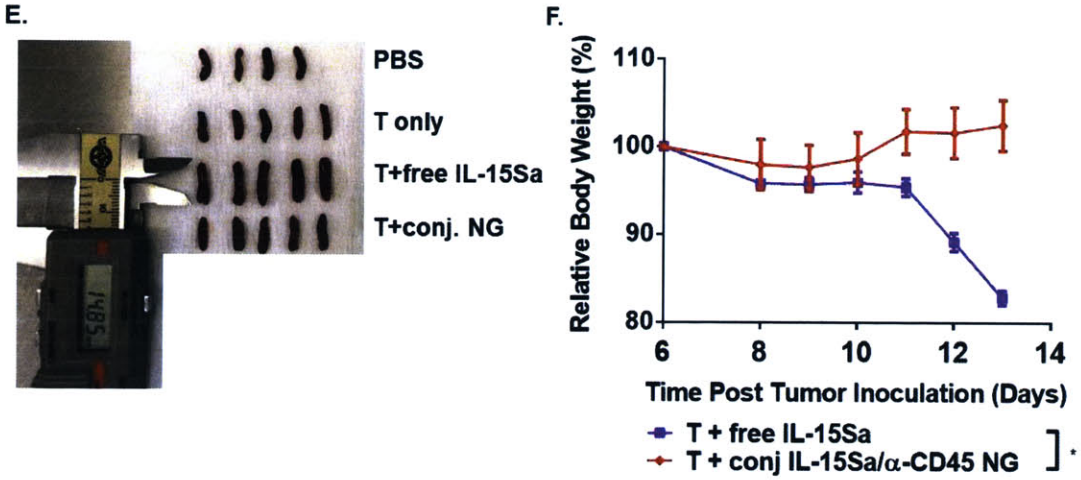

Figure 3-11: Surface anchoring IL15-Sa/anti-CD45 nanogels allow greater ACT T-cells expansion in tumor bearing mice without toxicity. B16F10 tumor cells ($0.5x10^6$) were injected subcutaneously into $Thy1.2^+$ C57Bl/6 mice on day 0 and allowed to establish tumor for 5 days. Animals were then sublethally lymphodepleted by irradiation on day 5 and received i.v. adoptive transfer of 13.5×10^6 activated pmel-1 $Thy1.1^+$ $CD8^+$ T-cells the next day. For one group of mice, T cells were conjugated with IL-15Sa/α-CD45 nanogel before adoptive transfer. Other groups of mice receive PBS, T cells only or T cells with equivalent dose of systemic free IL-15Sa (56.9 μg). On day 13, mice were sacrificed and tumor were processed and analyzed by flow cytometry. Body weight of mice was monitored daily. (**A**) Timeline of injections and necropsy. (**B**) Quantification of percentage of $CD8^+$ $Thy1.1^+$ T-cells in tumor (left) and number of Ki67+ transferred T cells (middle) and transferred T-cells per g of tumor (right). (**C**) Number of adoptively transferred T-cells in inguinal lymph nodes and spleen. (**D**) Free IL-15Sa at 57 μg caused non-specific expansion of transferred T-cells (left), endogenous CD8 T-cells (middle) and Tregs (right) in blood while IL-15Sa/anti-CD45 nanogels did not. (**E**) Size of spleens from each group on day 13. (**F**) Body weight was normalized to day 0 body weight and average body weight was plotted over time. n=4-5 animals/group. *, $p<0.05$; **, $p<0.01$; ***, $p<0.001$; ****, $p<0.0001$.

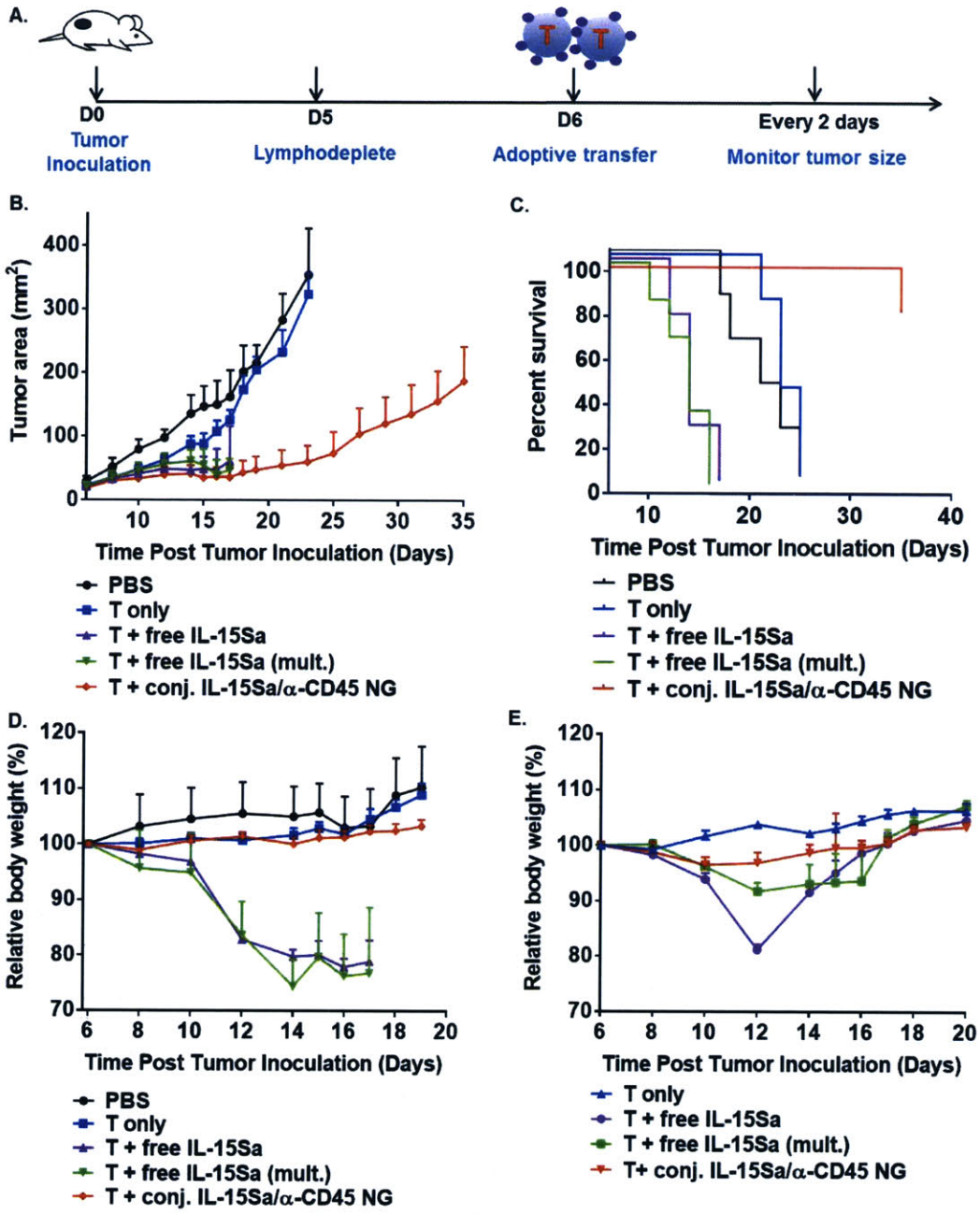

Figure 3-12: Surface anchoring nanogels suppress tumor growth and prolong survival of mice without overt toxicity. (**A-D**) B16F10 tumor cells ($0.5x10^6$) were injected subcutaneously into Thy1.2$^+$ C57Bl/6 mice on day 0 and allowed to establish tumor for 5 days. Animals were then sublethally lymphodepleted by irradiation and received i.v. adoptive transfer of 11×10^6 activated pmel-1 Thy1.1$^+$ CD8$^+$ T-cells the next day (day 6). For one group of mice, T cells were conjugated with IL-15Sa/α-CD45 nanogel before adoptive transfer. Other groups of mice receive PBS, T cells only or T cells with equivalent dose of systemic free IL-15Sa (40 μg) or 10 μg IL-15Sa. The group received 10 μg of IL15-Sa was boosted with three more doses at 10 μg on day

8/10/12. Tumor size and body weight of mice were monitored every two days. (**A**) Timeline of experiment. (**B**) Average tumor growth curve of PBS group (black), T only group (blue), T-cells with 40 μg IL-15Sa (purple), T-cells with 10 μg x4 IL-15Sa (green) and T-cells with conjugated nanogels (red). (**C**) Survival curve of different groups. (**D**) Body weight was normalized to day 0 body weight and average body weight was plotted over time. (**E**) With the same experiment timeline, 14×10^6 T-cells with conjugated IL-15Sa/anti-CD45 nanogels. For control groups, free IL-15Sa at nanogels equivalent dose (20 μg) or 5 μg or were injected i.v. immediately after adoptive transfer. The group received 5 μg IL15-Sa was boosted with three more doses of 5 μg IL15-Sa on day 9/12/15. n=4-5 animals/group. *, $p<0.05$; **, $p<0.01$; ***, $p<0.001$.

3.4 Conclusions

We identified CD45 as a receptor capable of blocking internalization of lipid vesicles bound to T-cells, and via a biotin labeled targeting-liposome system found that CD45 could dominate the internalization kinetics when co-crosslinked with rapidly-internalizing receptors. Applying this approach for modulating internalization to a novel protein-based nanoparticle system developed in our laboratory, we demonstrated that IL-15Sa nanogels with surface decorated anti-CD45 could be retained on cell surfaces for at least 7 days, eliciting prolonged stimulation of IL-15 signaling pathway. Surface anchoring nanogels also induced much stronger proliferation of transferred T-cells both *in vitro* and in tumor bearing mice without systemic toxicity observed in equivalent dose of free IL-15Sa. With the successful application of CD45 in nanogel system, we believe that anti-CD45 can also be generally employed to decorate a broad range of nanoparticles to prolong their stability on cell surface for extracelluar drug delivery, tracking or diagnostic purposes.

4 Arming adoptively transferred T-cells with immunosuppression-reverting drugs

4.1 Introduction

In adoptive T-cell therapy (ACT), tumor-specific lymphocytes are either isolated from patient tumor biopsies, activated and expanded *ex vivo* then infused back into patients, or alternatively, polyclonal peripheral T-cells are genetically transduced with a tumor-specific receptor to impart tumor specificity prior to infusion [34]. In phase I clinical trials, ACT has mediated up to 78% sustained complete remission in chronic lymphoblastic leukemia [39, 40]. Despite these promising results in early clinical findings, the objective response rates of ACT in solid tumors have been lower, for example 22% durable complete responses in patients with advanced metastatic melanoma [14, 36-38]. Poor *in vivo* functional persistence has been one of the limiting factors hindering the overall efficacy of adoptive T-cell therapy [34]. Although ACT T-cells are activated and primed *ex vivo*, they are usually quickly subjected to immunosuppression either in lymphoid organs or in the tumor microenvironment. Most ACT T-cells become non-functional before tumor eradication [44] owing to a variety of immunosuppression mechanisms in tumors including recruitment of suppressive host immune cells, activation of negative costimulatory signaling pathways, and secretion of immunosuppressive factors [10].

TGF-β, a pleiotropic cytokine, is one of the key immunosuppressive cytokines produced in the tumor microenvironment promoting evasion from the immune response (**Figure 4-1**) [133, 134]. TGF-β exerts its negative inhibitory effects by attenuating the potency of natural killer (NK) cells and promoting the generation of regulatory T lymphocytes (T_{regs}) [25, 135]. In addition, TGF-β suppresses both the activation and proliferation of cytotoxic T-cells (CTLs) and decreases CTLs' cytotoxicity by upregulating FoxP1 and inhibiting production of IFN-γ, perforin, Granzyme A and B as well as FasL in CTLs [26-29, 136, 137].

These findings motivate TGF-β synthesis, TGF-β interaction with its receptor and TGF-β downstream signaling transduction as potential therapeutic targets to enhance tumor immunotherapy. Indeed, soluble TGF-β receptor, which neutralizes TGF-β, suppressed pancreatic tumor growth in mice [30]. Transgenic mice with expression of a dominant-negative TGF-β type II receptor specifically in $CD4^+$ and $CD8^+$ T-cells reject B16F10 and EL4 tumors [31]. Adoptive transfer of tumor-specific $CD8^+$ T-cells bearing a non-functional TGF-β receptor also eradicated prostate cancer in mice [32]. Small molecule TGF-β receptor inhibitors have also shown efficacy in cancer treatment when used alone [138-140] or in combination with agonistic antibodies, cytokines, or chemotherapy [67, 141, 142]. Encouraged by these promising preclinical results, several small molecule inhibitors and neutralizing/blocking antibodies targeting TGF-β ligands or receptors have entered clinical trials (**Table 4-1**) [143]. However, the only published first-in-human dose study of TGF-β receptor small molecule inhibitor Galunisertib (LY2157299) used as a monotherapy in glioma patients revealed modest results [144]. For an ongoing study in advanced

hepatocellular carcinoma patients, Galunisertib had better efficacy in patients with high alpha-fetoprotein levels, but the overall response rate was still low [143, 145].

Despite some patients suffered from thrombocytopenia, ischemic stroke, pulmonary embolism and dyspnea by dosing with Galunisertib at 300 mg/day, Galunisertib is still approved to proceed to phase II clinical trials [144, 145]. Although no severe toxicities have been observed at the maximum tolerated doses tested to date in clinical trials, toxicities might emerge with higher doses which are much needed to improve efficacy. As TGF-β is required to maintain homeostasis of immune cells [25], systemic blockade of TGF-β signaling pathway might lead to autoimmune and inflammatory diseases. This is predicted by studies of TGF-β knockout mice, which develop multifocal inflammation and autoimmune disease [146, 147]. Humans deficient in TGF-β might suffer from autoimmune diseases such as rheumatoid arthritis and systemic lupus erythematosus [148, 149]. In addition, the pleiotropic nature of TGF-β renders complete systemic inhibition unsafe. TGF-β has been known to suppress tumor initiation and development in early stage [134, 150] and chronic systemic inhibition of TGF-β might increase the chance of spontaneous cancer [151]. Chronic inflammation in skin and gut due to lack of TGF-β also created pre-cancerous conditions [152, 153]. In addition, prolonged exposure to TGF-β receptor inhibitors has caused drug resistance and resulted in more aggressive tumors in murine model [154]. Thus, strategies to target TGF-β receptor inhibitors to adoptively transferred T-cells or tumor microenvironment are urgently needed to improve efficacy by increasing local concentration of TGF-β receptor inhibitor while minimizing systemic side effects.

However, targeting the tumor microenvironment via systemic administration is proven difficult. Although various reports have claimed targeted delivery of drugs to tumor microenvironment [73-76], a closer look revealed that "targeted" nanoparticles enter the tumor via enhanced permeability and retention (EPR) effect. The resulting increased efficacy of such treatments is generally due to improved internalization of particles due to tumor-particle ligands interaction in the tumor site [77, 78]. Strategies using T-cells themselves as delivery vehicles of supporting drugs to the tumor microenvironment have recently been reported. Cytokine- or drug-loaded nanoparticles (NPs) were conjugated to the surfaces of T-cells *ex vivo* prior to transfer into tumor-bearing recipients, generating T-cell "pharmacytes" [71, 72, 155]. ACT T-cells could also be specifically armed *in vivo* by antibody/cytokine coupled targeting immunoliposomes to allow repeatedly stimulation by supporting adjuvant drugs [79]. ACT T-cells then carried these drug cargos into tumor during infiltration. These approaches increased the potency of adjuvant drugs while simultaneously minimizing systemic exposure to the supporting signals.

In this chapter, we report on initial therapy results for targeted delivery of SB525334 (SB), a potent small molecule inhibitor of TGF-β receptor I (ALK5) [156], to ACT T-cells by using both "pharmacyte" and *in vivo* targeting boost strategies. We first synthesized and characterized liposomes encapsulating SB. We then demonstrated SB in liposomes was as effective as its free form in inhibiting the TGF-β signaling pathway and maintaining T-cell proliferation and cytotoxicity *in vitro*. However, it was unclear if more sustained TGF-β inhibition would be achieved by liposomes bound to the ACT T-cells surface that continuously release drug over several days, or alternatively through liposomes that are internalized and degraded in the endolysosomal pathway. To compare these two pathways

for liposome targeting to ACT cells, we selected two candidate target receptors: (1) Thy1.1, a congenic quick internalizing cell surface receptor uniquely expressed by the transferred T-cells [79]; and (2) a surface retaining receptor- CD45 which in preliminary experiments staining with antibody alone we found did not appear to exhibit rapid internalization. The density of granzyme B^+ ACT T-cells infiltrating tumors was 2.5-fold higher for pmel-1 T-cells conjugated with anti-CD45 SB liposomes compared to the T-cells alone or T-cells + systemic SB groups. By contrast, animals receiving anti-Thy1-targeted SB liposomes showed a mean density of granzyme B^+ pmel-1 T-cells in tumors only 1.4-fold greater than T-cells alone, a difference that was not statistically significant. Thus, in the setting of pre-loading T-cells with liposomes *in vitro*, binding to T-cells through the non-internalizing receptor CD45 elicited greater granzyme expression in ACT T-cells systemically and particularly led to greater donor T-cell infiltration of tumors, which correlated with greater therapeutic efficacy. Nevertheless, as a proof of concept, anti-Thy1.1 liposomes repeatedly re-armed ACT T-cells with SB via *in vivo* targeting and slowed down tumor growth more than anti-CD45 liposomes. This demonstrated the feasibility of *in vivo* re-arming of ACT T-cells with supporting drug by using targeting liposomes. Comparison between different targeting liposomes might also provide us with insights into designing and selecting the right targeting liposomes or combination of them for specific delivery of immunosuppression-reverting drugs to ACT T-cells. This targeting liposome platform can also be applicable to other supporting drugs including cytokines and agonist antibodies.

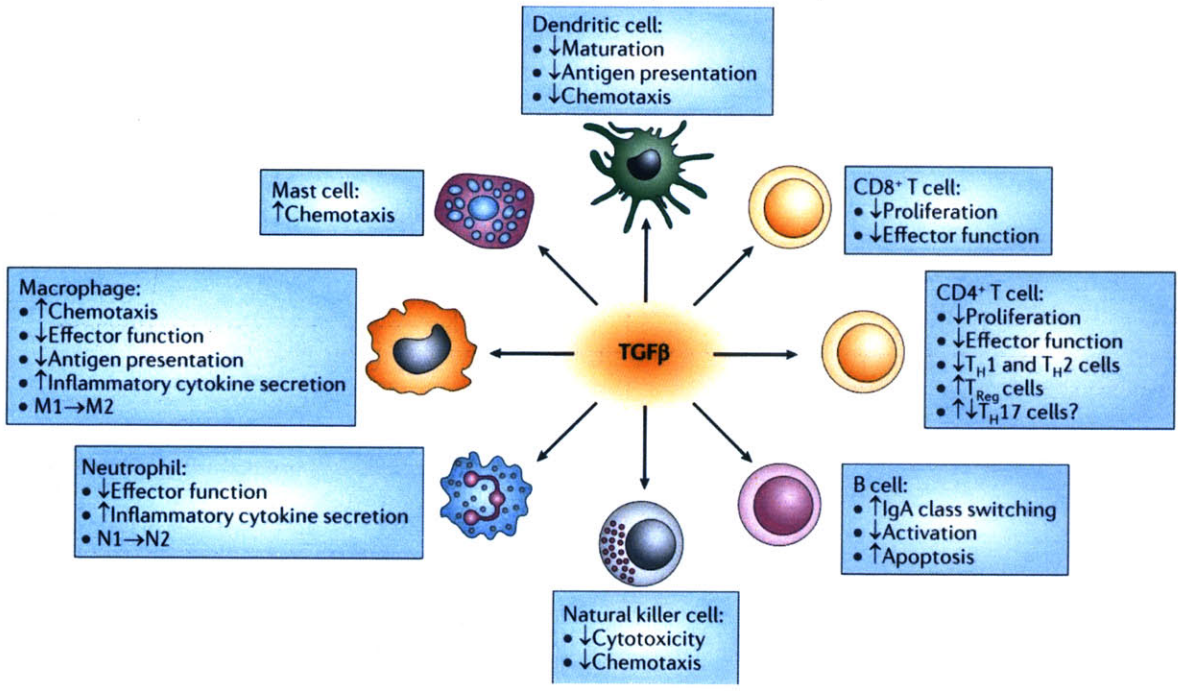

Figure 4-1: TGF-β effects on immune cells. Reproduced from Akhurst, *et al.* [133].

TGFβ pathway inhibitors in development in cancer.

Name	Targets	Trial identifier	Current status
TGFβ ligand inhibitors			
Lerdelimumab (CAT-152) Genzyme®	TGFβ2		Development stopped
Metelimumab Genzyme®	TGFβ1		Development stopped
Fresolimumab (GC1008) Genzyme®/Aventis®	TGFβ1, -β2, -β3	NCT00356460 NCT00923169 NCT01472731 NCT01112293 NCT01401062	Results in RCC, melanoma, mesothelioma and glioma; combination phase I/II in progress in breast cancer
LY2382770 Eli Lilly®	TGFβ1		In progress outside oncology
Trabedersen (AP12009) Antisens Pharma®	TGFβ2	NCT00844064 NCT00431561 NCT00761280	Results in glioma, PDAC, CRC, melanoma and glioblastoma
Lucanix (Belagenpumatucel-L) NovaRx Corporation®	TGFβ2	NCT01058785 NCT00676507	Results in glioma and NSCLC; combination phase I in progress
FANG™ Vaccine (rhGMCSF/shRNAfurin) Gradalis®	TGFβ1, -β2	NCT01061840 NCT01309230 NCT01505166 NCT01453361	In progress in melanoma, CRC and ovarian cancer
Disitertide (P144) Digna Biotech®	TGFβ1		In progress outside oncology
TGFβ receptor inhibitors			
Galunisertib (LY2157299) Eli Lilly®	TGFβRI	NCT01246986 NCT01373164 NCT01220271 NCT02178358 NCT01582269	Phase II in progress in PDAC, HCC, glioma and glioblastoma
TEW-7197 MedPacto®	TGFβRI	NCT02160106	Phase I in progress
PF-03446962 Pfizer®	ALK-1 (TGFβRI)	NCT00557856 NCT01337050 NCT01911273 NCT01486368 NCT01620970 NCT02116894	Results of phase I; phase II results pending in HCC and in progress in malignant pleural mesothelioma and refractory urothelial carcinoma; combination phase I in progress with regorafenib in CRC
IMC-TR1	TGFβRII	NCT01646203	Phase I in progress

Table 4-1: TGF-β pathway inhibitors in cancer clinical trials. Reproduced from Neuzillet, *et al.* [143].

4.2 Materials and methods

4.2.1 Materials

1,2-distearoyl-*sn*-glycero-3-phosphoethanolamine-N-[maleimide(poly ethylene glycol)-2000 (maleimide-PEG$_{2000}$-DSPE), cholesterol, hydrogenated Soy L-α-phosphatidylcholine (HSPC), 1,2-Dioleoyl-sn-glycero-3-phosphocholine (DOPC) and 1,2-dimyristoyl-sn-glycero-3-phosphocholine (DMPC) were from Avanti Polar Lipids (Alabaster, AL) and dissolved in ethanol before use. Anti-Thy1.1 (clone 19E12) and Anti-CD45 (clone HB220) were purchased from BioXCell (West Lebanon, NH). Ethanol was from VWR (Radnor, PA). F(Ab')$_2$ Preparation Kits, BCA Protein Assay Kits, and 7k MWCO Zeba spin desalting columns were from Pierce Thermo Scientific (Rockford, IL). Protein A agarose columns and Amicon Ultra-15 30kDa MWCO Centrifugal Filter Units were from Millipore (Billerica, MA). ACK lysis buffer and 1,1'-Dioctadecyl-3,3,3',3'-Tetramethylindodicarbocyanine, 4-Chlorobenzenesulfonate Salt (DiD) were obtained from Invitrogen Life Technologies (Grand Island, NY). Dithiothreitol (DTT), Concanavalin A Type VI (ConA), and Triton X-100 were

from Sigma-Aldrich (St. Louis, MO) and used as received. Recombinant interleukin-2 (IL-2) and interleukin-7 (IL-7) were obtained from PeproTech (Rocky Hill, NJ). Ficoll-Pague Plus was from GE Health Care (Waukesha, WI). EasySep™ Mouse $CD8^+$ T Cell Enrichment Kit was from Stemcell (Vancouver, BC, Canada). SB525334 was from Selleckchem (Houston, TX). Recombinant mouse TGF-β1 was bought from R&D systems (Minneapolis, MN). Hank's Balanced Salt Solution (HBSS) were purchased from (Gibco-Invitrogen, Carlsbad, CA). B16F10 melanoma cells were from American Type Culture Collection (Manassas, VA). Anti-mouse CD16/32 (clone 93), anti-mouse Thy1.1-PE (clone HIS51), anti-mouse CD8a-FITC (clone 53-6.7), anti-mouse CD8a-APC-Cy7 (clone 53-6.7), anti-mouse CD4-FITC (clone GK1.5), anti-mouse CD4-Percp-Cy5.5 (clone GK1.5), anit-mouse NK1.1-FITC (clone PK136), Foxp3-PE-Cy7 (FJK-16s), and anti-perforin-PE (clone dG9) were purchased from eBiosceince (San Diego, CA). Anti-pSmad2-APC (clone 072-670), cytoperm/cytofix buffer kit and Perm Buffer III were bought from BD Biosciences (San Jose, CA). Anti-human/mouse Granzyme B-APC (clone GB11) was obtained from BioLegend (San Diego, CA). Live/Dead fixable Aqua dead cell stain kit and mouse anti-CD3/CD28 dynabeads were obtained from Life Technologies (Grand Island, NY). AccuCount rainbow fluorescent count beads (10.1 μm) was bought from Spherotech (Lake forest, IL).

4.2.2 Preparation of targeting ligands- antibody $F(Ab)_2$

Monoclonal antibodies (Abs) against Thy1.1 and CD45 were digested with pepsin to generate $F(Ab')_2$ using a $F(Ab')_2$ Preparation Kit following the manufacturer's instructions, and characterized by gel electrophoresis. Antibodies or $F(Ab')_2$ used for liposome coupling were concentrated by using centrifugal filter units (Amicon Ultra-15 30kDa MWCO) and their concentration were measured by infrared spectroscopy (Direct Detect, Millipore, Billerica, MA).

4.2.3 Liposome synthesis

Liposomes were prepared by ethanol dilution. Briefly, a lipid solution (0.8 mg in 150 μl ethanol) composed of maleimide-PEG_{2000}-DSPE)/ cholesterol / HSPC in a 2.5/30/67.5 molar ratio was combined with SB (500 μg in 100 μl ethanol). The drug/lipid solution was added dropwise at 200 μl/min via a syringe pump (New Era Pump Systems, NE-1000) to a 5 ml deionized water reservoir in a glass vial with vigorous stirring at 1100 rpm (RT 10 power stir plate, IKA). After lipid/drug addition was complete, the bulk aqueous solution was further stirred at a lower speed for 2 min (200 rpm, power 4 on VWR 371 hot plate/stirrer). Solvent and free SB were removed using centrifugal filter units (Amicon Ultra-15 30kDa MWCO) by concentrating the preparation to ~200 μL followed by washing 1X with 5 ml PBS. For low-T_m and medium-T_m liposomes, equivalent moles of DOPC and DMPC were used to replace HSPC. For experiments with fluorescently-labeled liposomes, 0.1 mol% of a fluorescent lipophilic tracer dye DiD was added to the initial lipid mixture.

For rehydration synthesis method, vacuum dried lipid films composed of maleimide-PEG_{2000}-DSPE/ cholesterol / HSPC in a molar ratio of 2.5/27.5/69 together with 1% of DiD were rehydrated in 250 μl of 50 mM HEPES/150 mM NaCl-buffer (pH6.5). Lipids were vortexed every 10 min for 1 hr at 62°C to form vesicles and size extruded through a polycarbonate membrane (0.2 μm). After washing in excess phosphate buffered saline (PBS) pH7.4 and spinning down by ultracentrifugation at 110,000xg for 4 hr, liposomes were re-suspended in 100 μl PBS per 1.4 mg of lipids.

4.2.4 Characterization of liposomes and drug loading quantification

Liposome sizes were characterized by dynamic light scattering (90Plus Particle Size Analyzer, Brookhaven, Holtsville, NY). To quantify drug loading, liposomes were dissolved in a lipid-dissolving buffer (LDB, aqueous 38 vol% ethanol containing 1.5 vol% Triton X) followed by measurement of SB absorbance at 338 nm by spectrometer (Thermo scientific MULTISKAN GO) for drug quantification.

4.2.5 Release kinetics

Liposomes (0.8 mg) were resuspended in 1 ml PBS supplemented with 10% fetal bovine serum in Eppendorf tubes at 37°C on a rotator. At each time point, three tubes were sampled. For each sample, 100 µl of mixture were taken for measuring total amount of drug while 200 µl of mixture were spun down (Airfuge® Air-Driven, Beckman Coulter) at 160,000xg for 45 minutes, and 100 µl of supernatant was taken for quantification of released drug. Both mixture and supernatant were added to 400 µl LDB (total 500 µl) for absorbance measurements at 338 nm.

4.2.6 Coupling of ligands to liposome surface

Antibodies/F(Ab')$_2$ (2-5 mg/ml) were treated with 1.8 mM DTT in the presence of 10 mM EDTA at 25°C for 20 min to expose hinge region free thiols. DTT was subsequently removed using Zeba desalting columns before mixing with maleimide-bearing liposomes (1 mg protein/1 mg lipid) in PBS pH 7.4. After incubation for 9 hr at 25°C on a rotator, antibody-conjugated liposomes were washed in excess PBS pH7.4 and pelleted by ultracentrifugation at 110,000xg for 2.5 hr. Conjugated vesicles were then re-suspended in 500 µl PBS per 1.6 mg of lipids before spinning at 800xg for 3.5 minutes using a bench top centrifuge machine (Eppendorf centrifuge 5424) to remove a small fraction of aggregates/drug precipitates that formed during overnight incubation with the antibodies. Liposomes in the supernatants were used for *in vitro* experiments or T-cell conjugation.

4.2.7 Quantification of ligands coupled to liposomes

Anti-Thy1.1-FITC or anti-CD45-FITC were concentrated to 3-5 mg/ml using Ultra-15 Centrifugal Filters before coupling to liposomes as previously described. After liposomes were solubilized in 2% Triton X-100 at 37°C for 5 min with gentle vortexing, FITC fluorescence was measured at ex/em wavelengths of 490/520nm using a fluorescence plate reader (Tecan Systems, San Jose, CA) and converted to protein concentrations using standard curves prepared from serial dilutions of neat anti-Thy1.1-FITC or anti-CD45-FITC stock solutions.

4.2.8 Activation of Pmel-1 Thy1.1$^+$ CD8$^+$ T cells

Animals were purchased from Jackson Laboratories and cared for in the USDA-inspected MIT Animal Facility under federal, state, local and NIH guidelines for animal care. Spleens from pmel-1 Thy1.1$^+$ mice were ground through a 70 µm cell strainer and red blood cells were removed by incubating with ACK lysis buffer (1 ml per spleen) for 4 min at 25°C. After 1 wash in PBS, the remaining cells were cultured at 37°C in RPMI 1640 medium containing 10% fetal calf serum (FCS). ConA at a final concentration of 2 µg/ml and IL-7 at

1 ng/ml were added to activate and expand splenocytes. After two days, dead cells were removed by Ficoll-Pague Plus gradient separation and $CD8^+$ T-cells were isolated via magnetic negative selection using an EasySep™ Mouse $CD8^+$ T Cell Enrichment Kit. Purified $CD8^+$ T-cells were re-suspended at 0.75×10^6 per ml RPMI containing 10 ng/ml recombinant murine IL-2. After 24 hr, cells were washed 3 times in PBS and re-suspended in 100×10^6 per ml of complete RPMI for liposome conjugation or adoptive transfer.

4.2.9 *In vitro* liposome binding to T cells

Anti-Thy1.1 liposomes (1 mg) were incubated with 120×10^6 activated pmel-1 $Thy1.1^+$ T-cells in 10 ml complete RPMI supplemented with 10% FCS for 20 min at 37°C with gentle agitation every 10 min. After incubation, T-cells were spun down and supernatants were collected for conjugation efficiency measurement. After 1 wash in ice cold PBS, T-cells with conjugated liposomes were re-suspended at 100 $x10^6$ /ml in PBS for adoptive transfer.

4.2.10 Titration of liposome concentration for *in vitro* conjugation

Varying concentrations of DiD-labeled anti-Thy1.1-Lip and anti-CD45-Lip were added to 5 $\times10^6$ activated pmel-1 $Thy1.1^+$ T-cells. The total volume for all groups was topped up with RPMI with 10% FCS to 280 µl and incubated at 37°C for 20 min. After two washes in ice cold PBS to remove unbound liposomes, cells were resuspended in FACS buffer and analyzed by flow cytometry on a BD FACS Canto.

4.2.11 Evaluation of TGF-β signaling and granzyme B expression of T-cells

For short incubations with TGF-β1 (1 hr), activated Pmel-1 $CD8^+$ T-cells ($1x10^6$) were treated with serum-free RPMI, TGF-β1 alone (1.5 nM), SB (2 µM) alone or both for 1 hr at 37°C in 220 µl serum-free RPMI. For extended incubations with TGF-β1 (12 hr, 36 hr, 60 hr), activated pmel-1 $CD8^+$ T-cells were expanded in IL-2 (10 ng/ml) for one day, and then T-cells (0.5 $x10^6$) were treated with complete RPMI, TGF-β1 alone (1.5 nM), SB alone (2 µM), TGF-β1 and SB together, equivalent doses of liposomal SB, or 2X equivalent doses of SB in liposomes in the presence of TGF- β1 at 37°C. All T-cells were incubated in complete RPMI supplemented with 5 ng/ml IL-2. After incubation, T-cells were spun down and washed 1X with ice cold PBS followed by Aqua live dead staining and intracellular staining for phosphorylated Smad2 and granzyme B. T-cells were analyzed on a FACS Canto flow cytometer after staining.

4.2.12 *In vitro* T-cells proliferation assay

Naïve $CD8^+$ T cells were isolated from Pmel-1 splenocytes via magnetic negative selection using an EasySep™ Mouse $CD8^+$ T Cell Enrichment Kit, and re-suspended at 10 $\times10^6$ /ml in pre-warmed serum-free RPMI. Carboxyfluorescein succinimidyl ester (CFSE) was added to the cells at a final concentration of 2 µM, which were incubated at 37°C for 15 minutes. Staining was quenched by adding a 1:1 volume ratio of cold RPMI with 10% FBS and cells were spun down followed by two more washes in cold RPMI with FBS. Anti-CD3/CD28 beads were added to CFSE-stained naïve $CD8^+$ T-cells (0.15 $x10^6$) at a 1:1 beads:T-cells ratio before treatment with TGF-β1 alone (1.2 nM), SB alone (1.6 µM), both drugs, or equivalent doses of liposomal SB in the presence of TGF- β1 in 280 µl complete RPMI media with 10% FBS at 37°C. Two days after activation, T-cells were mixed with

counting beads, washed once with FACS buffer before analysis by flow cytometry on a BD FACS Canto.

4.2.13 *In vivo* tumor therapy using T-pharmacytes

B16F10 melanoma cells were suspended at 0.5×10^6 cells in 100 µl HBSS and inoculated subcutaneously (*s.c.*) to induce tumors in C57Bl/6 mice (6-8 weeks old, Jackson Laboratory, Bar Harbor, ME) (day 0). Animals were then sublethally lymphodepleted by total body irradiation (5 Gy) 5 days post tumor inoculation (day 5) and received i.v. adoptive transfer of 8×10^6 activated pmel-1 Thy1.1$^+$ CD8$^+$ T-cells the next day. For T-pharmacyte groups, T cells were either conjugated with anti-CD45 liposomes or anti-Thy1.1 liposomes encapsulating SB before adoptive transfer. Other groups of mice either receive equivalent doses of systemic free SB (1 µg) in addition to T-cells or T-cells alone. After four days, mice in respective groups were boosted with 12×10^6 activated T-cells and 1.5 µg drugs either in liposomes or free form same as the first dose. Mice were sacrificed three days after boost for flow cytometric analysis.

4.2.14 *In vivo* targeting by anti-CD45-Lip

Animals were sublethally lymphodepleted by total body irradiation (5 Gy) and received i.v. adoptive transfer of 15×10^6 activated pmel-1 Thy1.1$^+$ CD8$^+$ T-cells the next day. Mice were either receive liposomes without targeting ligands or anti-CD45-Lips (0.5 mg) two days after adoptive transfer. One day after injection of ACT T-cells, mice were sacrificed for flow cytometric analysis.

4.2.15 Necropsy and sample preparation for flow cytometry analysis

Inguinal lymph nodes and spleens were ground through a 70 µm cell strainer and washed once with ice cold PBS. Splenocytes were treated with ACK lysis buffer (1 ml per spleen) for 4 min at 25°C to remove red blood cells before washing in ice cold FACS buffer (PBS with 1% BSA). Blood samples were lysed with 2X 1ml ACK lysis buffer for 5 min at 25°C and then washed 1x with ice cold PBS. Tumors were weighed and ground through a 70 µm cell strainer and washed once with ice cold FACS buffer. All cells were added with counting beads and washed in ice cold PBS once before Aqua live/dead staining. After Aqua staining, cells were washed 1x in FACS buffer followed by surface-staining with Ab. Cells were then surface-stained for Thy1.1, CD8, CD4 and NK 1.1, washed 2X in FACS buffer and fixed before splitting into two halves for intracellular staining of p-Smad2 and granzyme B. Samples for p-Smad2 study were permeabilized in BD PERM Buffer III while others were treated with BD Cytofix/cytoperm buffer. After intracellular staining, cells were washed once in FACS buffer and re-suspended in FACS buffer before analyzing on a BD LSR Fortessa flow cytometer. All data was processed using FlowJo software.

4.2.16 *In vivo* tumor therapy

B16F10 tumor cells ($0.5\text{x}10^6$) were injected subcutaneously into Thy1.2$^+$ C57Bl/6 mice on day 0 and allowed to establish tumor for 6 days. Animals were then sublethally lymphodepleted by irradiation (5 Gy) on day 5 and received i.v. adoptive transfer of 12×10^6 activated pmel-1 Thy1.1$^+$ CD8$^+$ T-cells the next day. For T-pharmacyte groups, T cells were either conjugated with anti-CD45-Lip or anti-Thy1.1-Lip encapsulating SB before adoptive

transfer. Other groups of mice either receive equivalent dose of systemic free SB (1.5 μg) in addition to T-cells or T-cells alone. On day 8 and 10, mice were boosted with either 0.6 mg of anti-Thy1.1-Lip or anti-CD45-Lip loaded with SB or equivalent dose of systemic drug (5 μg). Tumor size were monitored every two days afterwards. Tumor area was calculated as the product of 2 measured orthogonal diameters (D_1xD_2). Body mass of treated mice was measured daily as an indicator of overall body condition and systemic toxicity.

4.2.17 Statistical analysis

Statistical analysis was done using GraphPad Prism software and two-tailed unpaired t-tests were conducted between groups of experimental data. Graphs show the mean ± SEM of sample groups. Graphs show the mean ± SEM of sample groups. Tumor areas were compared using two-tailed unpaired student t-test, and Kaplan-Meier survival curves were compared by log rank test.

4.3 Results and discussion

4.3.1 Synthesis and characterization of TGF-β inhibitor-loaded liposomes

To encapsulate the hydrophobic TGF-β inhibitor SB (abbreviated henceforth as TGF-βI), which has poor solubility in water but high solubility in ethanol (68 mg/ml), liposomes were formulated via ethanol dilution (**Schematic 4-1**). Lipids and SB were mixed in ethanol and added to an excess aqueous phase dropwise via a syringe pump, followed by removal of excess solvent and free drug by centrifugal filtration. We first evaluated the impact of membrane composition on drug loading in 2.5/30/67.5 mol ratio maleimide-PEG-DPSE/PC/cholesterol liposomes, testing lipids of varying liquid/gel state transition temperatures (T_ms). Liposomes formed using low-T_m DOPC (T_m= -20 °C) encapsulated only 8 ± 0.1 μg drug/mg liposomes, while higher T_m DMPC or HSPC lipids with more rigid membranes encapsulated 11 ± 0.1 μg and 12 ± 0.7 μg/mg liposomes, respectively (**Figure 4-2A**). Based on these results, we focused on HSPC-based liposomes for subsequent studies. The molar percentage of HSPC was then varied from 37% to 77% (with PEG-DSPE content fixed at 2.5 mol% and cholesterol amounts adjusted accordingly) to optimize the lipid composition for drug loading. Over this lipid composition range, TGF-βI loading was relatively constant (**Figure 4-2**). With lipid composition fixed at 67.5% HSPC, 30% cholesterol and 2.5% maleimide-PEG-DSPE, the concentration of TGF-βI in the initial lipid/drug mixture was also titrated. Drug loading reached a plateau around 12 μg/mg liposomes after TGF-βI concentration was raised above 2.4 mg/ml (**Figure 4-2C**). The best lipid composition and drug input amount were used to form liposomes via the lipid film rehydration method (co-drying the drug with the lipids), but this process yielded only 1± 0.2 μg/mg liposomes which was 12-fold less than the ethanol dilution process (**Figure 4-2D**). TGF-βI-loaded liposomes formed via ethanol dilution had a mean diameter of 83 ± 11 nm (**Figure 4-2E**) and released the drug over 3 days in the prescence of serum *in vitro* (**Figure 4-2F**).

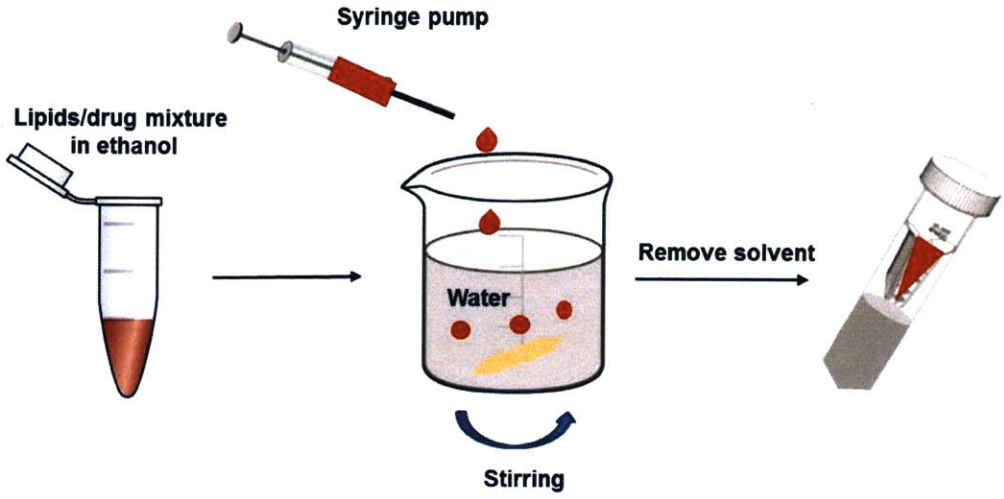

Schematic 4-1: Flow chart for synthesizing liposomes encapsulating hydrophobic small molecule drugs via nanoprecipitation.

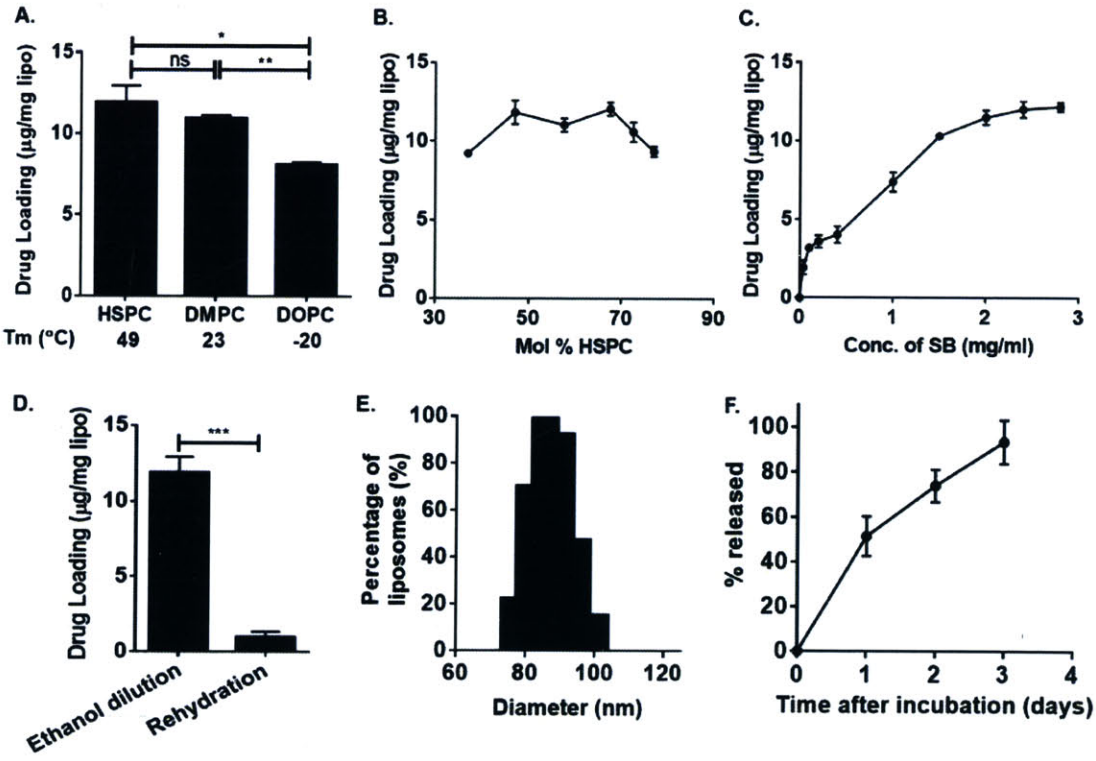

Figure 4-2: Characterization of TGF-βI-loaded liposomes. (**A**) Liposomes with a 2.5/30/67.5 mol ratio of maleimide-PEG-DSPE/cholesterol/PC were prepared using DOPC, DMPC, or

HSPC lipids and evaluated for encapsulation of SB by UV spectroscopy. (**B**) Liposomes containing a fixed 2.5 mol% maleimide PEG-DSPE were prepared with varying HSPC/cholesterol ratios and SB encapsulation was measured. (**C**) Drug loading as a function of SB concentration in the initial lipid/drug solution. (**D**) Comparison of lipid rehydration vs. ethanol dilution methods for SB encapsulation in maleimide-PEG-DSPE/cholesterol/HSPC 2.5/30/67.5 liposomes. (**E**) Typical particle size distributions for liposomes before antibody conjugation determined by dynamic light scattering. (**F**) Kinetics of SB release from liposomes at 37 °C in 10% FBS. Data shown are means ± SEM (n=3). *, $p<0.05$; **, $p<0.01$; ***, $p<0.001$, by two-tailed unpaired student t-test.

4.3.2 Free and liposomal SB block TGF- β signaling *in vitro*

When activated $CD8^+$ T-cells were treated with soluble TGF-β, the downstream signaling mediator Smad2 [25] was phosphorylated within an hour. The mean fluorescence intensity (MFI) of phospho-Smad2 (pSmad2) was raised 3-fold in TGF-β-pulsed cells compared to untreated T-cells (**Figure 4-3A, B**). However, incubation of cells with TGF-βI maintained p-Smad2 amounts at basal levels in the presence of TGF-β (**Figure 4-3A, B**). In order to evaluate the protective efficacy of SB at later time points and when it is encapsulated in liposomes, we incubated activated pmel-1 melanoma-specific $CD8^+$ T cells with liposomal SB (free liposomes with no targeting ligand) or equivalent doses of free drug in the presence of TGF-β1. After 36 hr incubation, TGF-β1 still upregulated p-Smad2 about 1.5-fold relative to untreated cells (**Figure 4-3C, D**). Encapsulated SB and its free form both downregulated p-Smad2 expression to basal levels, indicating liposomal formulation did not impair the drug function and the amount of drug released from liposomes during the assay time was sufficient to protect T-cells (**Figure 4-3C, D**). This protection was also dose dependent as doubling the amount of liposomal TGF-βI decreased pSmad2 levels further, even lower than that in untreated cells (**Figure 4-3C, D**). This might be due to the quenching of basal levels of TGF-β production in activated T-cells [26].

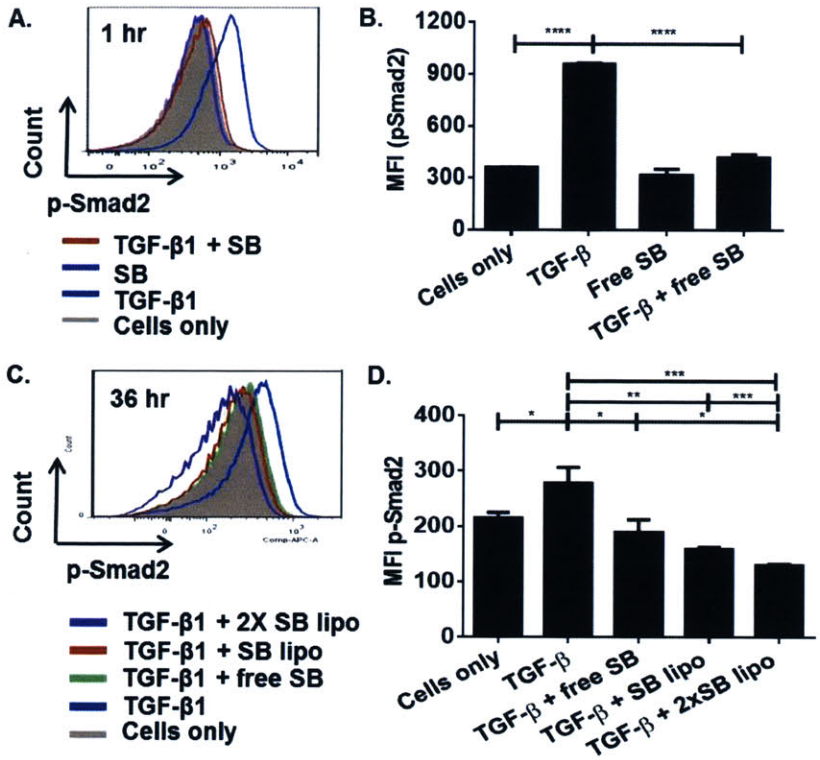

Figure 4-3: Free and liposomal SB block TGF-β signaling in activated T-cells. (**A-B**) Activated pmel-1 $CD8^+$ T-cells were treated with PBS, TGF-β alone (1.5 nM), SB (2 μM) alone or both drugs for 1 hr at 37°C, and pSmad2 levels were evaluated by intracellular staining and flow cytometry. (**A**) Overlay of representative histograms of pSmad2 expression. (**B**) Quantification of mean fluorescence intensity of pSmad2 in T-cells under different treatments (*n* = 3 samples/group). (**C-D**) Activated pmel-1 $CD8^+$ T-cells expanded for 1 day in IL-2 were incubated with TGF-β alone (1.5 nM), SB (2 μM) alone, TGF-β with SB, or TGF-β combined with equivalent doses of liposomal SB at 37°C for 36 hrs, followed by intracellular staining for pSmad2. Shown are histograms of pSma2 expression (**C**) and quantification of mean fluorescence intensity of pSmad2 (*n* = 4 samples/group) (**D**) *, $p<0.05$; **, $p<0.01$; ***, $p<0.001$; ****, $p<0.0001$, by two-tailed unpaired student t-test.

4.3.3 Liposomal SB maintains cytotoxicity and proliferation of T-cells in the presence of immunosuppression *in vitro*

Next we sought to assess the potency of liposomal SB in restoring the cytotoxic potenital of TGF-β-treated T-cells. TGF-β suppressed granzyme B expression to levels ~40% of that in untreated activated T-cells. Addition of free TGF-βI to TGF-β-treated cells partially restored granzyme B expression to 70% of untreated cells while liposomal SB maintained 80% of granzyme levels by MFI (**Figure 4-4A, B**). Granzyme B maintenance due to liposomal SB was also dose dependent as doubling the concentration of liposomes further restored over

90% of granzyme B levels (**Figure 4-4B**). Both free and liposomal SB were effective in maintaining granzyme B expression over 60 hr of culture in the presence of TGF-β (**Figure 4-4C**).

TGF-β is also known to block proliferation of T-cells [26-28]. We found that TGF-β treatment could modestly limit T-cell expansion even in response to strong stimulation by anti-CD3/anti-CD28 beads, as evidenced by CFSE dilution and total cell counts (**Figure 4-4D-F**). By contrast, T-cells activated in the presence of TGF-β together with liposomal SB or free TGF-βI were stimulated to divide and expand similarly to untreated cells (**Figure 4-4D-F**). Together, these results demonstrate that SB can be released from liposomes at concentrations relevant to maintaining T-cell proliferation and expression of key effector genes over several days.

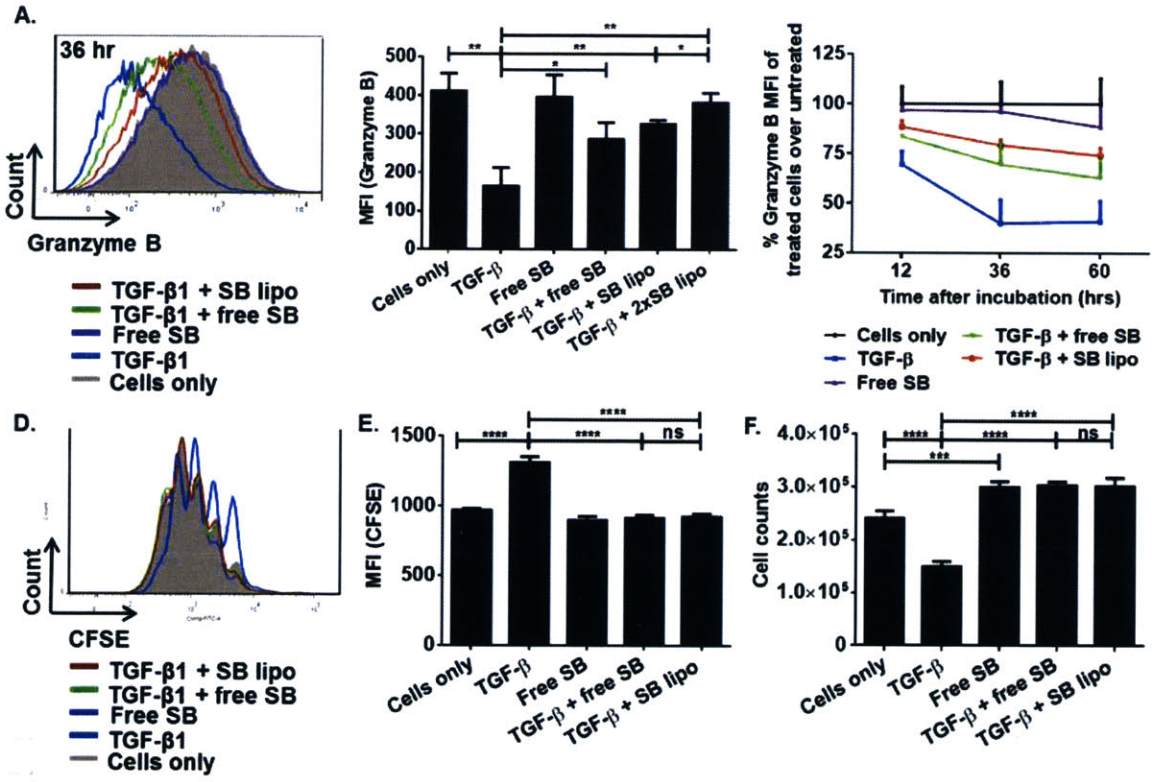

Figure 4-4: Liposomal SB maintains granzyme expression in activated T-cell and proliferates T-cells in the presence of immune suppression *in vitro*. (A-C) Activated pmel-1 $CD8^+$ T-cells expanded for 1 day in IL-2 were replated in 5 ng/ml IL-2 for 12 to 60 hr with or without TGF-β1 alone (1.5 nM), SB (2 μM) alone, both TGF-β1 and free SB or equivalent doses of liposomal SB at 37°C, followed by intracellular staining for granzyme B expression. Shown are histograms of granzyme B expression in T-cells (**A**), quantification of MFI (n = 3 samples/group) after 36 hr (**B**), and relative granzyme expression levels over time (**C**). **(D-F)** Naïve Pmel-1 $CD8^+$ T-cells were isolated from splenocytes, CFSE stained and activated by anti-CD3/CD28 beads with 1:1 beads to T-cells ratio. Naïve $CD8^+$ T-cells (0.15×10^6) were then treated with TGF-β1 alone (1.2 nM), SB alone (1.6 μM), both of them or equivalent dose of liposomal SB and TGF-β1 in complete RPMI media with 10% FCS at 37°C. Two days after

activation, T-cells were added counting beads, washed once with FACS buffer and resuspended in FACS buffer containing DAPI before analysis for flow cytometer. Shown are histograms of CFSE dilution patterns of T-cells (**D**), quantification of MFI (n = 4 samples/group) after two days (**E**), and number of cells under different treatment after two days (**F**). *, $p<0.05$; **, $p<0.01$; ***, $p<0.001$; ****, $p<0.0001$, by two-tailed unpaired student t-test.

4.3.4 Non-internalizing liposomes deliver TGF-β inhibitor more efficiently to transferred T-cells in T-pharmaycte setting

To deliver liposomal TGF-βI to adoptively-transferred T-cells in vivo, we tested the use of antibody-mediated targeting to permit pre-loading of T-cells with liposomes prior to infusion or for direct in vivo targeting of transferred cells. For this purpose, we reasoned that an important issue is the behavior of the target receptor on liposome binding. Classic studies with antibody-targeted liposomes delivering chemotherapy agents to tumor cells demonstrated that liposomes targeting internalizing receptors are more effective than liposomes targeting non-internalizing receptors [73] [157], suggesting that for such drugs, delivery of liposomes to endosomal compartments enhances drug delivery to the cytosol/nucleus. To support adoptively-transferred T-cells, it was unclear if more sustained TGF-β inhibition would be achieved by liposomes bound to the cell surface that continuously release drug over several days, or alternatively through liposomes that are internalized and degraded in the endolysosomal pathway.

To compare these two pathways for liposome targeting to ACT cells, we selected two candidate target receptors (**Figure 4-5A**). We previously demonstrated targeting of liposomes to ACT T-cells using antibodies against Thy1.1, a congenic internalizing cell surface receptor uniquely expressed by the transferred T-cells [79]. For comparison, we test liposomes targeted through an anti-CD45 antibody, which in preliminary experiments staining with antibody alone we found did not appear to exhibit rapid internalization (data not shown). In order to equalize the amount of drug loaded to T-cells via different targeting ligands, a titration of liposome concentrations for T-cell conjugation was conducted. A larger number of fluorescently labeled anti-CD45-Lip were loaded to T-cell surface due to more abundant expression of CD45 than Thy1.1 (**Figure 4-5B**). However, anti-Thy1.1-Lip bound to T-cells more efficiently than anti-CD45-Lip given the same concentration of liposomes (**Figure 4-5C**). By using the binding titration curve, we could choose the respective concentration of anti-CD45-Lip and anti-Thy1.1-Lip to allow the same number of liposomes thus the same amount of drug to be coupled to T-cells. We prepared empty liposomes conjugated with equivalent amounts of anti-Thy1.1 or anti-CD45 and assessed internalization by pmel-1 T-cells. Unlike anti-Thy1.1 liposomes, which were 70 % internalized by pmel-1 T-cells within 19 hr, anti-CD45 liposomes remained on cell surface through this time point (**Figure 4-5D**).

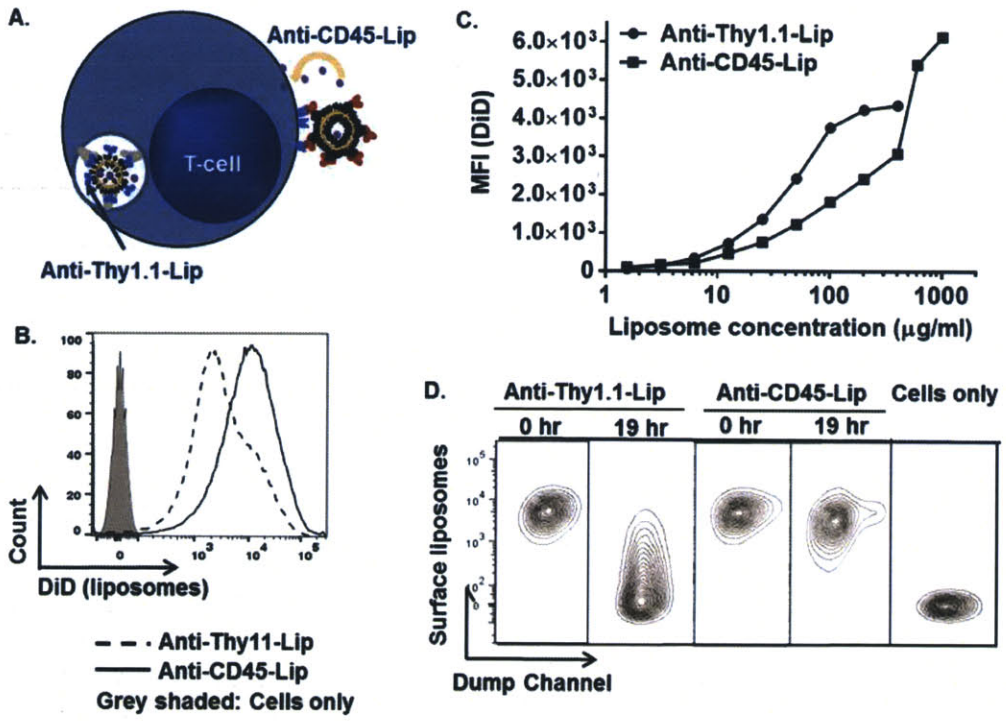

Figure 4-5: Different mechanism of delivering TGF-β inhibitor to T-cells via T-pharmacyte approach. (**A**) Schematic of two different mechanism of delivery. (**B-C**) Varying concentrations of DiD-labeled anti-Thy1.1-Lip and anti-CD45-Lip were incubated with5 $\times 10^6$ activated pmel-1 Thy1.1$^+$ T-cells at 37°C for 20 min. After two washes in ice cold PBS to remove unbound liposomes, cells were resuspended in FACS buffer and analyzed by flow cytometry on a BD FACS Canto. Shown are sample histogram of T-cell liposome fluorescence after 1 mg/ml anti-CD45-Lip and 0.4 mg/ml anti-Thy1.1-Lip were incubated with T-cells (**B**) and mean fluorescence of cells after conjugation with different concentrations of anti-CD45-Lip or anti-Thy1.1-Lip (**C**). (**D**) Sample FACS plots to show number of cells with surface liposomes at 0 hr and 19 hr when different targeting liposomes were used.

To test the impact of delivering TGF-βI to T-cells via these two different types of targeting liposomes, we tested the effect of liposome-mediated drug delivery to pmel-1 melanoma-specific CD8$^+$ T-cells in B16F10 melanoma tumor-bearing mice (**Fig. 5**). To focus on the question of whether binding to an internalizing vs. non-internalizing receptor was more effective for TGF-βI delivery, we first tested an experimental setting where T-cells were conjugated with TGF-βI-loaded liposomes *in vitro* prior to adoptive transfer, so that the liposomes could be compared under conditions where the same dose of liposomes/drug were coupled to the donor cells, and only the ACT cells were modified with liposomes. Activated pmel-1 CD8$^+$ T-cells were prepared and either left unmodified or conjugated with anti-Thy1- or anti-CD45-targeted SB liposomes *in vitro* prior to adoptive transfer into lymphodepleted B16F10 tumor-bearing mice. Control animals received unmodified T-cells followed by an equivalent total dose of systemic SB. Four days after adoptive transfer, all groups received a

second injection with the same combination of T-cells/liposomes/SB. Mice were sacrificed three days after the second T-cell infusion and tumors, spleen, and blood were processed and analyzed by flow cytometry (**Figure 4-6A**). Examining tumor size, only T-cells "backpacked" with CD45-binding liposomes elicited a statistically significant reduction in tumor area at this early time-point post treatment (**Figure 4-6B**). Flow cytometry analysis revealed that pmel-1 T-cells infiltrating tumors upregulated granzyme compared to ACT T-cells localized in the spleen, and T-cells conjugated with either Thy1-targeting or CD45-targeting SB liposomes exhibited higher granzyme levels than T-cells supported by systemic SB injection; systemic SB treatment did not increase T-cell granzyme expression above the T-cells alone group (**Figure 4-6C**). Increased granzyme expression was observed for liposome-treated T-cells in both the blood and tumors (**Figure 4-6D-E**). In addition, the density of granzyme B^+ ACT T-cells infiltrating tumors was 2.5-fold higher for pmel-1 T-cells conjugated with anti-CD45 SB liposomes compared to the T-cells alone or T-cells + systemic SB groups (**Figure 4-6F**). This higher number of granzyme B^+ ACT T-cells was not due to activation caused by binding to CD45 or Thy1.1 (**Appendix Figure 6-3**). By contrast, animals receiving anti-Thy1-targeted SB liposomes showed a mean density of granzyme B^+ pmel-1 T-cells in tumors only 1.4-fold greater than T-cells alone, a difference that was not statistically significant. Thus, in the setting of pre-loading T-cells with liposomes *in vitro*, binding to T-cells through the non-internalizing receptor CD45 elicited greater granzyme expression in ACT T-cells systemically and particularly led to greater donor T-cell infiltration of tumors, which correlated with greater therapeutic efficacy.

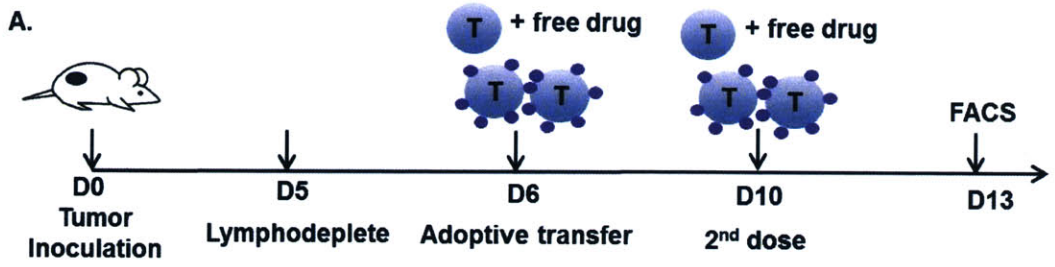
A.
+ free drug
+ free drug
FACS
D0
Tumor
Inoculation
D5
Lymphodeplete
D6
Adoptive transfer
D10
2nd dose
D13

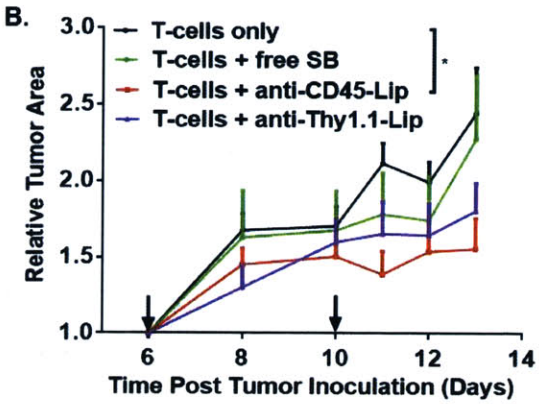
B.
T-cells only
T-cells + free SB
T-cells + anti-CD45-Lip
T-cells + anti-Thy1.1-Lip
Relative Tumor Area
Time Post Tumor Inoculation (Days)

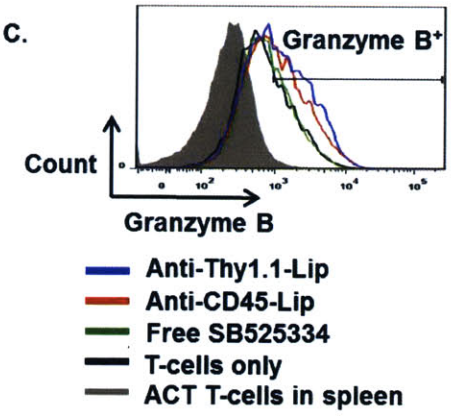
C.
Granzyme B+
Count
Granzyme B
Anti-Thy1.1-Lip
Anti-CD45-Lip
Free SB525334
T-cells only
ACT T-cells in spleen

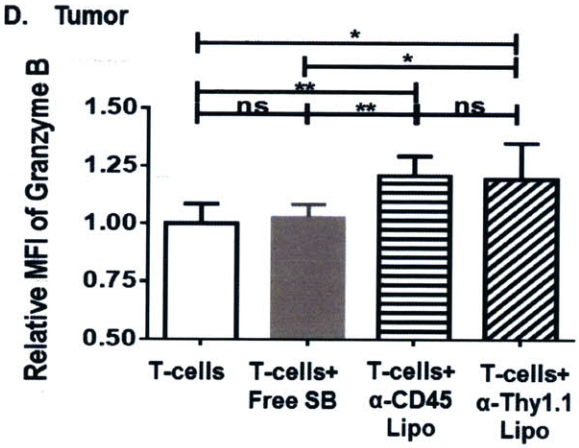
D. Tumor
Relative MFI of Granzyme B
T-cells
T-cells+ Free SB
T-cells+ α-CD45 Lipo
T-cells+ α-Thy1.1 Lipo

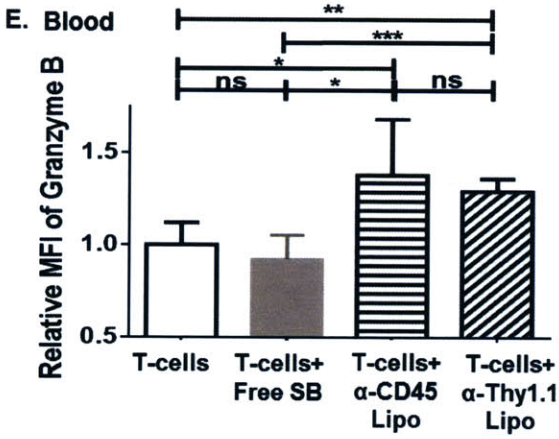
E. Blood
Relative MFI of Granzyme B
T-cells
T-cells+ Free SB
T-cells+ α-CD45 Lipo
T-cells+ α-Thy1.1 Lipo

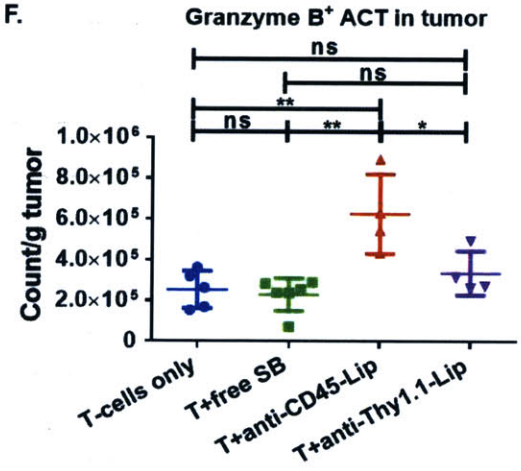
F.
Granzyme B+ ACT in tumor
Count/g tumor
T-cells only
T+free SB
T+anti-CD45-Lip
T+anti-Thy1.1-Lip

Figure 4-6: Pre-loading T-cells with SB liposomes targeting non-internalizing CD45 receptor leads to greater tumor infiltration by donor T-cells and enhanced therapeutic efficacy of ACT. B16F10 tumor cells (0.5x106) were injected subcutaneously into Thy1.2+ C57Bl/6 mice on day 0 and allowed to establish tumor for 6 days. Animals were then sublethally lymphodepleted by irradiation on day 5 and received i.v. adoptive transfer of 8 ×106 activated pmel-1 Thy1.1+ CD8+ T-cells the next day. For T-pharmacyte groups, T cells were either conjugated with anti-CD45 liposomes or anti-Thy1.1 liposomes encapsulating SB before adoptive transfer. Other groups of mice either receive equivalent dose of systemic free SB (1 μg) in addition to T-cells or T-cells alone. After four days, mice in respective group were boosted with 12×106 activated T-cells and 1.5 μg drugs either in liposomes or free form same as the first dose. Mice were sacrificed three days after boost. Tumor, lymph nodes, spleen and blood were processed and analyzed by flow cytometry. (**A**) Experimental timeline. (**B**) Relative average tumor growth curve normalized to day 6 tumor area. *, $p<0.05$, by two-tailed unpaired student t-test on tumor size on day 13. (**C**) Sample histograms to indicate granzyme B expression of tumor infiltrating adoptively transferred T-cells in different groups and gating to determine granzyme B+ ACT T-cells. (**D**) Shown are relative mean fluorescence intensity of granzyme B expression of granzyme B+ ACT T-cells in tumor. Value was normalized to T-cell only group. (**E**) Relative mean fluorescence intensity of granzyme B expression of ACT T-cells in blood. (**F**) Quantification of number of granzyme B+ CD8+ Thy1.1+ T-cells per gram of tumor. *, $p<0.05$; **, $p<0.01$, by two-tailed unpaired student t-test.

4.3.5 Anti-Thy1.1 liposomes encapsulating SB slow down tumor growth and outperform anti-CD45 liposomes for *in vivo* targeting

Although anti-CD45-Lip could deliver TGF-β inhibitor more efficiently after conjugating to T-cell surface, its overall efficacy might be impaired during in vivo targeting step as CD45 was expressed on the surface of all nucleated hematopoietic cells and their precursors [158, 159]. However, anti-Thy1.1-Lips could minimize off-targeting by binding to adoptively transferred T-cells specifically *in vivo*. To compare the therapeutic efficacy of two types of targeting liposomes in terms of *in vivo* targeting, B16F10 tumor cells were injected subcutaneously into Thy1.2$^+$ C57Bl/6 mice on day 0 and allowed to establish tumor for 6 days. Animals were then sublethally lymphodepleted by irradiation on day 5 and received i.v. adoptive transfer of activated pmel-1 Thy1.1$^+$ CD8$^+$ T-cells the next day. T cells were then either conjugated with anti-CD45-Lip or anti-Thy1.1-Lip encapsulating SB before adoptive transfer. Other groups of mice either receive equivalent dose of systemic free SB in addition to T-cells or T-cells alone. On day 8 and 10, mice were boosted with either anti-Thy1.1-Lip or anti-CD45-Lip loaded with SB or equivalent dose of systemic drug (**Figure 4-7A**). Anti-CD45-Lip group had negligible impact on tumor growth compared to equivalent dose of free SB or T-cells alone group. On the contrary, anti-Thy1.1-Lip slowed down tumor growth significantly and allowed longer survival compared to all other groups (**Figure 4-7B, C**). The low efficacy of anti-CD45-Lip is probably due to non-specific targeting of the liposomes to ACT T-cells as endogenous T-cells, peripheral B-cells, dendritic cells and macrophages all express CD45RB [119]. Anti-CD45-Lips bound to only 52% of ACT T-cells in blood and 25% in LN while a similar percentage of endogenous T-cells were also bound by anti-CD45-Lips (**Figure 4-7D, E**). However, anti-Thy1.1-Lip could target

specifically to ACT T-cells for drug delivery [79]. Non-targeting liposomes group did not give additional therapeutic efficacy compared to free drug indicating efficacy due to passive tumor targeting via enhanced permeability and retention (EPR) effect was minimal (**Figure 4-7B, C**).

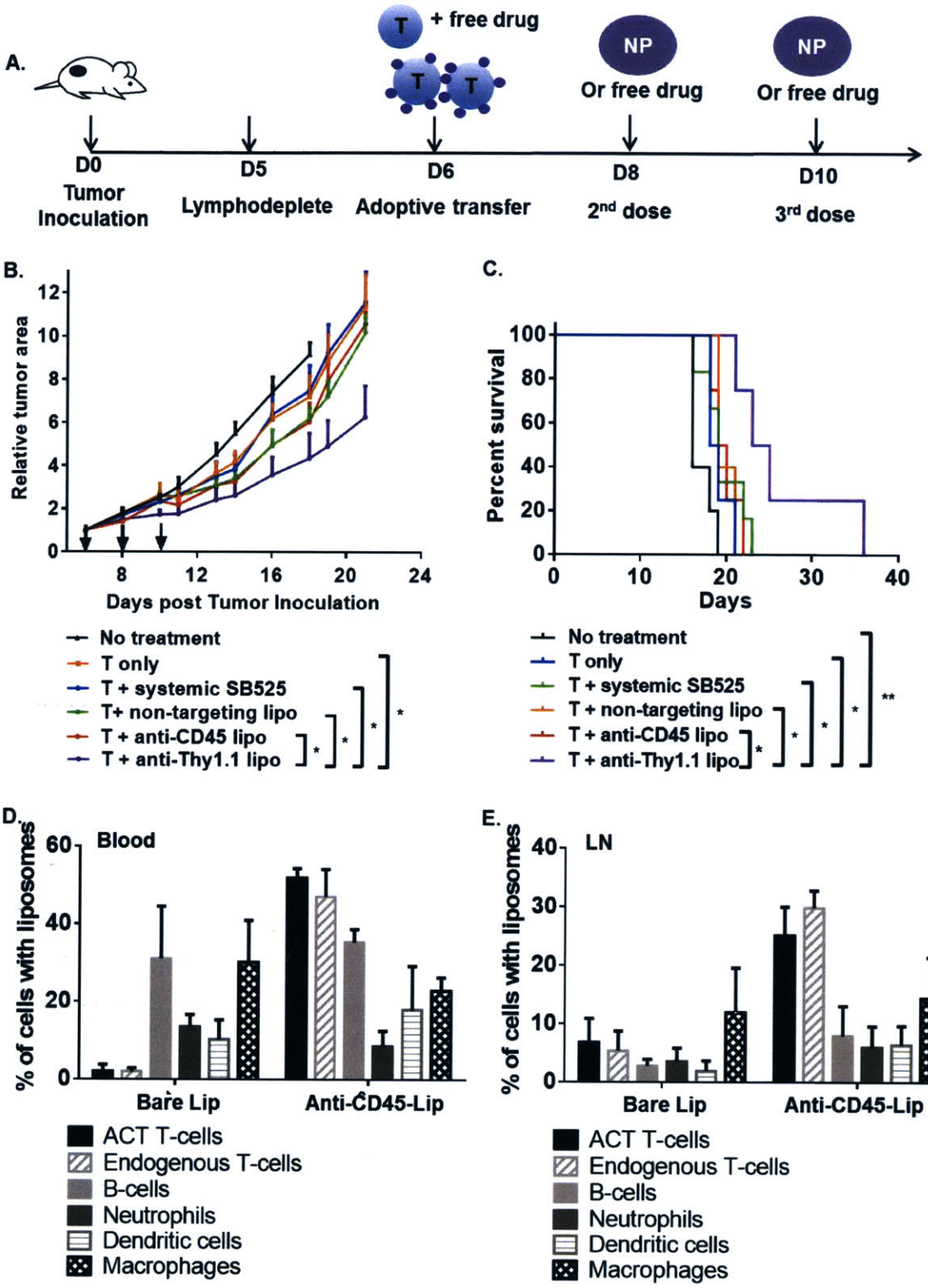
A.
T
+ free drug
T
T
NP
Or free drug
NP
Or free drug
D0
Tumor Inoculation
D5
Lymphodeplete
D6
Adoptive transfer
D8
2nd dose
D10
3rd dose
B.
Relative tumor area
Days post Tumor Inoculation
No treatment
T only
T + systemic SB525
T+ non-targeting lipo
T + anti-CD45 lipo
T + anti-Thy1.1 lipo
C.
Percent survival
Days
No treatment
T only
T + systemic SB525
T + non-targeting lipo
T + anti-CD45 lipo
T + anti-Thy1.1 lipo
D.
Blood
% of cells with liposomes
Bare Lip
Anti-CD45-Lip
ACT T-cells
Endogenous T-cells
B-cells
Neutrophils
Dendritic cells
Macrophages
E.
LN
% of cells with liposomes
Bare Lip
Anti-CD45-Lip
ACT T-cells
Endogenous T-cells
B-cells
Neutrophils
Dendritic cells
Macrophages

Figure 4-7: Anti-Thy1.1 liposomes encapsulating SB slow down tumor growth and outperforms anti-CD45 liposomes for *in vivo* targeting. B16F10 tumor cells ($0.5x10^6$) were injected subcutaneously into Thy1.2$^+$ C57Bl/6 mice on day 0 and allowed to establish tumor for 6 days. Animals were then sublethally lymphodepleted by irradiation on day 5 and received i.v. adoptive transfer of 12 $\times 10^6$ activated pmel-1 Thy1.1$^+$ CD8$^+$ T-cells the next day. For T-pharmacyte groups, T cells were either conjugated with anti-CD45-Lip or anti-Thy1.1-Lip encapsulating SB before adoptive transfer. Other groups of mice either receive equivalent dose of systemic free SB (1.5 μg) in addition to T-cells or T-cells alone. On day 8 and 10, mice were boosted with either 0.6 mg of anti-Thy1.1-Lip or anti-CD45-Lip loaded with SB or equivalent dose of systemic drug (5 μg). Tumor size were monitored afterwards. (**A**) Timeline of injections. (**B**) Average tumor area for all groups were plotted. Data shown are means ± SEM (n=4 to 6 animals per group). *P* value was determined by t-test for tumor areas on day 21. (**C**) Kaplan-Meier survival curve of different groups. Mice were considered dead when tumor size reached 150 mm^2. (**D-E**) Activated pmel-1 Thy1.1$^+$ CD8$^+$ T-cells (15×10^6) were adoptively transferred 1 day after lymphodepletion. Fluorescently labeled Liposomes without antibody coupling and anti-CD45-Lip (0.5 mg) were injected i.v. two days after adoptive transfer. Mice were sacrificed one day after injection of liposomes. Blood and LN were processed and analyzed by flow cytometry. Shown are percentage of respective cells types labeled with liposome fluorescence in blood (**D**) and LN (**E**).

4.4 Conclusions and future directions

Here we synthesized and characterized targeting liposomes encapsulating a potent TGF-β receptor inhibitor, SB525334. To elucidate if more sustained TGF-β inhibition would be achieved by liposomes bound to the ACT T-cells surface that continuously release drug over several days, or alternatively through liposomes that are internalized and degraded in the endolysosomal pathway, we synthesized liposomes targeting to two different receptors to represent the two mechanisms respectively. Firstly, Thy1.1 is a congenic quick internalizing cell surface receptor uniquely expressed by the transferred T-cells. Secondly, a surface retaining receptor- CD45 which in preliminary experiments staining with antibody alone we found did not appear to exhibit rapid internalization. The density of granzyme B$^+$ ACT T-cells infiltrating tumors was 2.5-fold higher for pmel-1 T-cells conjugated with anti-CD45 SB liposomes compared to the T-cells alone or T-cells + systemic SB groups. By contrast, animals receiving anti-Thy1-targeted SB liposomes showed a mean density of granzyme B$^+$ pmel-1 T-cells in tumors only 1.4-fold greater than T-cells alone, a difference that was not statistically significant. Thus, in the setting of pre-loading T-cells with liposomes *in vitro*, binding to T-cells through the non-internalizing receptor CD45 elicited greater granzyme expression in ACT T-cells systemically and particularly led to greater donor T-cell infiltration of tumors, which correlated with greater therapeutic efficacy. Nevertheless, as a proof of concept, anti-Thy1.1 liposomes allowed specific re-arming of ACT T-cells with SB by *in vivo* targeting and slowed down tumor growth significantly compared to equivalent dose of free drug and anti-CD45 liposomes.

These might provide us with insights into designing and selecting the right targeting liposomes or combination of them for specific delivery of immunosuppression-reverting

drugs or cytokines to transferred T-cells. So far we have tried targeting supporting cytokine and immunosuppression-blocking drugs to tumor-specific adoptively transferred T-cells, with the goal of optimally sustaining the anti-tumor activity of exogenous anti-tumor lymphocytes. The majority of our efforts have been focused on the setting of ACT due to the clinical promise of this approach. However, the laborious nature of ACT in the clinic, the challenge of successfully isolating/preparing autologous T-cells to treat all patients, potential safety issues with genetically modified T-cells make alternatives based on bolstering the patient's endogenous immune system also very attractive. Next we are hoping to test whether targeting approaches can be used to amplify endogenous anti-tumor T-cell responses by using targeting ligands such as anti-CD8 or tumor antigen peptides to direct liposomes to tumor-specific T-cells.

5 Conclusions and future work

5.1 Conclusions

Poor *in vivo* functional persistence due to immunosuppression is one of the major limiting factors for adoptive T-cell therapy. Augmenting the function and proliferation of adoptively transferred T-cells *in vivo* by using biomaterials is gaining more attention [160]. In this thesis, we demonstrated success in both 1) repeatedly reloading supporting drugs to T-cells through T-cell-targeted drug carriers and 2) extending the functional life span of drug carriers conjugated to T-cells surfaces prior to transfer in the adoptive T-cell therapy setting.

We firstly synthesized and characterized antibody-, cytokine- or combinations of antibody/cytokine-decorated immunoliposomes targeting unique cell surface antigens or activation markers on T-cells, respectively. Targeting liposomes bound to ACT T-cells specifically *in vitro,* and further, anti-Thy1.1-Lip labeled nearly 100% of transferred T-cells in systemic compartments and most of transferred T-cells in lymph nodes *in vivo* following a single injection. IL-2-Fc-Lip was able to repeatedly boost transferred T-cells *in vivo* in tumor-bearing animals and suppress tumor growth significantly. These results demonstrate the concept of repeated targeting of ACT T-cells for adjuvant stimulation *in vivo* and set the stage for functional targeting of supporting adjuvant drugs to T-cells in chapter 4.

We then focused on prolonging the life span of adjuvant drug carriers on T-cell surfaces, thus increasing the duration of initial support to T-cells. Identification of CD45 as a receptor capable of blocking internalization of lipid vesicles bound to T-cells allowed us to modulate internalization of a novel protein-based nanoparticle system developed in our laboratory. We demonstrated that IL-15Sa nanogels with surface-decorated anti-CD45 could be retained on cell surfaces for at least 10 days, eliciting prolonged stimulation of the IL-15 signaling pathway. Surface anchored nanogels also induced much stronger proliferation of transferred T-cells both *in vitro* and in tumor bearing mice without the systemic toxicity observed in equivalent doses of free IL-15Sa. With the successful application of CD45 in the nanogel system, we believe that anti-CD45 can also be generally employed to decorate a broad range of nanoparticles to prolong their stability on cell surface for extracelluar drug delivery, tracking or diagnostic purposes.

Building on the results from chapters 2 and 3, we used both anti-CD45 and anti-Thy1.1 targeting liposomes to deliver immunosuppression-reverting drug to ACT T-cells *in vivo*. We formulated liposomes encapsulating SB525334 via ethanol dilution and demonstrated that liposomal SB525334 effectively maintained T-cell proliferation and cytotoxicity *in vitro*. To elucidate if more sustained TGF-β inhibition would be achieved by liposomes bound to the ACT T-cells surface that continuously release drug over several days, or alternatively through liposomes that are internalized and degraded in the endolysosomal pathway, quick internalizing anti-Thy1.1 liposomes and surface anchoring anti-CD45 liposomes were used to represent the two mechanisms respectively. In the setting of pre-loading T-cells with liposomes *in vitro*, binding to T-cells through the non-internalizing receptor CD45 elicited greater granzyme expression in ACT T-cells systemically and particularly led to greater donor T-cell infiltration of tumors, which correlated with greater therapeutic efficacy.

Nevertheless, as a proof of concept, anti-Thy1.1 liposomes allowed specific re-arming of ACT T-cells with SB by *in vivo* targeting and slowed down tumor growth significantly compared to equivalent dose of free drug and anti-CD45 liposomes.

In overall, this thesis described a targeting nanoparticle platform which is able to specifically provide various kind of drugs including cytokines and immunosuppression-reverting drugs to adoptively transferred T-cells. It also can provide insights into designing and selecting the right targeting nanoparticles or combinations of them depending on the nature of choice drug.

5.2 Future directions

Due to the multiplicity and redundancy of tumor suppression mechanisms, combination of drugs targeting several pathways in parallel might improve the therapeutic outcome significantly.

We have tried targeting supporting cytokine and immunosuppression-blocking drugs to tumor-specific adoptively transferred T-cells, with the goal of optimally sustaining the anti-tumor activity of exogenous anti-tumor lymphocytes. The majority of our efforts have been focused on the setting of ACT due to the clinical promise of this approach. However, the laborious nature of ACT in the clinic, the challenge of successfully isolating/preparing autologous T-cells to treat all patients, potential safety issues with genetically modified T-cells make alternatives based on bolstering the patient's endogenous immune system also very attractive. Next we are hoping to test whether targeting approaches can be used to amplify endogenous anti-tumor T-cell responses elicited by a vaccination. Our lab has created a potent amphiphile vaccine to induce 30-fold increases in endogenous tumor-specific cytotoxic T-cells [60]. We can use targeting ligand such as anti-CD8 to target $CD8^+$ T cells or use tumor antigen peptide to direct to tumor-specific T-cells generated. This approach would enable T-cell-targeted drugs to be more broadly applied clinically in a variety of cancer therapy settings.

6 Appendix

6.1 Supplementary data

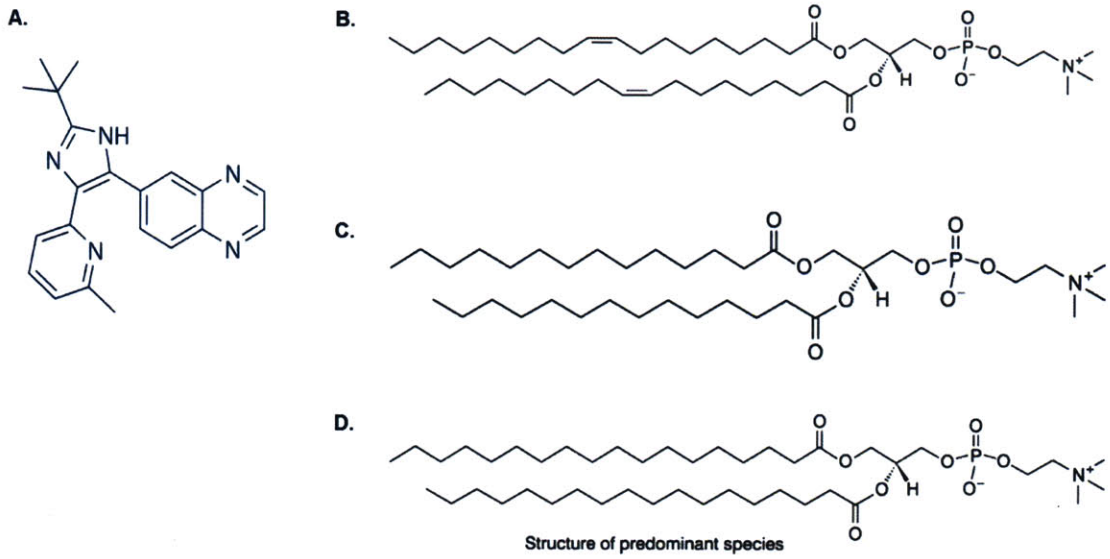

Figure 6-1: Structure of SB525334 and lipids used. (**A**) Structure of SB525334. (**B**) Structure of DOPC. (**C**) Structure of DMPC. (**D**) Structure of HSPC.

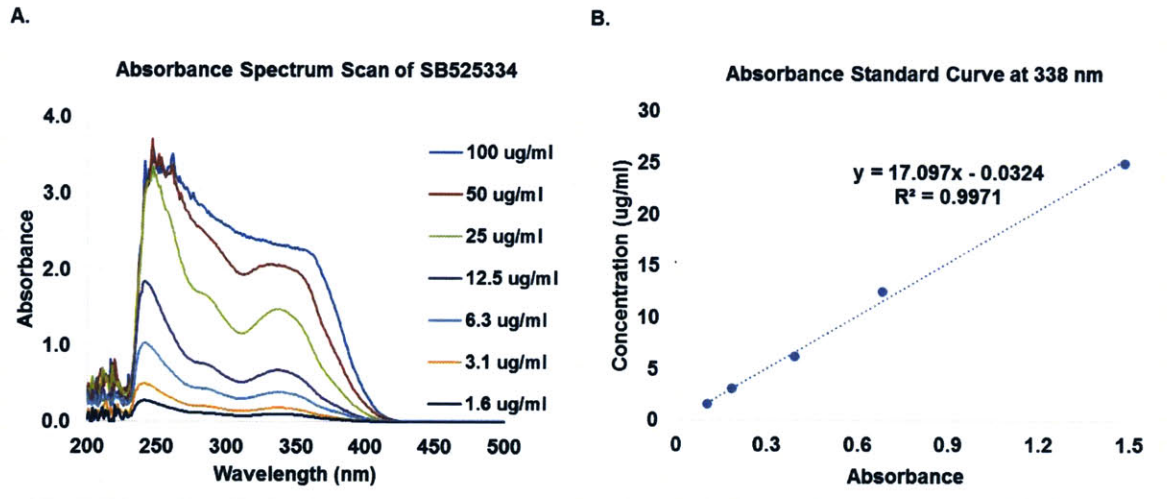

Figure 6-2: Absorbance of SB525334. Make respective concentrations of SB525334 in 38 vol% ethanol and 1.5 vol% Triton X in DI water. (**A**) Scan the absorbance of SB525334 from wavelength 200 nm to 500 nm and plot absorbance against wavelength. (**B**) Absorbance at 338 nm were plotted against concentration of SB525334 in the sample.

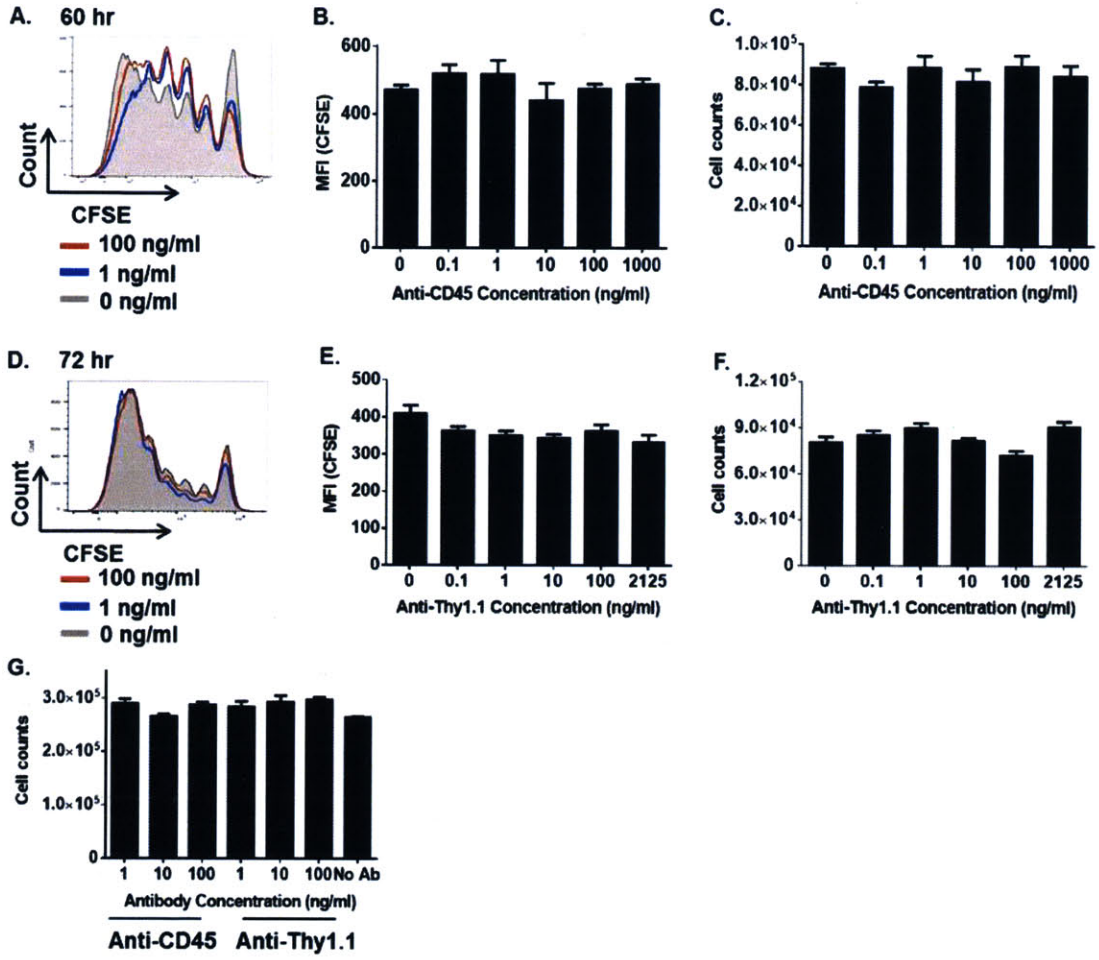

Figure 6-3: Soluble anti-CD45 and anti-Thy1.1 have negligible effect on T-cell activation and proliferation in the presence of anti-CD3/CD28 beads. (**A-F**) Naïve Pmel-1 $CD8^+$ T-cells were isolated from splenocytes, CFSE stained and activated by anti-CD3/CD28 beads with 1:1 beads to T-cells ratio. Naïve $CD8^+$ T-cells were treated with different concentrations of anti-CD45 and anti-Thy1.1 at 37°C. About three days after activation with anti-CD45 (60hr) or anti-Thy1.1 (72 hr), T-cells were added counting beads, washed once with FACS buffer and resuspended in FACS buffer containing DAPI before analysis for flow cytometer. Shown are histograms of CFSE dilution patterns of T-cells treated with anti-CD45 (**A**), quantification of MFI (n = 4 samples/group) (**B**), and number of cells under different treatment after three days (**C**). Histograms of CFSE dilution patterns of T-cells treated with anti-Thy1.1 (**D**), quantification of MFI (n = 4 samples/group) (**E**), and number of cells under different treatment after three days (**F**) are shown. (**G**) Activated pmel-1 $CD8^+$ T-cells were replated in 5 ng/ml IL-2 for 2 days with different concentrations of anti-CD45 or anti-Thy1.1. Shown are number of cells under different treatment after two days.

6.2 Protocols

6.2.1 Liposome formation via rehydration and antibody coupling

1. Dry lipids by purging N_2 gas and then in vacuum drier overnight.
2. Hydrate each 2 µmol lipids in 250 µl of 50 mM HEPES/150 mM NaCl-buffer at pH 6.5).
3. Vortex every 10 minutes for 1 hr at 62 °C.
4. Pre-warm size extrusion pad to about 60 °C. Pre-wet membrane filter supporter and membrane filter in PBS. Assemble size extrusion kit.
5. Size extrusion for 21 times by using 200 nm membrane.
6. Add liposomes to disposable ultracentrifuge tubes and top up with sterile phosphate buffered saline (PBS).
7. Spin down by ultracentrifugation at 30,000 rpm for 3 hr at 4 °C.
8. Antibody conjugation.
   Antibody Solution preparation: (at least 0.7 mg Ab per µmol of liposome)
   a. 100 µl of 0.5M EDTA + 4.9 ml of PBS to make 10 mM EDTA.
   b. Add 10 µl of DTT at 150 mM to 140 µl of 10 mM EDTA to make 150 µl of DTT at 10 mM.
   c. Add respective amount of EDTA (0.5M) and DTT solution (10 mM) to make final concentration of Ab solution at 10 mM EDTA and 1.8 mM DTT and.
   d. Let mixtures sit at room temp for 20 min.
   e. While waiting, equilibrate 7kD MWCO Zeba desalt columns with 10 mM EDTA solution prepared. Remove buffer by centrifuging for 1 min at 1300xg using bench-top centrifuge. Add 200 µl of 10 mM EDTA to the column and spin for 1 min at 1300xg. Repeat two times.
   f. Add 200 µl Ab solution into each column and spin for 3 min at 1300xg to remove DTT.
   g. Re-suspend every 1 µmol high TM liposomes in 50 µl sterile PBS.
   h. Add desalted Ab solution to liposomes. Top up to 500 µl per batch (2 µmol) liposome.
   i. Leave them on rotator at room temperature overnight for Ab coupling
9. Next day (at least 12 hr later), transfer samples to ultracentrifuge tubes and top up with STERILE PBS IN THE HOOD. Spin down at 30,000 rpm for 3 hr at 4 °C.
10. Remove supernatant and re-suspend each µmol liposome in 50 µl of sterile PBS.

6.2.2 Pmel-1 primary T-cells activation

Day 0:

1. Extract Pmel-1 mice's spleens and store temporarily in RPMI in an ice bucket.
2. Put 70 µm cell strainer on top of 50 ml tube and wet the strainer with 1ml of cold PBS. Put 5 spleens on each cell strainer. Cut the spleens with scissors and grind them. Rinse cell strainer with PBS to wash down cells.
3. Remove cell strainer and top up tube to 50 ml with PBS. Spin down at 1700 rpm, 4 °C for 6 min.
4. Aspirate supernatant. Re-suspend pellet in 1 ml of ACK lysing buffer (AKL) per spleen.

5. After 4 minutes, filter the cell solution through a 70 μm cell strainer to a new 50 ml tube. Top up to 50 ml with PBS, take out a aliquot for counting and spin down cells.
6. While waiting for spinning down, prepare activation medium (Complete RPMI with ConA and IL-7). To each 50 ml of RPMI, add 20 μl of ConA at 5mg/ml (final conc. 2 μg/ml) and 10 μl of IL-7 at 5 ng/ml (final conc. 1 ng/ml).
7. Aspirate supernatant. Re-suspend pellet in prepared activation medium. Rule of thumb: generally 1 spleen (6 weeks) in 10 ml per 10 cm petri dish
8. Add 10ml of cell solution to each cell culture petri dish. Incubate at 37 °C.

Day 2 (48 hr later)

1. Warm up PBS to room temperature.
2. Transfer the T-cells to 50 ml tubes. Rinse each petri dish with 4 ml PBS (at room temperature) twice.
3. Spin down the cells at 4 °C, 1700 rpm for 6 minutes and re-suspend in PBS. Top up to 50 ml with PBS and spin down again.
4. Re-suspend cells in 20ml PBS at ROOM TEMPERATURE.
5. Add 20 ml Ficoll at the bottom GENTLY. Should observe two clear layers of liquid. Do not disturb interface.
6. Centrifuge at 22°C, 1500 rpm for 15 minutes. Unleash brake.
7. Use 25 ml pipet tips to take out the interface between PBS and ficoll. Top up to 50mL with PBS.
8. Centrifuge at 4 °C, 1700 rpm for 6 minutes. Aspirate supernatant. Re-suspend cells in T-cells isolation buffer.
9. Top up to 50 ml with isolation buffer, count cells and spin down at 4 °C, 1700 rpm for 6 min.
10. Aspirate supernatant. Re-suspend cells in 100 million per ml in isolation buffer.
11. Proceed to T-cells isolation.
12. After T cell isolation, re-suspend T-cells in RPMI containing IL-2 at final conc. 10 ng/ml and 0.75 million cells/ml.
13. Add 10 ml of cells to each petri dish.

Day3 (72hrs later)

1. Spin down cells 4 °C, 1700 rpm for 6 min.
2. Wash two more times with PBS.
3. Re-suspend T-cells for experiments.

6.2.3 Intracellular staining of phosphorylated Smad2

1. Wash cells in PBS, spin at 1800 rpm for 5 min at 4°C (subsequent spins will be with these conditions unless otherwise noticed).
2. Aspirate cells, then re-suspend in 200 μl of PBS.
3. Add 1μl of dissolved aqua live/dead dye to each well.
4. Incubate cells for 30 min at room temperature (RT) in the dark.
5. Spin cells out of PBS.
6. Aspirate cells, then wash once in FACS buffer (1%BSA).

7. Add 200 µl of BD cytofix/cytoperm solution (BD Bioscience) to each well for fixation. Incubate for 20 min in the dark at 4°C.
9. Spin cells out of fixation solution at 2300 rpm for 5 min at 4°C (all subsequent spins will be at 2300 rpm).
10. Suspend cells in pre-chilled perm buffer III (pre-chilled to -20°C) (BD Bioscience) and incubate for 20 min at 4°C in the dark.
11. Spin cells out of perm buffer III and aspirate.
12. Suspend cells in 50 µl of staining solution (anti-p-Smad2-APC 1:50 dilution in FACS buffer) and incubate for 20 min at RT in the dark.
13. Top up cells with 150 µl FACS buffer and spin.
14. Aspirate cells, then re-suspend in 200 µ FACS buffer and proceed to analysis by flow cytometer.

References

1. Urruticoechea, A., et al., *Recent advances in cancer therapy: an overview.* Curr Pharm Des, 2010. **16**(1): p. 3-10.
2. Chabner, B.A. and T.G. Roberts, Jr., *Timeline: Chemotherapy and the war on cancer.* Nat Rev Cancer, 2005. **5**(1): p. 65-72.
3. Vanneman, M. and G. Dranoff, *Combining immunotherapy and targeted therapies in cancer treatment.* Nat Rev Cancer, 2012. **12**(4): p. 237-51.
4. Cohen, M.H., et al., *Approval summary for imatinib mesylate capsules in the treatment of chronic myelogenous leukemia.* Clin Cancer Res, 2002. **8**(5): p. 935-42.
5. O'Brien, S.G., et al., *Imatinib compared with interferon and low-dose cytarabine for newly diagnosed chronic-phase chronic myeloid leukemia.* N Engl J Med, 2003. **348**(11): p. 994-1004.
6. Huang, M., et al., *Molecularly targeted cancer therapy: some lessons from the past decade.* Trends Pharmacol Sci, 2014. **35**(1): p. 41-50.
7. Sierra, J.R., V. Cepero, and S. Giordano, *Molecular mechanisms of acquired resistance to tyrosine kinase targeted therapy.* Mol Cancer, 2010. **9**: p. 75.
8. O'Hare, T., et al., *Pushing the limits of targeted therapy in chronic myeloid leukaemia.* Nat Rev Cancer, 2012. **12**(8): p. 513-26.
9. Dunn, G.P., L.J. Old, and R.D. Schreiber, *The three Es of cancer immunoediting.* Annu Rev Immunol, 2004. **22**: p. 329-60.
10. Rabinovich, G.A., D. Gabrilovich, and E.M. Sotomayor, *Immunosuppressive strategies that are mediated by tumor cells.* Annu Rev Immunol, 2007. **25**: p. 267-96.
11. Steinman, R.M., D. Hawiger, and M.C. Nussenzweig, *Tolerogenic dendritic cells.* Annu Rev Immunol, 2003. **21**: p. 685-711.
12. Khong, H.T. and N.P. Restifo, *Natural selection of tumor variants in the generation of "tumor escape" phenotypes.* Nat Immunol, 2002. **3**(11): p. 999-1005.
13. Holko, P. and P. Kawalec, *Economic evaluation of sipuleucel-T immunotherapy in castration-resistant prostate cancer.* Expert Rev Anticancer Ther, 2014. **14**(1): p. 63-73.
14. Restifo, N.P., M.E. Dudley, and S.A. Rosenberg, *Adoptive immunotherapy for cancer: harnessing the T cell response.* Nat Rev Immunol, 2012. **12**(4): p. 269-81.
15. Kantoff, P.W., et al., *Sipuleucel-T immunotherapy for castration-resistant prostate cancer.* N Engl J Med, 2010. **363**(5): p. 411-22.
16. Mellman, I., G. Coukos, and G. Dranoff, *Cancer immunotherapy comes of age.* Nature, 2011. **480**(7378): p. 480-9.
17. Hodi, F.S., et al., *Improved survival with ipilimumab in patients with metastatic melanoma.* N Engl J Med, 2010. **363**(8): p. 711-23.
18. Maus, M.V., et al., *Adoptive immunotherapy for cancer or viruses.* Annu Rev Immunol, 2014. **32**: p. 189-225.
19. Lee, S. and K. Margolin, *Cytokines in cancer immunotherapy.* Cancers (Basel), 2011. **3**(4): p. 3856-93.
20. Schwartzentruber, D.J., *Guidelines for the safe administration of high-dose interleukin-2.* J Immunother, 2001. **24**(4): p. 287-93.
21. Rosenberg, S.A., et al., *Experience with the use of high-dose interleukin-2 in the treatment of 652 cancer patients.* Ann Surg, 1989. **210**(4): p. 474-84; discussion 484-5.
22. Conlon, K.C., et al., *Redistribution, hyperproliferation, activation of natural killer cells and CD8 T cells, and cytokine production during first-in-human clinical trial of*

recombinant human interleukin-15 in patients with cancer. J Clin Oncol, 2015. **33**(1): p. 74-82.
23. Yu, H., M. Kortylewski, and D. Pardoll, *Crosstalk between cancer and immune cells: role of STAT3 in the tumour microenvironment.* Nature Reviews Immunology, 2007. **7**(1): p. 41-51.
24. Gerlini, G., et al., *Metastatic melanoma secreted IL-10 down-regulates CD1 molecules on dendritic cells in metastatic tumor lesions.* Am J Pathol, 2004. **165**(6): p. 1853-63.
25. Li, M.O., et al., *Transforming growth factor-beta regulation of immune responses.* Annu Rev Immunol, 2006. **24**: p. 99-146.
26. Kehrl, J.H., et al., *Production of transforming growth factor beta by human T lymphocytes and its potential role in the regulation of T cell growth.* J Exp Med, 1986. **163**(5): p. 1037-50.
27. Wrzesinski, S.H., Y.Y. Wan, and R.A. Flavell, *Transforming growth factor-beta and the immune response: implications for anticancer therapy.* Clin Cancer Res, 2007. **13**(18 Pt 1): p. 5262-70.
28. Thomas, D.A. and J. Massague, *TGF-beta directly targets cytotoxic T cell functions during tumor evasion of immune surveillance.* Cancer Cell, 2005. **8**(5): p. 369-80.
29. Ahmadzadeh, M. and S.A. Rosenberg, *TGF-beta 1 attenuates the acquisition and expression of effector function by tumor antigen-specific human memory CD8 T cells.* J Immunol, 2005. **174**(9): p. 5215-23.
30. Rowland-Goldsmith, M.A., et al., *Soluble type II transforming growth factor-beta (TGF-beta) receptor inhibits TGF-beta signaling in COLO-357 pancreatic cancer cells in vitro and attenuates tumor formation.* Clin Cancer Res, 2001. **7**(9): p. 2931-40.
31. Gorelik, L. and R.A. Flavell, *Immune-mediated eradication of tumors through the blockade of transforming growth factor-beta signaling in T cells.* Nat Med, 2001. **7**(10): p. 1118-22.
32. Zhang, Q., et al., *Adoptive transfer of tumor-reactive transforming growth factor-beta-insensitive CD8+ T cells: eradication of autologous mouse prostate cancer.* Cancer Res, 2005. **65**(5): p. 1761-9.
33. Rosenberg, S.A., et al., *Adoptive cell transfer: a clinical path to effective cancer immunotherapy.* Nat Rev Cancer, 2008. **8**(4): p. 299-308.
34. June, C.H., *Principles of adoptive T cell cancer therapy.* J Clin Invest, 2007. **117**(5): p. 1204-12.
35. Park, T.S., S.A. Rosenberg, and R.A. Morgan, *Treating cancer with genetically engineered T cells.* Trends Biotechnol, 2011. **29**(11): p. 550-7.
36. Rosenberg, S.A., et al., *Durable complete responses in heavily pretreated patients with metastatic melanoma using T-cell transfer immunotherapy.* Clin Cancer Res, 2011. **17**(13): p. 4550-7.
37. Yee, C., et al., *Adoptive T cell therapy using antigen-specific CD8+ T cell clones for the treatment of patients with metastatic melanoma: in vivo persistence, migration, and antitumor effect of transferred T cells.* Proc Natl Acad Sci U S A, 2002. **99**(25): p. 16168-73.
38. Morgan, R.A., et al., *Cancer regression in patients after transfer of genetically engineered lymphocytes.* Science, 2006. **314**(5796): p. 126-9.

39. Kalos, M., et al., *T cells with chimeric antigen receptors have potent antitumor effects and can establish memory in patients with advanced leukemia.* Sci Transl Med, 2011. **3**(95): p. 95ra73.
40. Maude, S.L., et al., *Chimeric antigen receptor T cells for sustained remissions in leukemia.* N Engl J Med, 2014. **371**(16): p. 1507-17.
41. Grupp, S.A., et al., *Chimeric antigen receptor-modified T cells for acute lymphoid leukemia.* N Engl J Med, 2013. **368**(16): p. 1509-18.
42. Louis, C.U., et al., *Antitumor activity and long-term fate of chimeric antigen receptor-positive T cells in patients with neuroblastoma.* Blood, 2011. **118**(23): p. 6050-6.
43. Rosenberg, S.A. and N.P. Restifo, *Adoptive cell transfer as personalized immunotherapy for human cancer.* Science, 2015. **348**(6230): p. 62-68.
44. Kalos, M. and C.H. June, *Adoptive T cell transfer for cancer immunotherapy in the era of synthetic biology.* Immunity, 2013. **39**(1): p. 49-60.
45. Dudley, M.E., et al., *Cancer regression and autoimmunity in patients after clonal repopulation with antitumor lymphocytes.* Science, 2002. **298**(5594): p. 850-4.
46. Besser, M.J., et al., *Adoptive transfer of tumor-infiltrating lymphocytes in patients with metastatic melanoma: intent-to-treat analysis and efficacy after failure to prior immunotherapies.* Clin Cancer Res, 2013. **19**(17): p. 4792-800.
47. Besser, M.J., et al., *Clinical responses in a phase II study using adoptive transfer of short-term cultured tumor infiltration lymphocytes in metastatic melanoma patients.* Clin Cancer Res, 2010. **16**(9): p. 2646-55.
48. Rubinstein, M.P., et al., *Ex vivo interleukin-12-priming during CD8(+) T cell activation dramatically improves adoptive T cell transfer antitumor efficacy in a lymphodepleted host.* J Am Coll Surg, 2012. **214**(4): p. 700-7; discussion 707-8.
49. Prieto, P.A., et al., *Enrichment of CD8+ cells from melanoma tumor-infiltrating lymphocyte cultures reveals tumor reactivity for use in adoptive cell therapy.* J Immunother, 2010. **33**(5): p. 547-56.
50. Kobayashi, H., et al., *Phase I/II study of adoptive transfer of gammadelta T cells in combination with zoledronic acid and IL-2 to patients with advanced renal cell carcinoma.* Cancer Immunol Immunother, 2011. **60**(8): p. 1075-84.
51. Markley, J.C. and M. Sadelain, *IL-7 and IL-21 are superior to IL-2 and IL-15 in promoting human T cell-mediated rejection of systemic lymphoma in immunodeficient mice.* Blood, 2010. **115**(17): p. 3508-19.
52. Kerkar, S.P., et al., *Tumor-specific CD8+ T cells expressing interleukin-12 eradicate established cancers in lymphodepleted hosts.* Cancer Res, 2010. **70**(17): p. 6725-34.
53. Hsu, C., et al., *Cytokine-independent growth and clonal expansion of a primary human CD8+ T-cell clone following retroviral transduction with the IL-15 gene.* Blood, 2007. **109**(12): p. 5168-77.
54. Hoyos, V., et al., *Engineering CD19-specific T lymphocytes with interleukin-15 and a suicide gene to enhance their anti-lymphoma/leukemia effects and safety.* Leukemia, 2010. **24**(6): p. 1160-70.
55. Zhang, L., et al., *Tumor-infiltrating lymphocytes genetically engineered with an inducible gene encoding interleukin-12 for the immunotherapy of metastatic melanoma.* Clin Cancer Res, 2015. **21**(10): p. 2278-88.
56. Eton, O., et al., *Phase I trial of subcutaneous recombinant human interleukin-2 in patients with metastatic melanoma.* Cancer, 2002. **95**(1): p. 127-34.

57. Hill, H.C., et al., *Cancer immunotherapy with interleukin 12 and granulocyte-macrophage colony-stimulating factor-encapsulated microspheres: coinduction of innate and adaptive antitumor immunity and cure of disseminated disease.* Cancer Res, 2002. **62**(24): p. 7254-63.
58. June, C.H., *Adoptive T cell therapy for cancer in the clinic.* J Clin Invest, 2007. **117**(6): p. 1466-76.
59. Moon, J.J., B. Huang, and D.J. Irvine, *Engineering Nano- and Microparticles to Tune Immunity.* Advanced Materials, 2012. **24**(28): p. 3724-3746.
60. Liu, H.P., et al., *Structure-based programming of lymph-node targeting in molecular vaccines.* Nature, 2014. **507**(7493): p. 519-+.
61. Kim, J., et al., *Injectable, spontaneously assembling, inorganic scaffolds modulate immune cells in vivo and increase vaccine efficacy.* Nat Biotechnol, 2015. **33**(1): p. 64-72.
62. Hanes, J., et al., *Controlled local delivery of interleukin-2 by biodegradable polymers protects animals from experimental brain tumors and liver tumors.* Pharm Res, 2001. **18**(7): p. 899-906.
63. Alshamsan, A., et al., *The induction of tumor apoptosis in B16 melanoma following STAT3 siRNA delivery with a lipid-substituted polyethylenimine.* Biomaterials, 2010. **31**(6): p. 1420-8.
64. Kimura, K., et al., *Pathogenic role of B cells in anti-CD40-induced necroinflammatory liver disease.* Am J Pathol, 2006. **168**(3): p. 786-95.
65. Kwong, B., *Liposome-anchored local delivery of immunomodulatory agents for tumor therapy*, in *Biological Engineering*. 2012, Massachusetts Institute of Technology: http://hdl.handle.net/1721.1/76115.
66. Kwong, B., et al., *Localized immunotherapy via liposome-anchored Anti-CD137 + IL-2 prevents lethal toxicity and elicits local and systemic antitumor immunity.* Cancer Res, 2013. **73**(5): p. 1547-58.
67. Park, J., et al., *Combination delivery of TGF-beta inhibitor and IL-2 by nanoscale liposomal polymeric gels enhances tumour immunotherapy.* Nat Mater, 2012. **11**(10): p. 895-905.
68. Fadel, T.R., et al., *A carbon nanotube-polymer composite for T-cell therapy.* Nature Nanotechnology, 2014. **9**(8): p. 639-647.
69. Perica, K., et al., *Magnetic Field-Induced T Cell Receptor Clustering by Nanoparticles Enhances T Cell Activation and Stimulates Antitumor Activity.* Acs Nano, 2014. **8**(3): p. 2252-2260.
70. Stephan, S.B., et al., *Biopolymer implants enhance the efficacy of adoptive T-cell therapy.* Nat Biotechnol, 2015. **33**(1): p. 97-101.
71. Stephan, M.T., et al., *Therapeutic cell engineering with surface-conjugated synthetic nanoparticles.* Nat Med, 2010. **16**(9): p. 1035-41.
72. Stephan, M.T., et al., *Synapse-directed delivery of immunomodulators using T-cell-conjugated nanoparticles.* Biomaterials, 2012. **33**(23): p. 5776-87.
73. Allen, T.M., *Ligand-targeted therapeutics in anticancer therapy.* Nat Rev Cancer, 2002. **2**(10): p. 750-63.
74. Ruoslahti, E., S.N. Bhatia, and M.J. Sailor, *Targeting of drugs and nanoparticles to tumors.* J Cell Biol, 2010. **188**(6): p. 759-68.

75. Mamot, C., et al., *Epidermal growth factor receptor (EGFR)-targeted immunoliposomes mediate specific and efficient drug delivery to EGFR- and EGFRvIII-overexpressing tumor cells.* Cancer Res, 2003. **63**(12): p. 3154-61.
76. Sacchetti, C., et al., *In vivo targeting of intratumor regulatory T cells using PEG-modified single-walled carbon nanotubes.* Bioconjug Chem, 2013. **24**(6): p. 852-8.
77. Iyer, A.K., et al., *Exploiting the enhanced permeability and retention effect for tumor targeting.* Drug Discov Today, 2006. **11**(17-18): p. 812-8.
78. Kirpotin, D.B., et al., *Antibody targeting of long-circulating lipidic nanoparticles does not increase tumor localization but does increase internalization in animal models.* Cancer Res, 2006. **66**(13): p. 6732-40.
79. Zheng, Y., et al., *In vivo targeting of adoptively transferred T-cells with antibody- and cytokine-conjugated liposomes.* J Control Release, 2013. **172**(2): p. 426-35.
80. Topalian, S.L., et al., *Safety, activity, and immune correlates of anti-PD-1 antibody in cancer.* N Engl J Med, 2012. **366**(26): p. 2443-54.
81. Fahmy, T.M., J.P. Schneck, and W.M. Saltzman, *A nanoscopic multivalent antigen-presenting carrier for sensitive detection and drug delivery to T cells.* Nanomedicine : nanotechnology, biology, and medicine, 2007. **3**(1): p. 75-85.
82. Tsai, S., et al., *Reversal of autoimmunity by boosting memory-like autoregulatory T cells.* Immunity, 2010. **32**(4): p. 568-580.
83. Clemente-Casares, X., et al., *Peptide-MHC-based nanovaccines for the treatment of autoimmunity: a "one size fits all" approach?* Journal of molecular medicine (Berlin, Germany), 2011. **89**(8): p. 733-742.
84. Wang, X., et al., *A transgene-encoded cell surface polypeptide for selection, in vivo tracking, and ablation of engineered cells.* Blood, 2011. **118**(5): p. 1255-63.
85. Kalos, M., *Biomarkers in T cell therapy clinical trials.* J Transl Med, 2011. **9**: p. 138.
86. Minami, Y., et al., *The IL-2 receptor complex: its structure, function, and target genes.* Annu Rev Immunol, 1993. **11**: p. 245-68.
87. Baudino, L., et al., *Crucial role of aspartic acid at position 265 in the CH2 domain for murine IgG2a and IgG2b Fc-associated effector functions.* J Immunol, 2008. **181**(9): p. 6664-9.
88. Overwijk, W.W., et al., *Tumor regression and autoimmunity after reversal of a functionally tolerant state of self-reactive CD8+ T cells.* J Exp Med, 2003. **198**(4): p. 569-80.
89. Lowenthal, J.W., et al., *High and low affinity IL 2 receptors: analysis by IL 2 dissociation rate and reactivity with monoclonal anti-receptor antibody PC61.* J Immunol, 1985. **135**(6): p. 3988-94.
90. Lowenthal, J.W., et al., *Similarities between interleukin-2 receptor number and affinity on activated B and T lymphocytes.* Nature, 1985. **315**(6021): p. 669-72.
91. Murphy, R.F., S. Powers, and C.R. Cantor, *Endosome pH measured in single cells by dual fluorescence flow cytometry: rapid acidification of insulin to pH 6.* J Cell Biol, 1984. **98**(5): p. 1757-62.
92. Klebanoff, C.A., et al., *Sinks, suppressors and antigen presenters: how lymphodepletion enhances T cell-mediated tumor immunotherapy.* Trends Immunol, 2005. **26**(2): p. 111-7.
93. Dudley, M.E., et al., *A phase I study of nonmyeloablative chemotherapy and adoptive transfer of autologous tumor antigen-specific T lymphocytes in patients with metastatic melanoma.* J Immunother, 2002. **25**(3): p. 243-51.

94. Konrad, M.W., et al., *Pharmacokinetics of recombinant interleukin 2 in humans.* Cancer Res, 1990. **50**(7): p. 2009-17.
95. Sieber, T., et al., *Selective internalization of monoclonal antibodies by B-cell chronic lymphocytic leukaemia cells.* British Journal of Haematology, 2003. **121**(3): p. 458-461.
96. Sapra, P. and T.M. Allen, *Internalizing antibodies are necessary for improved therapeutic efficacy of antibody-targeted liposomal drugs.* Cancer Res, 2002. **62**(24): p. 7190-4.
97. Gao, H., et al., *Ligand modified nanoparticles increases cell uptake, alters endocytosis and elevates glioma distribution and internalization.* Sci Rep, 2013. **3**: p. 2534.
98. Henriksen, L., et al., *Internalization mechanisms of the epidermal growth factor receptor after activation with different ligands.* PLoS One, 2013. **8**(3): p. e58148.
99. Shukla, G.S. and D.N. Krag, *Cancer cell-specific internalizing ligands from phage displayed beta-lactamase-peptide fusion libraries.* Protein Eng Des Sel, 2010. **23**(6): p. 431-40.
100. Moon, J.J., et al., *Interbilayer-crosslinked multilamellar vesicles as synthetic vaccines for potent humoral and cellular immune responses.* Nat Mater, 2011. **10**(3): p. 243-51.
101. Waldmann, T.A., *The biology of interleukin-2 and interleukin-15: implications for cancer therapy and vaccine design.* Nat Rev Immunol, 2006. **6**(8): p. 595-601.
102. Fehniger, T.A., M.A. Cooper, and M.A. Caligiuri, *Interleukin-2 and interleukin-15: immunotherapy for cancer.* Cytokine Growth Factor Rev, 2002. **13**(2): p. 169-83.
103. Fehniger, T.A. and M.A. Caligiuri, *Interleukin 15: biology and relevance to human disease.* Blood, 2001. **97**(1): p. 14-32.
104. Budagian, V., et al., *IL-15/IL-15 receptor biology: A guided tour through an expanding universe.* Cytokine & Growth Factor Reviews, 2006. **17**(4): p. 259-280.
105. Marks-Konczalik, J., et al., *IL-2-induced activation-induced cell death is inhibited in IL-15 transgenic mice.* Proc Natl Acad Sci U S A, 2000. **97**(21): p. 11445-50.
106. Dubois, S., et al., *IL-15Ralpha recycles and presents IL-15 In trans to neighboring cells.* Immunity, 2002. **17**(5): p. 537-47.
107. Waldmann, T.A., et al., *Safety (toxicity), pharmacokinetics, immunogenicity, and impact on elements of the normal immune system of recombinant human IL-15 in rhesus macaques.* Blood, 2011. **117**(18): p. 4787-95.
108. Berard, M., et al., *IL-15 promotes the survival of naive and memory phenotype CD8+ T cells.* J Immunol, 2003. **170**(10): p. 5018-26.
109. Liu, K., et al., *IL-15 mimics T cell receptor crosslinking in the induction of cellular proliferation, gene expression, and cytotoxicity in CD8+ memory T cells.* Proc Natl Acad Sci U S A, 2002. **99**(9): p. 6192-7.
110. Mueller, K., O. Schweier, and H. Pircher, *Efficacy of IL-2- versus IL-15-stimulated CD8 T cells in adoptive immunotherapy.* Eur J Immunol, 2008. **38**(10): p. 2874-85.
111. Liu, R.B., et al., *IL-15 in tumor microenvironment causes rejection of large established tumors by T cells in a noncognate T cell receptor-dependent manner.* Proc Natl Acad Sci U S A, 2013. **110**(20): p. 8158-63.
112. Klebanoff, C.A., et al., *IL-15 enhances the in vivo antitumor activity of tumor-reactive CD8+ T cells.* Proc Natl Acad Sci U S A, 2004. **101**(7): p. 1969-74.
113. Rubinstein, M.P., et al., *Converting IL-15 to a superagonist by binding to soluble IL-15R{alpha}.* Proc Natl Acad Sci U S A, 2006. **103**(24): p. 9166-71.

114. Han, K.P., et al., *IL-15:IL-15 receptor alpha superagonist complex: high-level co-expression in recombinant mammalian cells, purification and characterization.* Cytokine, 2011. **56**(3): p. 804-10.
115. Sneller, M.C., et al., *IL-15 administered by continuous infusion to rhesus macaques induces massive expansion of CD8+ T effector memory population in peripheral blood.* Blood, 2011. **118**(26): p. 6845-8.
116. Sahaf, B., et al., *Lymphocyte surface thiol levels.* Proc Natl Acad Sci U S A, 2003. **100**(7): p. 4001-5.
117. Yu, A., et al., *Efficient internalization of IL-2 depends on the distal portion of the cytoplasmic tail of the IL-2R common gamma-chain and a lymphoid cell environment.* J Immunol, 2000. **165**(5): p. 2556-62.
118. Hemar, A., et al., *Endocytosis of interleukin 2 receptors in human T lymphocytes: distinct intracellular localization and fate of the receptor alpha, beta, and gamma chains.* J Cell Biol, 1995. **129**(1): p. 55-64.
119. Trowbridge, I.S. and M.L. Thomas, *CD45: an emerging role as a protein tyrosine phosphatase required for lymphocyte activation and development.* Annu Rev Immunol, 1994. **12**: p. 85-116.
120. Osinalde, N., et al., *Interleukin-2 signaling pathway analysis by quantitative phosphoproteomics.* J Proteomics, 2011. **75**(1): p. 177-91.
121. Lesage, S., et al., *CD4+ CD8+ thymocytes are preferentially induced to die following CD45 cross-linking, through a novel apoptotic pathway.* J Immunol, 1997. **159**(10): p. 4762-71.
122. Klaus, S.J., S.P. Sidorenko, and E.A. Clark, *CD45 ligation induces programmed cell death in T and B lymphocytes.* J Immunol, 1996. **156**(8): p. 2743-53.
123. Fortin, M., et al., *Apoptosis mediated through CD45 is independent of its phosphatase activity and association with leukocyte phosphatase-associated phosphoprotein.* J Immunol, 2002. **168**(12): p. 6084-9.
124. Hand, T.W., et al., *Differential effects of STAT5 and PI3K/AKT signaling on effector and memory CD8 T-cell survival.* Proc Natl Acad Sci U S A, 2010. **107**(38): p. 16601-6.
125. Tripathi, P., et al., *STAT5 is critical to maintain effector CD8+ T cell responses.* J Immunol, 2010. **185**(4): p. 2116-24.
126. Johnston, J.A., et al., *Tyrosine phosphorylation and activation of STAT5, STAT3, and Janus kinases by interleukins 2 and 15.* Proc Natl Acad Sci U S A, 1995. **92**(19): p. 8705-9.
127. Schluter, C., et al., *The cell proliferation-associated antigen of antibody Ki-67: a very large, ubiquitous nuclear protein with numerous repeated elements, representing a new kind of cell cycle-maintaining proteins.* J Cell Biol, 1993. **123**(3): p. 513-22.
128. Scholzen, T. and J. Gerdes, *The Ki-67 protein: from the known and the unknown.* J Cell Physiol, 2000. **182**(3): p. 311-22.
129. Yerushalmi, R., et al., *Ki67 in breast cancer: prognostic and predictive potential.* Lancet Oncol, 2010. **11**(2): p. 174-83.
130. Inwald, E.C., et al., *Ki-67 is a prognostic parameter in breast cancer patients: results of a large population-based cohort of a cancer registry.* Breast Cancer Res Treat, 2013. **139**(2): p. 539-52.

131. Wrzesinski, C., et al., *Increased intensity lymphodepletion enhances tumor treatment efficacy of adoptively transferred tumor-specific T cells.* J Immunother, 2010. **33**(1): p. 1-7.
132. Eisenman, J., et al., *Interleukin-15 interactions with interleukin-15 receptor complexes: characterization and species specificity.* Cytokine, 2002. **20**(3): p. 121-9.
133. Akhurst, R.J. and A. Hata, *Targeting the TGFbeta signalling pathway in disease.* Nat Rev Drug Discov, 2012. **11**(10): p. 790-811.
134. Yang, L., Y. Pang, and H.L. Moses, *TGF-beta and immune cells: an important regulatory axis in the tumor microenvironment and progression.* Trends Immunol, 2010. **31**(6): p. 220-7.
135. Laouar, Y., et al., *Transforming growth factor-beta controls T helper type 1 cell development through regulation of natural killer cell interferon-gamma.* Nat Immunol, 2005. **6**(6): p. 600-7.
136. Stephen, T.L., et al., *Transforming Growth Factor beta-Mediated Suppression of Antitumor T Cells Requires FoxP1 Transcription Factor Expression.* Immunity, 2014. **41**(3): p. 427-439.
137. Donkor, M.K., et al., *T Cell Surveillance of Oncogene-Induced Prostate Cancer Is Impeded by T Cell-Derived TGF-beta 1 Cytokine.* Immunity, 2011. **35**(1): p. 123-134.
138. Tran, T.T., et al., *Inhibiting TGF-beta signaling restores immune surveillance in the SMA-560 glioma model.* Neuro Oncol, 2007. **9**(3): p. 259-70.
139. Uhl, M., et al., *SD-208, a novel transforming growth factor beta receptor I kinase inhibitor, inhibits growth and invasiveness and enhances immunogenicity of murine and human glioma cells in vitro and in vivo.* Cancer Res, 2004. **64**(21): p. 7954-61.
140. Tanaka, H., et al., *Transforming growth factor beta signaling inhibitor, SB-431542, induces maturation of dendritic cells and enhances anti-tumor activity.* Oncol Rep, 2010. **24**(6): p. 1637-43.
141. Bhola, N.E., et al., *TGF-beta inhibition enhances chemotherapy action against triple-negative breast cancer.* J Clin Invest, 2013. **123**(3): p. 1348-58.
142. Garrison, K., et al., *The small molecule TGF-beta signaling inhibitor SM16 synergizes with agonistic OX40 antibody to suppress established mammary tumors and reduce spontaneous metastasis.* Cancer Immunol Immunother, 2012. **61**(4): p. 511-21.
143. Neuzillet, C., et al., *Targeting the TGFbeta pathway for cancer therapy.* Pharmacol Ther, 2015. **147**: p. 22-31.
144. Rodon, J., et al., *First-in-human dose study of the novel transforming growth factor-beta receptor I kinase inhibitor LY2157299 monohydrate in patients with advanced cancer and glioma.* Clin Cancer Res, 2015. **21**(3): p. 553-60.
145. Herbertz, S., et al., *Clinical development of galunisertib (LY2157299 monohydrate), a small molecule inhibitor of transforming growth factor-beta signaling pathway.* Drug Des Devel Ther, 2015. **9**: p. 4479-99.
146. Shull, M.M., et al., *Targeted disruption of the mouse transforming growth factor-beta 1 gene results in multifocal inflammatory disease.* Nature, 1992. **359**(6397): p. 693-9.
147. Aoki, C.A., et al., *Transforming growth factor beta (TGF-beta) and autoimmunity.* Autoimmun Rev, 2005. **4**(7): p. 450-9.
148. Ohtsuka, K., et al., *Decreased production of TGF-beta by lymphocytes from patients with systemic lupus erythematosus.* J Immunol, 1998. **160**(5): p. 2539-45.

149. Holmdahl, R., et al., *The molecular pathogenesis of collagen-induced arthritis in mice--a model for rheumatoid arthritis.* Ageing Res Rev, 2002. **1**(1): p. 135-47.
150. Akhurst, R.J. and R. Derynck, *TGF-beta signaling in cancer--a double-edged sword.* Trends Cell Biol, 2001. **11**(11): p. S44-51.
151. Guasch, G., et al., *Loss of TGFbeta signaling destabilizes homeostasis and promotes squamous cell carcinomas in stratified epithelia.* Cancer Cell, 2007. **12**(4): p. 313-27.
152. Hong, S., et al., *Connection between inflammation and carcinogenesis in gastrointestinal tract: Focus on TGF-beta signaling.* World Journal of Gastroenterology, 2010. **16**(17): p. 2080-2093.
153. Feagins, L.A., *Role of transforming growth factor-beta in inflammatory bowel disease and colitis-associated colon cancer.* Inflamm Bowel Dis, 2010. **16**(11): p. 1963-8.
154. Connolly, E.C., et al., *Outgrowth of drug-resistant carcinomas expressing markers of tumor aggression after long-term TbetaRI/II kinase inhibition with LY2109761.* Cancer Res, 2011. **71**(6): p. 2339-49.
155. Huang, B., et al., *Active targeting of chemotherapy to disseminated tumors using nanoparticle-carrying T cells.* Sci Transl Med, 2015. **7**(291): p. 291ra94.
156. Grygielko, E.T., et al., *Inhibition of gene markers of fibrosis with a novel inhibitor of transforming growth factor-beta type I receptor kinase in puromycin-induced nephritis.* J Pharmacol Exp Ther, 2005. **313**(3): p. 943-51.
157. Chen, S., et al., *Mechanism-based tumor-targeting drug delivery system. Validation of efficient vitamin receptor-mediated endocytosis and drug release.* Bioconjug Chem, 2010. **21**(5): p. 979-87.
158. Thomas, M.L., *The leukocyte common antigen family.* Annu Rev Immunol, 1989. **7**: p. 339-69.
159. Hermiston, M.L., Z. Xu, and A. Weiss, *CD45: a critical regulator of signaling thresholds in immune cells.* Annu Rev Immunol, 2003. **21**: p. 107-37.
160. Weber, J.S. and J.J. Mule, *Cancer immunotherapy meets biomaterials.* Nat Biotechnol, 2015. **33**(1): p. 44-5.